สำนักหอสมุดกลาง พระจอมเกล้าลาดกระบัง

SYNTHESIS, CHARACTERIZATION AND CATALYTIC ACTIVITY OF MOLYBDENUM (VI) OXIDE SUPPORTED SILICA CATALYSTS

E071863

LEENAWAT KANDA

เลขหมู่.......
เลขทะเบียน....71863
วัน,เดือน,ปี...30 มี.ค. 2554

b.......................
i.......................

A THESIS SUBMITTED IN PARTIAL FULFILLMENT

OF THE REQUIREMENT FOR THE DEGREE OF

MASTER OF SCIENCE IN CHEMISTRY

FACULTY OF SCIENCE

KING MONGKUT'S INSTITUTE OF TECHNOLOGY LADKRABANG

2011

KMITL-2011-SC-M-012-007

This material is reserved for educational use only, not allowed for commercial use.
Forbidden to modify the content, and cite the document when use.

COPYRIGHT 2011

FACULTY OF SCIENCE

KING MONGKUT'S INSTITUTE OF TECHNOLOGY LADKRABANG

This material is reserved for educational use only, not allowed for commercial use.

Forbidden to modify the content, and cite the document when use.

หัวข้อวิทยานิพนธ์	การสังเคราะห์ พิสูจน์เอกลักษณ์และความสามารถในการเร่งปฏิกิริยาของโมลิบดีนัม (VI) ออกไซด์บนตัวรองรับซิลิกา
นักศึกษา	นายลีนวัฒน์ กานต์ดา
รหัสนักศึกษา	49067803
ปริญญา	วิทยาศาสตรมหาบัณฑิต
สาขาวิชา	เคมี
พ.ศ.	2554
อาจารย์ที่ปรึกษาวิทยานิพนธ์	รศ.ดร. ตะวัน สุขน้อย

บทคัดย่อ

งานวิจัยนี้นำเสนอวิธีการประยุกต์และออกแบบการเตรียมสปีชีส์ของโมลิบดีนัมออกไซด์บนตัวรองรับซิลิกาให้มีลักษณะแตกต่างกันและนำไปศึกษาการเร่งปฏิกิริยาของบิวไทรัลดีไฮด์ โมลิบดีนัมออกไซด์บนตัวรองรับซิลิกาที่มีปริมาณโมลิบดีนัมออกไซด์ (1-20 %โมล) และอุณหภูมิในการแคลไซน์ (500-700 องศาเซลเซียส) ต่างๆนั้นถูกเตรียมโดยวิธีการโซล-เจลและอิมเพร็กเนชั่น จากผลการทดลองพบว่าตัวเร่งปฏิกิริยาที่เตรียมโดยวิธีการโซล-เจลมีพื้นที่ผิวจำเพาะสูง (214-722 ตร.ม./กรัม) และมีการกระจายตัวของขนาดรูพรุนต่ำกว่าตัวเร่งปฏิกิริยาที่เตรียมโดยวิธีการอิมเพร็กเนชั่น (159-378 ตร.ม./กรัม) โดยพื้นที่ผิวจำเพาะจะมีค่าลดลงเรื่อยๆเมื่อเพิ่มปริมาณโมลิบดีนัมออกไซด์บนตัวรองรับ จากการพิสูจน์เอกลักษณ์ด้วยเทคนิคการเลี้ยวเบนของรังสีเอ็กซ์พบว่าจะเกิดลักษณะของผลึกอัลฟาโมลิบดีนัมออกไซด์เมื่อปริมาณโมลิบดีนัมออกไซด์บนตัวรองรับสูงกว่า 10 %โมล อย่างไรก็ตามที่ปริมาณโมลิบดีนัมออกไซด์เท่ากัน (20 %โมล) พบว่าตัวเร่งปฏิกิริยาที่เตรียมโดยวิธีการอิมเพร็กเนชั่นมีความเป็นผลึกของอัลฟาโมลิบดีนัมออกไซด์สูงกว่าตัวเร่งปฏิกิริยาที่เตรียมโดยวิธีการโซล-เจล จากผลการวิเคราะห์โดยกล้องจุลทรรศน์อิเล็กตรอนแบบส่องผ่านพบว่าตัวเร่งปฏิกิริยาที่มีปริมาณโมลิบดีนัมออกไซด์บนตัวรองรับต่ำกว่า 3 %โมลจะมีการกระจายตัวของโมลิบ ดีนัมออกไซด์สูง และเมื่อทำการวิเคราะห์ลักษณะสปีชีส์ของโมลิบดีนัมออกไซด์โดยเทคนิคการวัดความสามารถในการเกิดปฏิกิริยารีดักชั่นและเทคนิคดิฟฟิวซ์รีเฟลกแทนซ์อัลตราไวโอเลตสเปก โตรสโคปีพบว่าลักษณะสปีชีส์แบบพอลิเมอริกและคริสตัลไลน์โมลิบดีนัมออกไซด์จะพบมากในตัวเร่งปฏิกิริยาที่เตรียมโดยทั้งวิธีการโซล-เจลและอิมเพร็กเนชั่นที่มีปริมาณโมลิบดีนัมออกไซด์สูง (20 %โมล) ในทางกลับกันลักษณะสปีชีส์แบบโอลิโกเมอริกและไอโซเลตโมลิบดีนัมออกไซด์จะพบเฉพาะในตัวเร่งปฏิกิริยาที่เตรียมโดยวิธีการโซล-เจลที่มีปริมาณโมลิบดีนัมออกไซด์ต่ำ (1-3 %โมล) อย่างไรก็ตามตัวเร่งปฏิกิริยาที่มีปริมาณโมลิบดีนัมออกไซด์ต่ำ (1-3 %โมล)ที่เตรียม

This material is reserved for educational use only, not allowed for commercial use.
Forbidden to modify the content, and cite the document when use.

โดยวิธีการอิมเพร็กเนชั่นนั้นจะพบลักษณะสปีชีส์แบบพอลิเมอริกและคริสตัลไลน์โมลิบดีนัมออกไซด์เป็นส่วนใหญ่ มากไปกว่านั้นลักษณะสปีชีส์แบบโอลิโกเมอริกและไอโซเลตโมลิบดีนัมออกไซด์สามารถเกิดการรวมตัวกันกลายเป็นลักษณะสปีชีส์แบบพอลิเมอริกและคริสตัลไลน์โมลิบดีนัมออกไซด์เมื่อเพิ่มอุณหภูมิในการแคลไซน์จาก 500 ไปจนถึง 700 องศาเซลเซียส จากผลการทดสอบประสิทธิภาพในการเร่งปฏิกิริยาพบว่าตัวเร่งปฏิกิริยาที่มีลักษณะสปีชีส์แบบไอโซเลตโมลิบดีนัมออกไซด์จะมีประสิทธิภาพสูงในการเร่งปฏิกิริยาคอนเดนเซชั่น ในทางกลับกันตัวเร่งปฏิกิริยาที่มีลักษณะสปีชีส์แบบพอลิเมอริกและคริสตัลไลน์โมลิบดีนัมออกไซด์จะมีประสิทธิภาพและความจำเพาะเจาะจงสูงในการเร่งปฏิกิริยาดีคาร์บอนิลเลชั่น

This material is reserved for educational use only, not allowed for commercial use.
Forbidden to modify the content, and cite the document when use.

Thesis Title	Synthesis, Characterization and Catalytic activity of Molybdenum (VI) oxide supported Silica catalysts
Student	Leenawat Kanda
Student ID	49067803
Degree	Master of Science
Program	Chemistry
Year	2011
Thesis Advisor	Assoc. Prof. Dr. Tawan Sooknoi

ABSTRACT

This work focuses on the preparation of molybdenum oxide supported silica with different surface molybdenum oxide species and the activity of the prepared catalysts was tested for the conversion of butyraldehyde. Molybdenum oxide supported silica catalysts (MoO_3/SiO_2) with different MoO_3 loadings (1-20 mol %) and calcination temperature (500-700 °C) were prepared by sol-gel and impregnation method. The catalysts prepared by sol-gel method exhibited high specific surface area (214-722 m^2/g) and low pore size distribution as compared to those prepared by impregnation method (159-378 m^2/g). Upon increasing the MoO_3 loading the surface area of the catalysts decreased gradually. The formation of crystalline α-MoO_3 was observed when MoO_3 loading is higher than 10 mol %. However, at the same molybdenum oxide content (i.e. 20 mol % MoO_3), the catalysts prepared by impregnation method show higher crystallinity as compared to that prepared by sol-gel method. TEM analysis showed that at low MoO_3 loading (< 3 mol %), a highly dispersion of molybdenum oxide was observed. TPR and DR-UV analysis revealed that polymeric (*Pm*) and crystalline MoO_3 (*Mc*) species are predominant for the catalyst with high molybdenum oxide loading (20 mol %) for both preparation methods. In contrast, the oligomeric MoO_3 (*Oc*) species and the well-dispersed isolated MoO_3 species (*Im*) are the main species for the catalysts obtained from sol-gel method at low molybdenum oxide loading (1-3 mol %). However, polymeric (*Pm*) and crystalline MoO_3 (*Mc*) species are predominant for those prepared by impregnation method. Moreover, the increase in calcination temperature from 500 to 700 °C causes the isolated (*Im*) and oligomeric MoO_3 (*Oc*) species tend to agglomerate to polymeric and crystalline MoO_3 (*Mc*) species. The catalytic activity results showed that the

This material is reserved for educational use only, not allowed for commercial use.
Forbidden to modify the content, and cite the document when use.

catalysts with isolated MoO_3 (*Im*) species (1-3 mol %) exhibited high activity for the condensation reaction. In contrast, the catalysts with polymeric (*Pm*) and crystalline MoO_3 (*Mc*) species (20 mol %) showed high activity and selectivity for the decarbonyltaion reaction.

This material is reserved for educational use only, not allowed for commercial use.
Forbidden to modify the content, and cite the document when use.

ACKNOWLEDGEMENTS

For the thesis completion, I would like to gratefully thank to my advisor, Assoc. Prof. Dr. Tawan Sooknoi for his supports, supervisions, inspiration, suggestions and encouragements throughout this thesis. Also, I wish also gratefully thank to Assoc. Prof. Dr. Sakda Trisak for his stimulating suggestions and encouragement in research in inorganic chemistry.

I wish to thank Asst. Prof. Dr. Punnama Siriphannon, Asst. Prof. Dr. Pachernchai Chaiyasith and Dr. Khamphee Phomphrai for serving as the chairperson and the committee and valuable comments.

I also appreciate the supports from the Department of Chemistry, Faculty of Science, King Mongkut's Institute of Technology Ladkrabang for the equipments, chemicals and facilities.

I would like to extend my sincere appreciation to all of my teachers, my friend and my research group for their constant guidance advice, support and encouragement.

Sincere thanks to Dr. Artit Ausavasukhi and Mr. Nipat peamaroon for their advices, suggestions and kindness.

Finally, I deeply appreciate and thank my parents and my family for their love, supports and encouragements.

Leenawat kanda

This material is reserved for educational use only, not allowed for commercial use.
Forbidden to modify the content, and cite the document when use.

TABLE OF CONTENTS

This material is reserved for educational use only, not allowed for commercial use.

Forbidden to modify the content and cite the document when use.

TABLE OF CONTENTS (Continued)

This material is reserved for educational use only, not allowed for commercial use.

Forbidden to modify the content and cite the document when use.

TABLE OF CONTENTS (Continued)

This material is reserved for educational use only, not allowed for commercial use.

Forbidden to modify the content and cite the document when use.

LIST OF TABLES

This material is reserved for educational use only, not allowed for commercial use.

Forbidden to modify the content and cite the document when use.

LIST OF TABLES (Continued)

Table Page

APPENDICES

This material is reserved for educational use only, not allowed for commercial use.

Forbidden to modify the content and cite the document when use.

LIST OF FIGURES

Figures Page

CHAPTER 2

This material is reserved for educational use only, not allowed for commercial use.
Forbidden to modify the content and cite the document when use.

LIST OF FIGURES (Continued)

Figures Page

This material is reserved for educational use only, not allowed for commercial use.
Forbidden to modify the content and cite the document when use.

LIST OF FIGURES (Continued)

This material is reserved for educational use only, not allowed for commercial use.
Forbidden to modify the content and cite the document when use.

LIST OF FIGURES (Continued)

Figures Page

APPENDICES

This material is reserved for educational use only, not allowed for commercial use.
Forbidden to modify the content and cite the document when use.

CHAPTER 1

INTRODUCTION

1.1 STATEMENT AND SIGNIFICANCE OF THE PROBLEMS

Transition metal oxides form a fascinating class of materials with extremely interesting structural, electronic, and magnetic behavior. From a chemical viewpoint, they play a fundamental role in heterogeneous catalysis of important chemicals, both in gas and liquid phase, as well as in acid–base and redox reaction of industrial processes. Indeed, supported transition metal oxide continues to grow at a rapid rate, reflecting the wide range of chemical reactions that can be enhanced by the use of them. Oxides of the group 5–7 metals (V, Nb, Ta, Cr, Mo, W, and Re) supported on a high surface area oxide material (SiO_2, Al_2O_3, TiO_2, ZrO_2, etc.) are recognized as industrially important catalysts for various chemical reactions **[1–5]**.

During the last decades a great deal of fundamental and applied research interest was focused on molybdenum oxide supported silica catalyst because of their numerous applications in petroleum refining and chemicals production. Since molybdenum oxide supported silica catalysts are excellent for selective oxidation of hydrocarbons **[6]**, oxidative dehydrogenation of alcohols **[7]**, deoxygenation of oxygenated compounds **[8]**. In fact, the catalytic activity of these catalysts depends on the degree of dispersion and structure of the active surface. Therefore, the activity and the selectivity are related to the nature of the active phase, which itself depends largely on the silica support structure and preparation methods **[9]**. Hence, surface structure controls the catalytic activity and selectivity, tailoring the surface properties and structures of catalyst support can provide an effect way to design the appropriate catalysts for certain applications. This can be achieved by understanding the interactions of the active surface with their environment (e.g., the underlying oxide support material and reactive environments). Accordingly, several studies have been devoted on "surface structures" of molybdenum oxide supported silica catalysts (MoO_3/SiO_2) to ascertain the factors controlling their transformation **[10-13]**. Despite the controversy still existing about the methods to identify the species of surface active sites, many studies claimed the existence of structure reactivity correlations as well as the identification of the active sites of bulk **[14]** and molybdenum oxide supported silica

This material is reserved for educational use only, not allowed for commercial use.
Forbidden to modify the content, and cite the document when use.

catalysts **[15]** generated under reaction conditions. Synthesis methods particularly used for preparing these types of catalysts have been developed. For examples, incipient wetness impregnation, immobilisation, grafting, co-pricipitation and sol-gel method were successfully applied. Among these, the catalysts prepared by sol-gel method generally possess high surface area and high dispersion of active sites. Especially, the alteration of active sites species, namely "crystalline MoO_3" (Mc), "polymeric" (*Pm*), oligomeric and the well- dispersed "isolated MoO_3 species" (*Im*) can be readily tailored and controlled in sol-gel synthesis **[16, 17]**. In addition, the loading amounts of molybdenum oxide and heat treatment **[18, 19]** also play a significant role on active sites structure and their catalytic activity. In general, when thermal energy is applied to a precursor compact, the compact is densified and the average grain size increases. The basic phenomena occurring during this process, called sintering, are densification and grain growth. Peculiarly, agglomeration and sintering of the active sites species during treating at high calcination temperature drastically affect the dispersion, active sites structure and catalytic activity of MoO_3/SiO_2 catalysts **[20]**.

According to the reasons above, in this thesis, sol-gel method will be used for preparing the catalysts. Beside, modification of the obtained catalysts by heat treatment with different temperature will also be studied. The catalytic activity and selectivity of the modified catalyst will be studied in the conversion of butyraldehyde as a model compound for this study. Since butyraldehyde is one of the most reactive oxygenated compound which exhibit high reactivity for many reactions such as hydrogenation, oxidation, condensation and deoxygenation. The aim of the present study is to understand the correlation between physico-chemical features of the catalysts and their catalytic activities in the conversion of butyraldehyde. In addition, the experiments will be done in order to propose the mechanism pathways and role of catalyst in the reaction process.

This material is reserved for educational use only, not allowed for commercial use.
Forbidden to modify the content, and cite the document when use.

1.2 GOAL AND OBJECTIVES

The specific objectives of this thesis are as follows:

1.2.1 To understand the effect of preparation method, MoO_3 loading and heat treatment on the active surface structure.

1.2.2 To understand the correlation between active sites species and their catalytic activities and selectivity in the conversion of light oxygenated compound.

1.3 SCOPES OF THE SYUDY

The scopes of this thesis are as follows:

1.3.1 Synthesis and modification of catalysts

1.3.1.1 Synthesis of molybdenum oxide supported silica catalysts (MoO_3/SiO_2) with different MoO_3 loadings (1-20 mol %) by sol-gel method.

1.3.1.2 Preparation of molybdenum oxide supported silica catalysts (MoO_3/SiO_2) with different MoO_3 loadings (3 and 20 mol %) by incipient wetness impregnation method.

1.3.1.3 Modification of the catalysts obtained in 3.3.1.1 and 3.3.1.2 by heat treatment with different temperature (500, 600 and 700 $^{\circ}C$)

1.3.2 Characterization of the catalysts

1.3.2.1 Investigate the physical properties of the catalysts using conventional techniques, such as inductively coupled plasma-atomic emission spectroscopy (ICP-AES), X-ray powder diffraction (XRD), scanning electron microscopy (SEM), gas adsorption analysis (Autosorb-1C) and transmission electron microscopy (TEM).

1.3.2.2 Investigate active sites of the catalysts by diffuse reflectance ultraviolet spectroscopy (DR-UV) and temperature programmed reduction (TPR).

1.3.2.3 Investigate acidity of the catalysts by temperature programmed desorption (TPD)

1.3.3 Catalytic testing of the catalysts

1.3.3.1 Investigate their catalytic activity and selectivity of modified catalysts

This material is reserved for educational use only, not allowed for commercial use.
Forbidden to modify the content, and cite the document when use.

with the conversion of butyraldehyde in a continuous fixed bed down flow reactor.

1.3.3.2 Study on effect of MoO_3 loading on support, effect of calcination temperature effect of preparation method and effect of reaction temperature.

1.3.4 Analysis of products

1.3.4.1 Determine the amount of product on-line by gas chromatograph equipped with a flame ionization detector (GC-FID)

1.3.4.2 Determine the qualitative of product by gas chromatograph-mass spectrometer (GC-MS).

1.4 EXPECTED RESULTS

1.4.1 This thesis would lead to provide basic insights into the surface structures of MoO_3/SiO_2 catalysts shedding light on the influences of preparation method, MoO_3 loading and heat treatment.

1.4.2 This thesis would provide a guide for tailoring the surface properties and structures of active sites for the desired reaction.

This material is reserved for educational use only, not allowed for commercial use.
Forbidden to modify the content, and cite the document when use.

CHAPTER 2

THEORYAND LITERATURE REVIEWS

2.1 TRANSITION METAL OXIDE

Transition metal oxides are technologically important materials that have found many applications. For example, in the chemical industry, these oxides are the functional components in the catalysts used in a large number of processes to convert hydrocarbons to other chemicals. They are also used as electrode materials in electrochemical processes. In the electronics industry, they are used to make conductors in films. The discovered high temperature superconductors are multi component transitional metal oxides. Among these applications, perhaps the use of transition metal oxides as catalysts is the most technologically advanced and economically important. It is also an area in which much progress has been made in recent years in terms of the understanding of the fundamental processes that occur, primarily because advances in instrumentation and experimental techniques have made it possible to study the chemistry of the interface between the transition metal oxide and the fluid phase in greater detail than ever before. In particular, developments in surface science techniques have provided very detailed pictures about the surface structures, chemical compositions, and electronic properties of the surfaces. Some of the chemical processes that make use of transition metal oxides are listed in **Table 2.1**. As can be seen from the table, many of the processes require high selectivity for a particular product, and many involve oxidation of the reactant molecules. In fact, selective oxidation, ammoxidation, and selective dehydrogenation probably constitute the most important catalytic uses of transition metal oxides. The different oxidation states available in these oxides make it possible to control the selectivity in oxidation with the properties of the oxides. Some transition metal oxides can also catalyze selective hydrogenation and are used in some commercial processes. As the demand for specialty chemicals (that is, specific chemicals for spccific processes) increases in the future, demand for high selectivity will increase in a wide variety of reactions including amination, alkylation, aldol condensation, carbonylation and deoxygenation.

This material is reserved for educational use only, not allowed for commercial use.
Forbidden to modify the content, and cite the document when use.

Table 2.1 Examples of Chemical Processes in which Transition Metal Oxides are Catalysts **[21]**

Process	**Examples**
Oxidation	Production of SO_3 from SO_2 and CO oxidation in emission control
Dehydrogenation (nonoxidative)	Production of styrene from ethyl benzene
Dehydrogenation (oxidative)	Production of formaldehyde from methanol and butadiene from butenes
Selective oxidation	Production of acrolein from propene and maleic anhydride from benzene or butane
Selective ammoxidation	Production of acrylonitrile from propene
Selective reduction	Reduction of NO, selective hydrogenation of unsaturated ketones.
Metathesis	Production of long chain alkenes
Water-gas shift	Production of hydrogen

In addition to being used as catalysts, transition metal oxides are also precursors for other important catalysts. The cobalt-molybdenum sulfide catalyst for hydrodesulfurization is an example. This catalyst is prepared by sulfiding cobalt-molybdenum oxide (often supported on alumina). Another example is the chromium-based catalyst for ethylene polymerization. The catalyst can be made from supported chromium oxide as a precursor. Finally, many noble metal catalysts are prepared by reduction of the corresponding oxides. In addition, these metal catalysts are often stored in air and are converted to their oxides during storage. It is quite conceivable that in these cases, the detailed structures, morphologies, or other properties of the transition metal oxide precursors could affect the properties of the final catalysts. Understanding catalysis requires an understanding of surface chemistry, which deals with the bonding and reaction of an adsorbate with the surface and the influence of the surface on the bonding and reaction between adsorbates. It is apparent that an important part of any effort toward obtaining such an understanding is the ability to characterize the physical and chemical properties of a surface. In recent years, much progress has been made in the understanding of metallic surfaces **[22-25]**. Progress has also been made, but at a slower pace, for the transition metal oxides because of the higher level of

This material is reserved for educational use only, not allowed for commercial use.
Forbidden to modify the content, and cite the document when use.

complexity in the experimental techniques involved. There are significant differences between the chemistry of transition metal oxides and the corresponding metals. **Table 2.2** provides a list of properties that are important in the surface chemistry of transition metal oxides. Many of them either do not apply or apply only to a limited extent to the metals. The ionicity of the lattice, which is often less than that predicted by the formal oxidation states, results in the presence of charged adsorbate species, and the common heterolytic dissociative adsorption of molecules (that is, a molecule AB is adsorbed as A^+ and B^-. Surface exposed cations and anions form acidic and basic sites as well as acid-base pair sites. The fact that the cations often have a number of commonly obtainable oxidation states has resulted in the ability of the oxides to undergo oxidation and reduction and the possibility of the presence of rather high densities of cationic and anionic vacancies.

Table 2.2 Properties that are important in the surface chemistry of transition metal oxides **[21]**

Properties of transition metal oxide surface
Presence of cations and anions in stoichiometric ratios and in well-defined spatial (structural) relationships
Possibility of covalent and ionic bonding between cations and anions
Presence of a strong electric field normal to the surface due to the coulombic nature of the ionic lattice
Presence of charged adsorbed species
Presence of surface acidity and basicity
Presence of cationic and anionic vacancies
Ability of cations to undergo oxidation and reduction
High mobility of lattice oxygen and the possibility that the lattice oxygen are reactants in a reaction
Interaction of the solid with incident photons that leads to photo-assisted surface chemical processes

This material is reserved for educational use only, not allowed for commercial use.
Forbidden to modify the content, and cite the document when use.

2.2 MOLYBDENUM (VI) OXIDE

Molybdenum trioxide is chemical compound with the formula MoO_3. This compound is produced on the largest scale of any molybdenum compound. It occurs as the rare mineral molybdite. Its chief application is as an catalyst and as a raw material for the production of molybdenum metal.

Table 2.3 Properties of molybdenum (VI) oxides **[26]**

Properties	
CAS number	1313-27-5
IUPAC Name	Molybdenum oxide
Empirical formula	MoO_3
Molar mass	143.94 g/mol
Appearance	yellow solid
Density	4.69 g/cm^3, solid
Melting point	795 °C
Boiling point	1155 °C
Solubility in water	0.1066 g/100 ml (18 °C) 2.055 g/100 ml (70 °C)
Std enthalpy of formation $\Delta_f H^\circ_{298}$	−745.17 kJ/mol
Standard molar entropy S°_{298}	77.78 J K^{-1} mol^{-1}

2.2.1 α-Molybdenum (VI) oxide

α-MoO_3 is the most stable phase of molybdenum (VI) oxide. It is composed of layers of distorted MoO_6 octahedra in an orthorhombic crystal. The unique layer structure made up of chains of octahedra that share coners. Two such chains are connected by sharing two edges of the octahedra to form a double chain. These double chains are then connected together in the third dimension (perpendicular to the plane of the double chain) by sharing coners to form a sheet-like structure. Thus for each octahedron, three O atoms are shared by three octahedra of the same double chain, two are shared by two octahedra of adjacent double chains, and one is

This material is reserved for educational use only, not allowed for commercial use.
Forbidden to modify the content, and cite the document when use.

unshared. This unshared unit is commonly referred to as a Mo=O unit. Finally, these two dimensional sheets are stacked on top of each other with rather weak interaction between layers

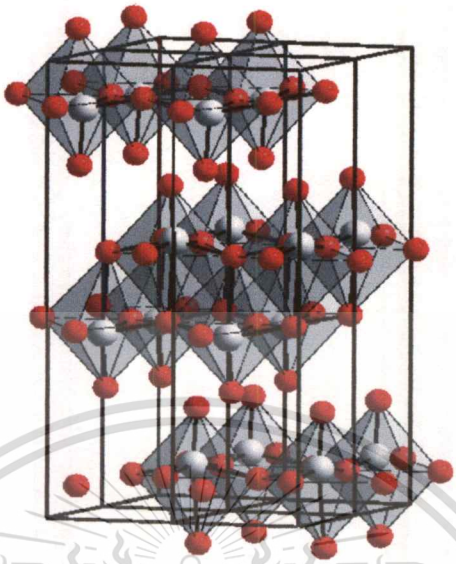

Figure 2.1 Crystal structure of α-MoO_3 [26]

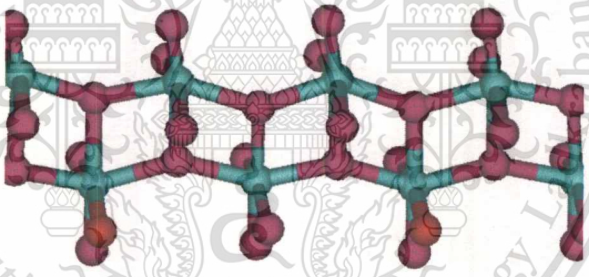

Figure 2.2 α-MoO_3 chains showing edge sharing [26]

α-MoO_3 has the space group of *Pbnm* with cell parameters a = 3.962 Å , b = 13.858 Å and c = 3.697 Å (ICSD-35076). It consists of double layers of linked distorted MoO_6 octahedra parallel to (010) planes. In each double layer MoO_6 octahedra form edge sharing zig-zag rows along the [001] direction and corner sharing rows along the [100] direction. The [100], [010] and [001] projected structures of MoO_3 are shown in **Figure 2.3**. Successive layers are held together by weak Van der Waals forces only, with easy cleavage along (010) planes.

This material is reserved for educational use only, not allowed for commercial use.
Forbidden to modify the content, and cite the document when use.

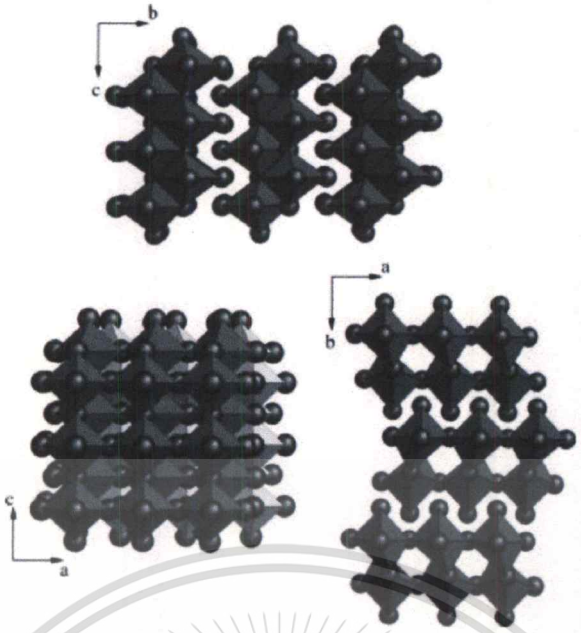

Figure 2.3 The [100], [010] and [001] projected structures of α-MoO_3 **[27]**

2.2.2 Hexagonal molybdenum (VI) oxide

Hexagonal molybdenum (VI) oxide (*P63/m* : $a = b = 10.584$ Å, $c = 3.7278$ Å, $\gamma = 120°$, ICSD-75417) : $Mo_{5.3}O_{14.5}(OH)_{2.8}(H_2O)_{1.36}(MoO_3.0.55H_2O)$ has been prepared by *Guo J.D. et al.*, **[28]** by ion-exchange reaction of $[NaxH_2O]Mo_{5.3}O_{17.3}H_{1.8}$ obtained by hydrothermal synthesis starting from Na_2MoO_4 solution at 150 °C for 3 days.

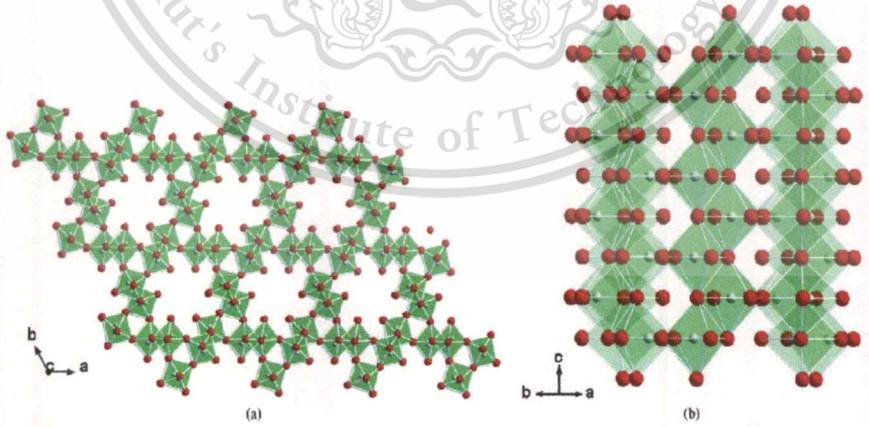

Figure 2.4 Schematic representation of the structure of hexagonal MoO_3 in the *a–b* plane (a) and in *c* direction (b). **[29]**

This material is reserved for educational use only, not allowed for commercial use.
Forbidden to modify the content, and cite the document when use.

2.2.3 Descriptions of the other phases

Triclinic Mo_9O_{26} (ζ -oxide). The ζ–phase has been obtained between 600 °C and 750 °C, and is the in sample of composition close to $MoO_{2.89}$. It is transformed into monoclinic Mo_9O_{26} (β'-oxide) when heated at 760 °C-780 °C (within 2 hours at 780 °C), and is slowly decomposed into MoO_3 and monoclinic Mo_4O_{11} (η-oxide) at 550°C. It forms almost-black, irregular, but rather flaky crystals, readily distinguishable from the other molybdenum (VI) oxides. With the aid of single crystal data, its powder pattern has been indexed and the following triclinic unit cell has been derived by least squares refinement

$$a = 8.145\ \text{Å} \quad b = 11.89\ \text{Å} \quad c = 19.66\ \text{Å} \quad V = 1779.5\ \text{Å}^3$$

$$\alpha = 95.47° \quad \beta = 90.39° \quad \gamma = 109.97°$$

As is the case with all the oxides below MoO_3 the electrical conductivity makes impossible the use of piezo-electrical methods for detection of any non-centrosymmetry. The density was found to be 4.74, which corresponds to 35.7 $MoO_{2.89}$ per unit cell and suggests a cell content of 4 formula units Mo_9O_{26}.

Mo_8O_{23} (β-oxide) and monoclinic Mo_9O_{26} (β'-oxide). These two phases, first described by *Hagg et al.,* **[30]** , have been obtained within the temperature ranges 650°C-780°C for Mo_8O_{23} (by decomposition of $Mo_{17}O_{47}$ even at 630°C; see below) and 750°C-780°C for monoclinic Mo_9O_{26}. Both decompose into MoO_3 and orthorhombic Mo_4O_{11} when heated at 785°C and 800°C. At temperatures below their formation regions they are, however, markedly stable; no change was actually observed after tempering Mo_8O_{23} for three days at 643°C or three weeks at 550°C and monoclinic Mo_9O_{26} three days at 700°C or one week at 648°C.

The structures of the two oxides have been determined by *Magneli* **[31]**. They constitute the first two members of series of structurally interrelated oxides of the general formula Me_nO_{3n-1}**[35]**. By substituting tungsten for part of the molybdenum, higher homologues in this series have been prepared, e.g. $(Mo, W)_{10}O_{29}$ and $(Mo, W)_{12}O_{35}$ **[33]**. The introduction of small proportion of tungsten has furthermore been found to extend the formation range for the β'-phase down to 650 °C **[33]**. The *d*-values of the power patterns of Mo_8O_{23} and monoclinic Mo_9O_{26} are listed in Ref **[36]**, and the unit cell dimensions are give in Table 2 of Ref **[33]**.

It has been pointed out earlier that, in view of it chemical properties, the "β-molybdenum (VI) oxide" of *Glemser et al.,* **[32]** is probably identical with the triclinic Mo_9O_{26} (ζ -oxide), while their "β-oxide" is Mo_8O_{23} monoclinic Mo_9O_{26} or mixture of these twophases. The resistivity measurements made **(Table 2.4)** strongly support this view: the triclinic Mo_9O_{26} is seen to have

This material is reserved for educational use only, not allowed for commercial use.
Forbidden to modify the content, and cite the document when use.

by far the highest resistivity of all the intermediate phases, as has the "β-oxide" according to *Glemser et al.,*.

$Mo_{17}O_{47}$ (x-oxide). In samples heated below about 560°C, a new phase appeared with a composition close to $MoO_{2.78}$. It decomposes into orthorhombic Mo_4O_{11} (γ-oxide) and Mo_8O_{23} (β-oxide) at 630°C, but does not change when kept at 590°C for one week.

Table 2.4 Specific electrical resistivity of molybdenum (VI) oxides (at room temperature).

Phase	**Resistivity (Ohm.cm)**
Mo_9O_{26} triclinic	~ 250
Mo_9O_{26} monoclinic	~ 3.7
Mo_8O_{23}	~ 1.2
$Mo_{17}O_{47}$	< 0.05
Mo_4O_{11} orthorhombic	~ 0.25
Mo_4O_{11} monoclinic	~ 0.2

The x-oxide forms long, flat, extremely thin, black needles and looks dark grey when powdered. Its powder pattern has revealed an orthorhombic unit cell with the dimensions

$$a = 21.61_5 \text{ Å} \quad b = 19.63_2 \text{ Å} \quad c = 3.951_5 \text{ Å}$$

The reflection absences found in the single crystal photographs are in accordance with the space groups No.32, *Pba2* and No.55 *Pbam*. The density was measured to be 4.72, which corresponds to 34.0 $MoO_{2.78}$ units per cell and suggests the formula $Mo_{17}O_{47}$, with 2 formula units per cell. The low electrical resistivity of this phase is noteworthy **(Table 2.4)**

υ-Oxide. A second phase not previously reported has been observed in preparations heated for a relatively short time below 530°C. The composition of this phase, called **υ**–oxide, seems to be in the neighbourhood of $MoO_{2.80}$, but it has not been possible to obtain it in a very pure state. With prolonged heating, it slowly decomposes into $Mo_{17}O_{47}$ (x-oxide) and MoO_3. It seems, therefore, probable that the **υ**–oxide is not stable within the temperature region investigated, but is formed in metastable state.

The unit cell is tetragonal with the dimensions

$$a = 45.99 \text{ Å}, \quad c = 3.937 \text{ Å}.$$

This material is reserved for educational use only, not allowed for commercial use.
Forbidden to modify the content, and cite the document when use.

The reflections hkl with h or k odd are absent for l=0 ; they are revealed in the layer line l=1 as very weak, diffuse spots growing stronger in the higher layer line. This phenomenon evidently indicates the presence of a sub cell of the dimensions

$$a' = 1/2a = 23.00 \text{ Å} \quad c' = c = 3.937 \text{ Å}.$$

The most probable space-group of the large cell is No.129, *P4/nmm*.

As it has not been possible to prepare the oxide in an amount sufficient for density determinations, no proposal of its formula can be given at present.

Orthorhombic Mo_4O_{11} (γ-oxide). The orthorhombic Mo_4O_{11} (γ-oxide) forms between 615°C and 800°C approximately. As was mentioned above, it is often found also in samples heated above this upper limit and furthermore sometimes in preparations treated at about 500°C. In these the monoclinic form, η-oxide (see below), by heating for three weeks at 550°C but remains unchanged after one week at 590°C.

The crystal structure has been determined by *Magnéli et al.*, [33] and the X-ray powder pattern is listed in Ref [36]. The unit cell dimensions are

$$a = 24.49 \text{ Å}, \quad b = 5.457 \text{ Å}, \quad c = 6.752 \text{ Å}, \quad V = 902.3 \text{ Å}^3.$$

Monoclinic Mo_4O_{11} (η-oxide). Below about 615°C another phase of composition $MoO_{2.75}$ is formed. This phase, (η-oxide), has previously been observed. As a product of thermal decomposition of MoO_3 in vacuo at 549°C and 608°C [34]. It is probably identical with the phase designated γ' by Glemser and Lutz which was rarely obtained at 600°C [32]. It remains unchanged after heating for two days at 634°C, but is transformed into the orthorhombic, high-temperature form (γ-oxide) within two weeks at 655°C.

This phase forms wine-red, rather irregular crystals, which are similar to those of the orthorhombic form (γ-oxide). The powder pattern has been evaluated with the aid of single crystal photographs, and the following unit cell has been derived

$$a = 24.54 \text{ Å}, \quad b = 5.439 \text{ Å}, \quad c = 6.701 \text{ Å}, \quad \beta = 94.28° \quad V = 891.8 \text{ Å}^3.$$

The observed density is 4.17, which is in good agreement with the value 4.168 calculated for Mo_4O_{11} with 4 formula units in the unit cell. The space group in probably No. 14, $P2_1/a$. The close similarity of the unit cell dimensions of the two Mo_4O_{11}- modification is striking; the slight monoclinic deformation of the η-oxide is the main difference. In addition there are many common features in the intensity distribution of the diffraction pattern indicating that the structures of the two oxides are probably interrelated. In view of this the sluggishness of the transformation between the two forms is remarkable. By means of differential thermal analysis no polymorphic

This material is reserved for educational use only, not allowed for commercial use.
Forbidden to modify the content, and cite the document when use.

transformation has been observed [37], which is not surprising in the light of the sluggishness of the transformation.

A few experimental have been carried out on the oxidation of molybdenum (VI) oxides in air at elevated temperatures. Finely ground specimens of the various oxides (except the υ–oxide) were heated in a muffle furnace at a few temperature within the region 230°C-350°C.

It was found that MoO_2 and triclinic Mo_9O_{26} (ζ-oxide) were the phases most resistant to oxide (hardly affected by heating for two days at about 270°C), while orthorhombic Mo_4O_{11} (γ-oxide) was the most sensitive phase (completely transformed to MoO_3 within 18 h at about 300°C). The high temperature forms of Mo_4O_{11} and Mo_9O_{26}, in a metastable state at the oxidation temperature, were much more rapidly oxidized than the low-temperature forms.

Indications from the powder photographs of intermediate stages in the course of oxidation were found only in the cases of monoclinic and orthorhombic Mo_4O_{11} heated at about 230°C and 270°C, at which temperatures quite new, somewhat diffuse pattern appeared in the photographs of partially oxidized products. In the samples treated at about 300°C and 350°C, this intermediate stage, here designated λ–oxide, was not observed. When a mixture of λ–oxide and MoO_3 (the mixture obtained by oxidizing orthorhombic Mo_4O_{11} for 13 days at about 230°C) was heated in vacuo at 390°C for 20 h, the lines of the λ–oxide disappeared: the sample consisted of MoO_3 and monoclinic Mo_4O_{11}. It is thus evident that the λ–oxide is unstable, at least at higher temperatures, and that it has a composition lying somewhere within the range $MoO_{2.75} \leq MoO_x < MoO_3$, but is probably not very close to the latter limit.

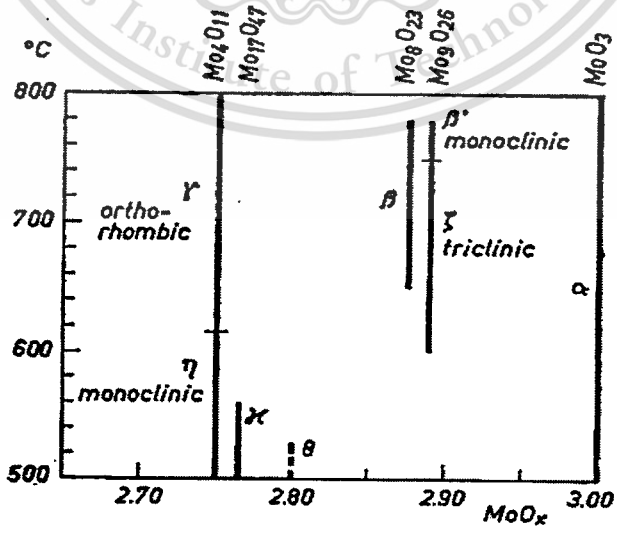

Figure 2.5 Formation, temperature vs composition diagram for molybdenum (VI) oxide

This material is reserved for educational use only, not allowed for commercial use.
Forbidden to modify the content, and cite the document when use.

2.3 SILICA

Silicon dioxide, silica, can be natural or synthetic,crystalline or amorphous. The building block of silica and the silicate structures is the SiO_4 tetrahedron, four oxygen atoms at the corners of a regular tetrahedron with a silicon ion at the centercavity or centroid **(Figure 2.6)**. The oxygen ion is so much larger than the Si^{4+} ion that the four oxygens of a SiO_4 unit are in mutual contact and the silicon ion is said to be in a tetrahedral hole. Natural silicas can be crystalline, as in quartz, cristobalite, tridymite, coesite, and stishovite, or amorphous, as in opal. Crystalline silica polymorphs are divided according to their framework density (SiO_2 groups per 1000 $Å^3$) into pyknosils and porosils, and the latter are further divided into clathrasils and zeosils depending on whether the pores are closed or open, that is, accessible to adsorption.

Familiarity with the structure of crystalline silica is helpful in understanding the bulk and surface structure of amorphous silica. All forms of silica contain the Si-O bond, which is the most stable of all Si-X element bonds. The Si-O bond length is about 0.162 nm, which is considerably smaller than the sum of the covalent radii of silicon and oxygen atoms (0.191 nm). The short bond length largely accounts for the partial ionic character of the single bond and is responsible for the relatively high stability of the siloxane bond. Although in most silicas and silicates the silicon atom is surrounded by four oxygen atoms, forming the tetrahedral unit $[SiO_4]^{4-}$, a sixfold octahedral coordination of the silicon atom has also been observed in stishovite and coesite.

The arrangements of $[SiO_4]^{4-}$ and $[SiO_6]^{8-}$ and the tendency of these units to form a three dimensional framework structure are fundamental to silica crystal chemistry.

This material is reserved for educational use only, not allowed for commercial use.
Forbidden to modify the content, and cite the document when use.

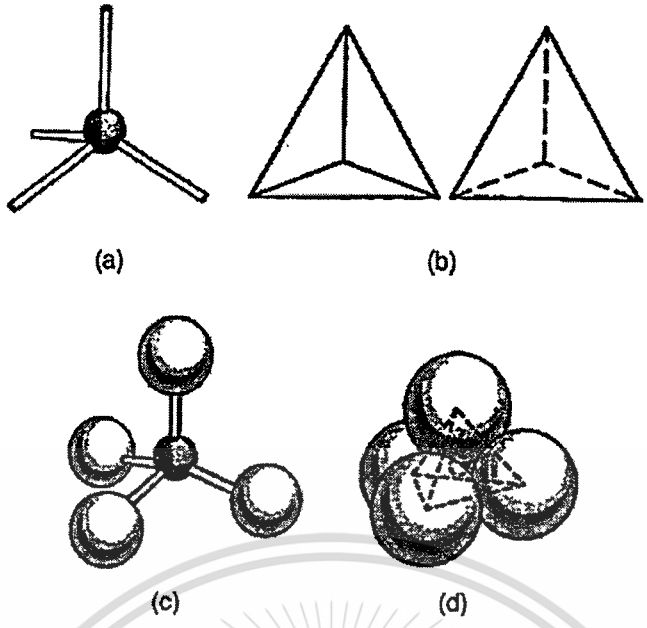

Figure 2.6 Tetrahedral coordination of oxygen ions with silicon: (a) ball and stick model, (b) solid tetrahedron, (c) skeletal tetrahedron, and (d) space-filling model based on packed spheres.

In amorphous silica the bulk structure is determined, as opposed to the crystalline silicas, by a random packing of $[SiO_4]^{4-}$ units, which results in a nonperiodic structure **(Figure 2.6)**. As a result of the structural differences the various silica forms have different densities **(Table 2.5)**. The structure, Si-O bond length, and Si-O-Si bond angle in crystalline and amorphous silicas have been studied by x-ray, electron, and neutron diffraction and by infrared spectroscopy. Three strong absorption bands at 800, 1100, and 1250 cm^{-1} measured by infrared transmission techniques are attributed to fundamental Si-O vibrations and do not differ greatly in the various silica modifications, whereas in the high-frequency region (2800–4000 cm^{-1}) certain distinct differences are observed. **Figure 2.8** is a schematic representation of adjacent SiO_4 tetrahedra that shows the Si-O-Si bond angle. Diffraction measurements have shown a difference between the Si-O-Si bond angle of quartz (142°), cristobalite (150°) and fused quartz (143°).

This material is reserved for educational use only, not allowed for commercial use.
Forbidden to modify the content, and cite the document when use.

สำนักหอสมุดกลาง พระจอมเกล้าลาดกระบัง

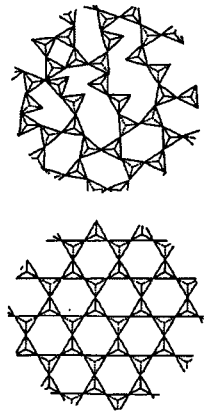

Figure 2.7 Two-dimensional representation of random versus regular packing of $(Si\text{-}O_4)^{4-}$ tetrahedra: amorphous (top) and crystalline silica (down).

Table 2.5 Density (d) of Crystalline and Amorphous Silicas

Silica	Density (g/ml at 273 K)
Coesite	3.01
α - Quartz	2.65
β - Quartz	2.53
β - Tridymite	2.26
β - Cristobalite	2.21
Amorphous silica	2.20

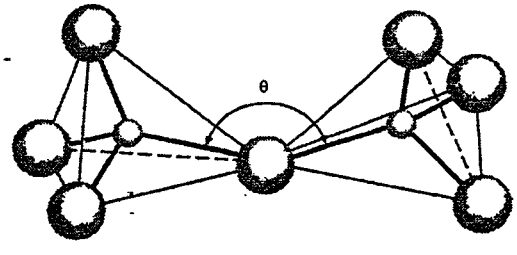

Figure 2.8 Schematic representation of adjacent SiO_4 tetrahedra that shows the Si-O-Si bond angle. Small circle, Si; large circle, O .

This material is reserved for educational use only, not allowed for commercial use.
Forbidden to modify the content, and cite the document when use.
71863

Silicas can be classified into *pyrogenic silicas* (aerosols and cabosils) and *silica gels*. Pyrogenic silicas are usually nonporous (*S*sp is about 200–400 $m^2.g^{-1}$), whereas the best known examples of silica gels – xerogel and aerogels obtained by polymerization of silicic acid – have a surface area above 500 $m^2.\ g^{-1}$ and pore diameters of about 2–10 nm. The fully hydroxylated surface of a silica gel consists of a layer of silanol groups (SiOH) and physically adsorbed water. Most of the water is removed upon drying in air at 400–500 K. In the spectra of silica-containing systems several absorption bands are observed in the region 3800–3400 cm^{-1}. Silanol groups are left on the surface and exist in three different configurations:

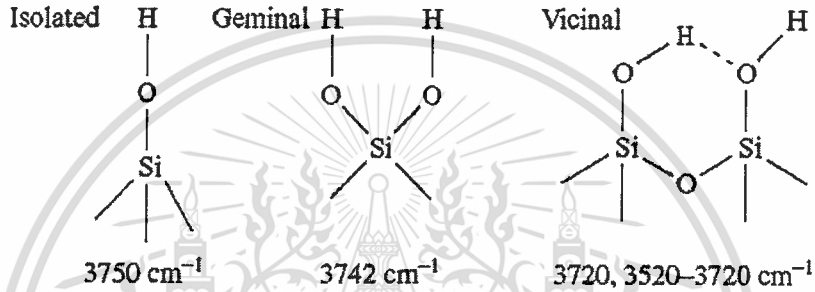

Figure 2.9 Three different configurations of silanol groups.

Isolated and vicinal groups may be hydrogen bonded to each other. The combination (νOH + δOH) band due to surface silanol lies at about 4550 cm^{-1} and allows distinction between OH species and molecular water. The combination band ($\nu_2 + \nu_3$) for the latter has been observed between 5100 and 5300 cm^{-1} (depending on the degree of hydration). The first overtone (ν_{02}) ofthe ν_{OH} mode at 3750 cm^{-1} (ν_{01}) was found at 7285 cm^{-1}. Silanol groups are progressively lost with increasing temperature with the formation of new surface siloxane groups:

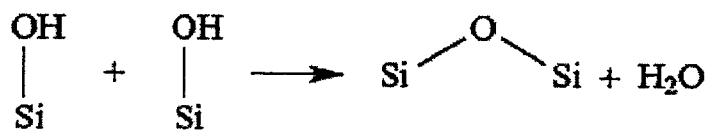

Figure 2.10 Formation of surface siloxane groups

This material is reserved for educational use only, not allowed for commercial use.
Forbidden to modify the content, and cite the document when use.

These newly formed siloxane bond are very reactive since dehydration leaves the surface in a strained condition. At temperatures greater than 973 K, complete removal of the silanol groups is observed, hence resulting in a significant change in surface morphology. In the case of nonporous SiO_2, for example, the following bands occur: 3747, 3725, 3700 cm^{-1}, with a very broad separate absorption at 3600–3200 cm^{-1}. Bands in the region 3800–3650 cm^{-1} correspond to stretching modes of OH groups which are not involved in (i.e. free of) hydrogen bonding. These groups include isolated OH (either external and internal to the lattice) and terminal hydroxyls of hydrogen-bonded sequences (either internal and external), whereas the bands in the 3650–3200 cm^{-1} region characterize the stretching modes of hydrogen-bonded OH groups (internal and external). Based on a computer graphic simulation and high-resolution microscopy results indicating that the exposed faces are regular and flat, the below interpretation has been suggested. Preferred exposures of the (010), (100), (001) and (101) faces on the nonporous SiO_2 cause the presence of the following types of SiOH groups.

On the (100) faces, the silanols are isolated, with an OH density of 3.1 OH/nm^2 and a minimum OH–OH distance of 0.36 nm, while on the 001 faces the hydroxyl density is about 5 OH/nm^2 and the minimum OH–OH distance is 0.25 nm. On the (101) faces, the situation is similar to that found on the [001] faces: the OH density is 3.8 OH/nm^2, and the minimum OH–OH distance is 0.25 nm. In all these cases silanols are isolated. On the (001) face, the structures are simultaneously present. The minimal OH.....OH distances are 0.25 nm (second structure), i.e. sufficiently low to ensure hydrogen bonding. The bending vibrations are also used to characterize the surface hydroxyls. Thus, the IR spectra of free silanol groups (3745 cm^{-1}) show combination bands with the in-plane δOH and out-of plane (or rotational) γOH vibrations. In the spectra taken at low temperature the OH band is split into two maxima at 840 and 765 cm^{-1} because of interactions with different ν Si–O stretching vibrations on different sites. Such a large difference between the frequencies of the two bending modes is typical of the type I hydroxyls.

This material is reserved for educational use only, not allowed for commercial use.
Forbidden to modify the content, and cite the document when use.

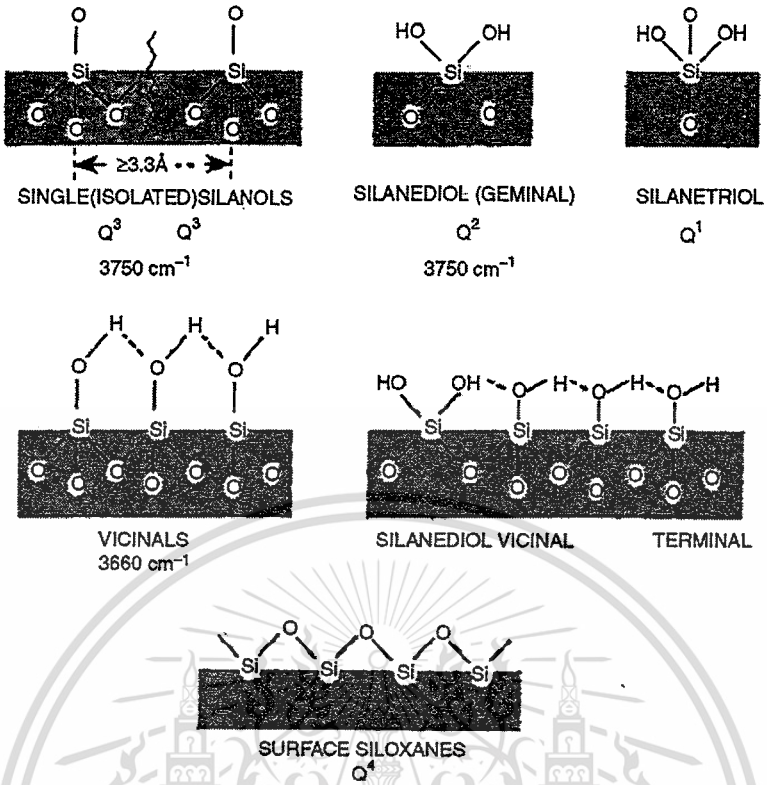

Figure 2.11 Silanol groups and siloxane bridges on the surface of colloidal silicas. Characteristic infrared bands at 3750 and 3660 cm^{-1} are shown for single and vicinal groups. Qn terminology is used in NMR; n indicates the number of bridging oxygens (-O-Si) bonded to the central silicon (n = 0–4).

Comprehensive studies by means of various physical and chemical methods showed that the pyrogenic silica surface is built up of regions with the structure of the (111) face and, to a lesser extent, the (100) face, of χ-crystobalite with silanol and silane diol end-groups, separated by a distance of 0.7 nm. The bulk phase of such SiO_2 samples consists of approximately equal amounts of the quartz and crystobalite structures. Results of the dehydration, dehydroxylation and rehydroxylation for amorphous silica surfaces have been examined. The number of silanol groups on silica gel has been estimated by using a variety of techniques.

The concentration of silanol groups on silica gel treated at 1073 K was measured as ca. 3 $\mu mol/m^2$. A model of the surface based on the examination of the crystal chemical structure of SiO_2 has been proposed by Chukin and Apretova. The IR spectra of dispersed silicas during the processes of desorption and adsorption of water and other molecules have been investigated. The interpretation of the absorption bands of dispersed silicas is based on a crystal chemical

This material is reserved for educational use only, not allowed for commercial use.
Forbidden to modify the content, and cite the document when use.

model of dispersed SiO_2. In this, primary globules of SiO_2 are spherical particles covered by SiO_2 chains of different lengths (peripheral structures). The spatial macrostructure of SiO_2 is produced by theinteraction between the peripheral structures of adjacent Si–O nuclei (see **Figure 2.12**). In recent years, some progress in the understanding of surface processes has been achieved by computer experiments which have revealed some characteristics of the systems investigated which were not available from direct experimental measurements. For example, in the case of SiO_2 computation of the atoms on isolated silica surface OH groups revealed that the splitting of the bending vibration is characteristic of two coupled oscillators of geminal silanol groups. All of the above models have analyzed the properties of OH groups characterized by the band at 3750 cm^{-1} and assigned this band to the OH^- ion, by comparison with the spectroscopic criteria for other OH^- containing species such as acidic OH groups, OH^- ions, HOH molecules and H_3O^+. In order to establish the structural chemistry features of the silica gel structure, spectra in the region of the skeleton Si–O vibrations have been investigated. A comparison of the silica gel spectrum with those of silicates which display such skeleton vibrations has shown that it is similar to the spectra of quartz and crystobalite, except that the band at ca. 1200 cm^{-1} in the spectrum of silica gel is characteristic of silicates with 'belt structures' (ksonotolite). On this basis, it was suggested that the silica gel structure consists of at least two irregularly interchanging regions: (i) crystallites which are close to the structure of crystobalite (three-dimensional polymeric skeleton), and (ii) a range between disordered crystals with silicon–oxygen two-dimensional layers and belts of the ksonotolite type. According to Chukin and Apretova, two types of hydroxyls, namely basic and acidic, correspond to these two types of structures; the OH^- ion (at 3750 cm^{-1}) can be assigned to the skeleton structure, and the weakly acidic OH group (at ca. 3630 cm^{-1}) to the belt structure. Because the 3720 and 3520 cm^{-1} bands have been interpreted as vibrations of the H^- ion and a weakly acidic Si–O–H group, respectively perturbed by the mutual hydrogen bond, it has been suggested that the two components of the silica gel structure are interrelated. One of the possible variants of a two-component structure of amorphous silica, together with the possible interpretations of the absorption bands, is depicted in **Figure 2.12**. A molecular dynamics computer simulation was carried out to investigate the spectral features of the geminal hydroxyl groups on a silica surface. The density of proton vibrational states and the IR stretching vibrations were calculated . Four intense peaks at 196, 600, 800 and 3736 cm^{-1} in the spectra obtained are ascribed to the 'out-of-plane-like' modes (196 cm^{-1}), the in-plane bending modes (600 and 800 cm^{-1}) and the stretching vibration (3736 cm^{-1}) of the general pair of OH groups. The in-plane

This material is reserved for educational use only, not allowed for commercial use.
Forbidden to modify the content, and cite the document when use.

spectral bending vibrations reveal a strong temperature dependence, unlike the bands of other vibrations.

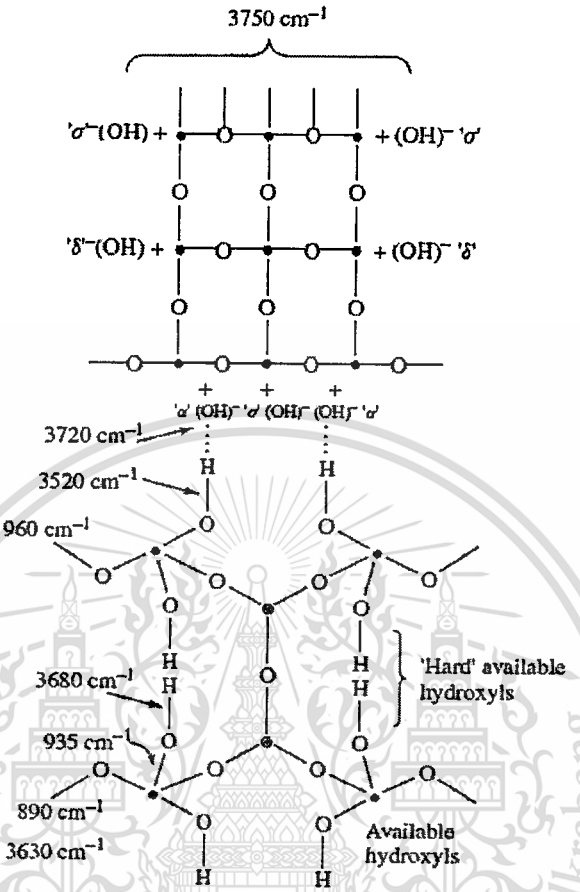

Figure 2.12 Model of the structure of dispersed silica according to Chukin and Apretova: O, oxygen atom; •, silicon atom

This material is reserved for educational use only, not allowed for commercial use.
Forbidden to modify the content, and cite the document when use.

2.4 SUPPORTED METAL OXIDE STRUCTURES

The nature of the supported metal oxide (SMO) species depends upon a number of factors: the preparation method (wet chemical synthesis plus calcination), chemical interactions between the support and surface layers, and surface density (surface oxide weight loading and specific surface area of the support oxide). **Figure 2.13** schematically demonstrates the various dehydrated surface structures commonly observed for a mono-oxo metal oxide: isolated, oligomeric, polymeric, and crystalline species. Several reviews comprehensively catalog the expected surface structures for transition metal mono- and polyoxoanions in four-, five-, and sixfold coordination under nonreaction conditions. Except at the extreme of the surface density scale, a distribution of structures is expected at any given surface density. In addition, transition from isolated to polymerized to crystalline species with increasing surface oxide content does not progress stepwise but rather through a continuum; except for the onset of crystallinity, there are no sharp surface density delineations between the various species. Still, the different surface species have been rigorously identified as active sites (or precursor to the active sites) for a number of reactions for some SMO catalyst compositions.

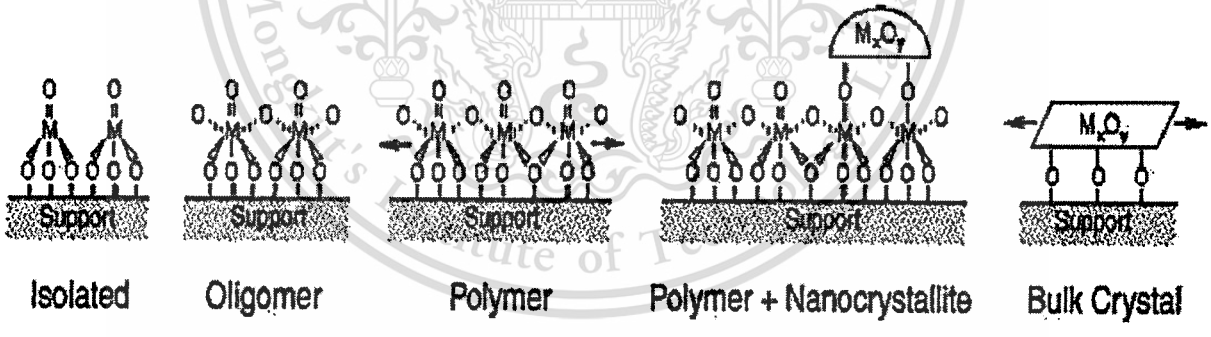

Figure 2.13 Schematic of surface structures of a generic mono-oxo metal oxide active phase on a metal oxide support. The active phase forms tetragonal structures at low loading (MO_4 coordination), distorted octahedral corner- and edge-sharing structures at intermediate loading (MO_6 coordination), and stoichiometric crystalline structures at high loading (M_xO_y).

This material is reserved for educational use only, not allowed for commercial use.
Forbidden to modify the content, and cite the document when use.

2.4.1 Isolated Species

The first structure in **Figure 2.13** is that of isolated species in tetrahedral coordination (MO_4), which are typically present at very low concentrations of surface oxide. Isolated species possess only M=O and, presumably, M-O-S bonds, where M represents the metal center of surface oxide, O an oxygen, and S the metal center of the support oxide. It is often difficult to obtain direct spectroscopic evidence of M-O-S bonds **[38]**, yet their existence is consistent with coordination models of surface oxides and infrared (IR) spectroscopy of support hydroxyl titrations **[38–41]**. Absent are M-O-M bridges, which appear in oligomeric and polymerized surface species. Only a few examples exist in the literature that positively identify isolated species as the key to catalytic activity, two of which are TiO_x/SiO_2 **[42]** and ZrO_x/SiO_2 **[43]** for methanol oxidation (x indicates the surface oxide exists in noncrystalline form). In these cases, the highest turnover frequencies (TOFs) for methanol consumption were observed at the lowest tested concentrations of supported titanate and zirconate, where isolated TiO_4 and ZrO_4 structures were shown to dominate. It was concluded that the number of Ti-O-Si and Zr-O-Si bonds were maximized in monomeric Ti and Zr sites, respectively. Significant TOF decreases concomitant with increasing surface oxide polymerization were rationalized to occur because the number of M-O-S bonds per active M site was reduced

2.4.2 Oligomeric and Polymerized Species

In addition to the M=O and M-O-S bonds also present in isolated species, increases in surface oxide concentration leads to condensation of surface oxoanions and the formation of bridging M-O-M bonds characteristic of oligomeric and polymeric species. **Figure 2.13** shows this for polyoxoanions in octahedral coordination (MO_6) possessing a combination of corner- and edge-sharing octahedra. Analogous to organic polymer nomenclature, oligomers (e.g., dimers, trimers) are generally considered to be of low molecular weight and incorporate only a limited number of active metal centers; polymers consist of larger domains that are often described as two- dimensional surface layers **[44,45]**. Rarely is a distinction between oligomers and polymers drawn, and usually only in relation to reference crystalline materials through fundamental spectroscopic investigations **[46,47]**. The formation of polymeric species is sensitive to the support composition. For example, due to unfavorable surface energy interactions, few oxides are known to form oligomeric/polymeric species supported on SiO_2 **[44, 45]**. A survey of

This material is reserved for educational use only, not allowed for commercial use.
Forbidden to modify the content, and cite the document when use.

catalysis literature reveals that for the majority of transition metal oxide catalyzed reactions, maximum TOFs most frequently correlate with maxima in polymeric surface species content. A limited subset of examples includes WO_x/ZrO_2 for *o*-xylene isomerization **[48]**, *n*-pentane isomerization **[41]** and 2-butanol dehydration **[49]**, MoO_x/Al_2O_3 and VO_x/Al_2O_5 for dimethyl ether oxidation **[50]** , MoO_x/Al_2O_3 for propane oxidative dehydrogenation [36] and MoO_x supported on TiO_2, ZrO_2, Al_2O_3, and Nb_2O_5 for methanol oxidation **[51]**.

2.4.3 Crystalline Species

Under the appropriate conditions (i.e., above monolayer coverage), well-dispersed amorphous surface oxides will nucleate into nanocrystalline primary particles and grow into microcrystallites **[52]**. Minimization of surface free energy is the driving force for the genesis and evolution of crystallite formation (i.e., sintering) for metal oxides. Two common conditions that lead to crystallite growth are (1) super saturation of the support oxide's capacity to stabilize on crystalline active oxide (i.e., above monolayer coverage) **[44, 52, 53]** and (2) unfavorable solid-solid chemical interactions between the surface and support oxides, such as strong electrostatic repulsion in the case of SiO_2 and typical transition metal oxide precursors **[44]**. These crystalline metal oxide species are characterized by well-defined unit cells exhibiting long-range order **[54]** amenable to x-ray diffraction investigation **[55, 56]**. These species have been referred to as nanocrystallites, microcrystallites, or bulk crystallites, terms that are often used interchangeably in supported metal oxide catalysis literature. To be precise, no official size delineation has been found for bulk crystallites, although presumably *nano* refers to < 100 nm and *micro* > 100 nm as per convention. The oxidative dehydrogenation (ODH) of isobutane to isobutene provides an interesting example where bulk crystalline Cr_2O_3 was demonstrated more active than supported CrO_x/Al_2O_3 catalysts, both with and without nanocrystallites of Cr_2O_3 **[57, 58]**. The supported materials were found less active but more selective than Cr_2O_3 due to slower dissociative O_2 adsorption and electron transfer from O_2 to O^{2-} (i.e., reoxidation), consistent with common partial oxidation behavior that higher product selectivity is obtained for higher oxygen bond energy **[59, 60]**. The higher activity of the bulk crystal was assigned to relatively more labile oxygen than that of the supported materials frustrated by Cr-O-Al bonds. Oxygen mobility was higher for Cr_2O_3 than CrO_x/Al_2O_3 due to (1) lower Cr-O bond energy as shown by ~4 times lower activation energy (E_a) for oxygen chemisorption over 250–375°C, (2) roughly twice the oxygen

This material is reserved for educational use only, not allowed for commercial use.
Forbidden to modify the content, and cite the document when use.

content removal, and (3) peak temperatures (T_p) of oxygen temperature programmed desorption (TPD) and hydrogen TPR lowered by ~40°C.

2.4.4 Molybdenum-Sillica Structure

The chemical reactions in the Mo/SiO_2 system caused by the deposition of the active component are confined (at least, at low molybdenum concentrations) to the surface, and bulk phases are not formed (there are no reports of the formation of silicon molybdates or of solid solutions). The MoO_3 phase is usually observed only for high surface concentrations of molybdenum. The state of the molybdenum ions in the system was studied by various methods (mainly by optical, and ESR spectroscopies). Most of these studies were aimed at the local surroundings of the molybdenum ions (mainly because of the nature of the chosen methods). The most important and complex problem seems to be to establish the relationship between the coordination state of the ion and the type of chemical compound formed on the carrier. XRD is the method traditionally used to solve this problem. However, as in the case of the Mo/SiO_2 system, it is applicable only at high concentrations of molybdenum, and therefore vibrational spectroscopy plays an important role in analysis of the structures of the molybdenum compounds formed on the surfaces of SiO_2. The coordination state of molybdenum at low concentrations was studied by ESR and UV spectroscopies. The formation of both tetrahedrally and octahedrally coordinated molybdenum ions was observed. The coordination state of molybdenum was identified from the ESR spectra of Mo^{5+} (used as a paramagnetic probe) on the basis of correspondence (well established in coordination chemistry) between the structure of the complex and the parameters of the ESR spectra. The ESR results agree well with those of diffuse reflectance spectroscopy. At low molybdenum concentrations, tetrahedral molybdenum ions are found on the SiO_2 surface irrespective of the method of preparing the catalyst. At higher concentrations, octahedral molybdenum ions are usually formed, as well as tetrahedral ions. However, there are also reports of molybdenum ions in the two coordination states in a 1:1 ratio at low enough surface concentration of molybdenum (0.1 Mo atom per nm^2). Whereas the tetrahedrally coordinated molybdenum ions are present as isolated ions in structures of the dimolybdate and MoO_3 type, the nature of the compounds in which the molybdenum is octahedrally coordinated is still problematic. *Castellan et al.* studied the Si–Mo system over a wide range of molybdenum concentrations by using a combination of physico-chemical methods: XRD, optical spectroscopy, electron microscopy, acidometric titration, etc. From the results

This material is reserved for educational use only, not allowed for commercial use.
Forbidden to modify the content, and cite the document when use.

obtained they constructed the phase diagram of molybdenum as a function of the molybdenum content of the catalyst **(Figure 2.14)**. This work led to the suggestion that molybdenum is present on the catalyst surface as isopoly and/or heteropoly acids, i.e. that it has a distorted octahedral coordination.

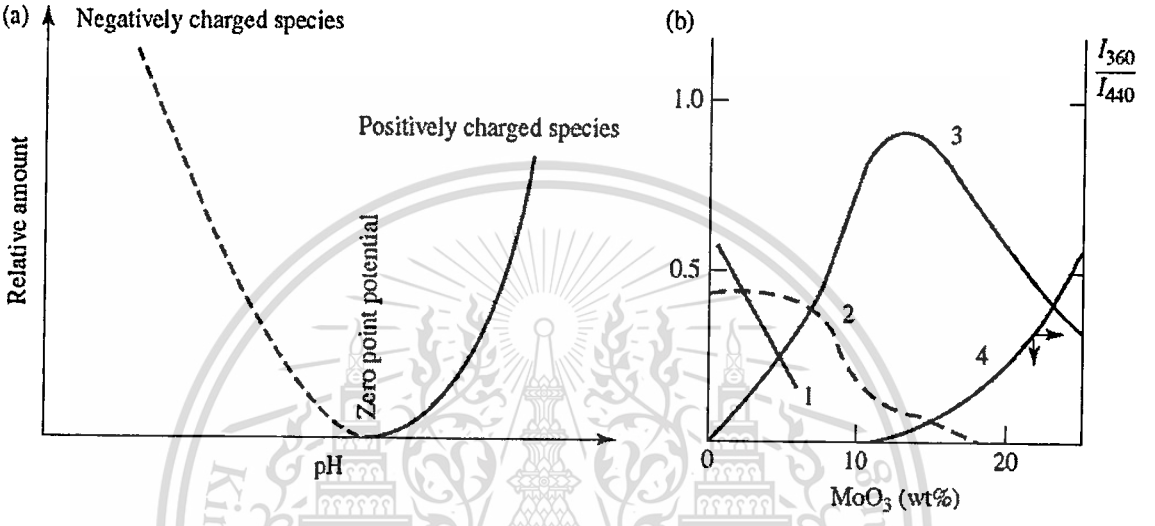

Figure 2.14 (a) Adsorption capacity of ionic species formed on a support as a function of pH (b) Distribution of the products in MoO_3/SiO_2 as a function of composition, established by titrations of (1) dimolybdate (DM), (2) molybdosilicic acid (MSA), (3) polymolybdate (PM), and (4) MoO_3. The proportions of MoO_3 (in relative units) was determined from the intensity ratios of the IR bands at 360 and 440 characteristic for MoO_3 and all molibdates, correspondingly.

Mo–Si oxide systems containing between 1 and 20 wt% of Mo have been studied **[61]** by ESR and IR spectroscopies. The results were used to correlate the octahedral coordination of molybdenum with the formation of heteropoly compounds at high molybdenum contents. By comparing the results of the ESR studies of the state of the molybdenum as function of the formation temperature of the sample it was concluded that identical changes in the state of the molybdenum take place in the supported Si–Mo–HPA **(Figure 2.15)** and in the molybdenum (VI) oxide catalyst synthesized in the SiO_2 surface (the anisotropic signal denotes stabilization of the molybdenum in a distorted octahedral coordination of C4v symmetry).

This material is reserved for educational use only, not allowed for commercial use.
Forbidden to modify the content, and cite the document when use.

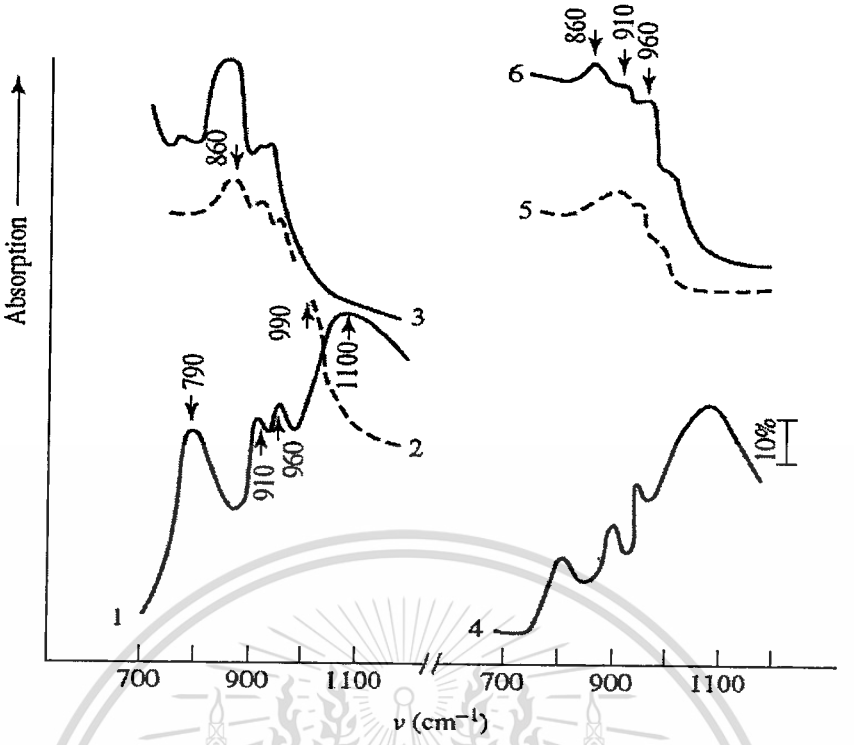

Figure 2.15 IR spectra of original HPA/SiO_2: (1) ordinary; (2) dehydrated at 673 K. IR spectra of: (3) ammonia paramolybdate; a Si–Mo catalyst, dried at (4) 383 K and dehydrated at (5) 673, 773 K and (6) 873 K. Spectra 2, 5, and 6 were obtained after subtraction of the spectra of SiO_2.

This material is reserved for educational use only, not allowed for commercial use.
Forbidden to modify the content, and cite the document when use.

2.5 SOL-GEL SYNTHESIS

The sol–gel process for preparing silica and silicates from metal alkoxide precursors is reviewed and compared to the processing of aqueous silicates. Sol–gel processing combines control of composition and microstructure at the molecular level with the ability to shape material in bulk, powder, fiber, and thin-film form. In sol–gel processing of metal alkoxides, hydrolysis reactions replace an alkoxide group with a hydroxyl group. Subsequent condensation reactions involving the hydroxyl groups produce siloxane bonds. The structure of the evolving silicates is a consequence of the successive polymerization, gelation, aging, drying, and heating steps. Often the structures of polymers, gels, and dried gels (either xerogels or aerogels) may be characterized on the 1–20-nm length scale by a mass or surface fractal dimension. On longer length scales, dried gels are micro- or mesoporous, with surface areas often exceeding 800 m^2/g. During heating, these gels undergo continued polymerization, structural relaxation, and viscous sintering; dense amorphous silica essentially indistinguishable from its conventionally prepared counterpart ultimately results.

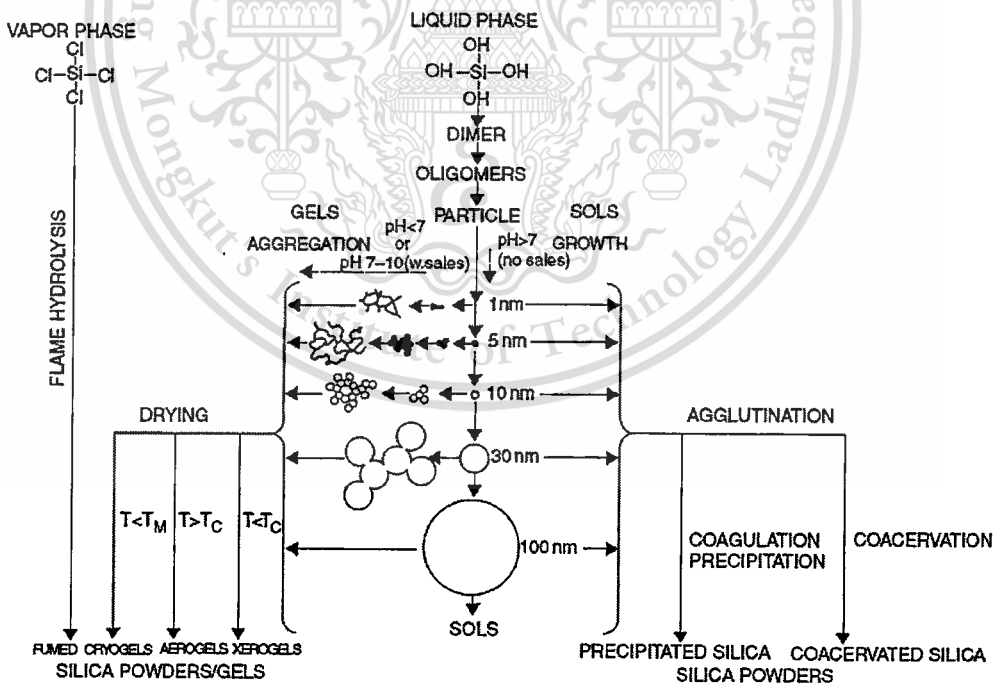

Figure 2.16 Formation of silica sols, gels, and powders by silica monomer condensation - polymerization followed by aggregation or agglutination and drying

This material is reserved for educational use only, not allowed for commercial use.
Forbidden to modify the content, and cite the document when use.

2.5.1 Fundamentals of Sol-gel process

A *sol* is a colloidal suspension of solid particles in a liquid. A *colloid* is a suspension in which the dispersed phase is so small (~1 nm - 1μm) that gravitational forces are negligible and interactions are dominated by short-range effects, such as van der Waals attraction and electrostatic forces resulting from surface charges. A *gel* can be interpreted to consist of continuous solid and liquid phases of colloidal dimensions. Continuity means that one could travel through the solid phase from one side of the sample to the other without having to enter the liquid; conversely, one could make the same trip entirely within the liquid phase. Since both phases are of colloidal dimension, a line segment originating in a pore and running perpendicularly into the nearest solid surface must re-emerge in another pore less than 1 μm away. Similarly, a segment originating within the solid phase and passing perpendicularly through the pore wall must re-enter the solid phase within a distance of 1 μm. Hence, in principle, *sol-gel* designates a process in which a gel is formed from the particles of a sol when attractive forces cause them to stick together in such a way as to form a network. In other words, sol-gel process should imply the formation of a gel by aggregation of particles in a sol. However, the term *sol-gel* is often used in literature to designate a process that leads to a gel (or sometimes merely to a slurry) from a homogeneous solution of soluble monomer precursors whatever the underlying physico-chemical mechanisms. Indeed, mechanisms other than aggregation have been suggested in various cases. For example, if a monomer can make more than two bonds, then there is no limit on the size of the molecule that can fill the space. If one molecule reaches macroscopic dimensions so that it extends throughout the solution, the substance is said to be a gel. Another example concerns the mechanism based on the separation of the initial homogeneous solution into two immiscible continuous and interconnected liquid phases, reminiscent of the structure of a gel, and called *spinodal phase separation*. The present review focuses on gels, as supported metallic catalyst precursors or catalyst support precursors, obtained from a homogeneous solution of monomer precursors. Gels obtained from the destabilization of a stable colloidal suspension, while representing an important class of sol-gel materials, are not presented here. Depending on whether the liquid in the wet gel is removed by evaporative drying or by supercritical drying, that is in pressure and temperature conditions beyond the critical point of the liquid, the resulting dry material is named *xerogel* or *aerogel* respectively. A third class of materials are *cryogels* dried by freeze-drying or lyophilization **[62]**.

This material is reserved for educational use only, not allowed for commercial use.
Forbidden to modify the content, and cite the document when use.

2.5.2 Hydrolysis and condensation of metal alkoxides

In theory, almost all metal oxides can be synthesized by sol-gel process. Among others, an abundant literature can be found on SiO_2, Al_2O_3, TiO_2, ZrO_2 as well as on the corresponding mixed oxides. Thus all porous oxide materials used in heterogeneous catalysis as catalyst support or precursors of catalyst supports can be prepared by sol-gel process. In the field of inorganic gels, the present review will focus mainly on silica gels. Probably the best starting materials for sol-gel preparations of metal oxides are the class of metalorganic compounds known as metal alkoxides **[63]**, which are focused on in the present paper. All metals form alkoxides which have the following general formula: $M(OR)_x$ where M is a metal (Si, Zr, Al, Ti, ...), R is an alkyl group (most often $-CH_3$, $-C_2H_5$, $-C_3H_7$ or $-C_4H_9$), and x is the valence state of the metal (for example, x = 4 with Si, Zr and Ti, and x = 3 with Al). Metal alkoxides, which are soluble in alcohol, are popular precursors because they are rapidly hydrolyzed to the corresponding hydroxide, except the most thoroughly studied among them, silicon tetraethoxide (or tetraethoxysilane, or tetraethyl orthosilicate, TEOS), $Si(OC_2H_5)_4$, which requires an acid or basic catalyst for hydrolysis. The reaction is called *hydrolysis*, because a hydroxyl ion becomes attached to the metal atom, as in the following reaction:

$$M(OR)_x + H_2O \longleftrightarrow HO\text{-}M(OR)_{x-1} + ROH$$

where, again, R is an alkyl group and therefore ROH is an alcohol. Depending on the amount of water and catalyst present, hydrolysis may go to completion, so that all of the OR groups are replaced by OH,

$$M(OR)_x + x\,H_2O \longleftrightarrow M(OH)_x + x\,ROH$$

or stop while the metal is only partially hydrolyzed, $M(OR)_{x-n}(OH)_n$. It can be mention that inorganic precursors as chlorides or nitrates can also be hydrolyzed. Two partially or completely hydrolyzed molecules can link together in a *condensation* reaction, such as

$$(OR)_{x-1}M\text{-}OH + HO\text{-}M(OR)_{x-1} \longleftrightarrow (OR)_{x-1}M\text{-}O\text{-}M(OR)_{x-1} + H_2O$$

or

$$(OR)_{x-1}M\text{-}OR + HO\text{-}M(OR)_{x-1} \longleftrightarrow (OR)_{x-1}M\text{-}O\text{-}M(OR)_{x-1} + ROH$$

This material is reserved for educational use only, not allowed for commercial use.
Forbidden to modify the content, and cite the document when use.

By definition, condensation liberates a small molecule, such as water or alcohol. This type of reaction can continue to build larger and larger silicon or aluminum or titanium or zirconium or containing molecules by a polymerization process in alcoholic medium. To summarize, the basic chemistry associated with formation of a typical sol-gel material such as silica gel is given in very simplified form in **Figure 2.17 [64]**.

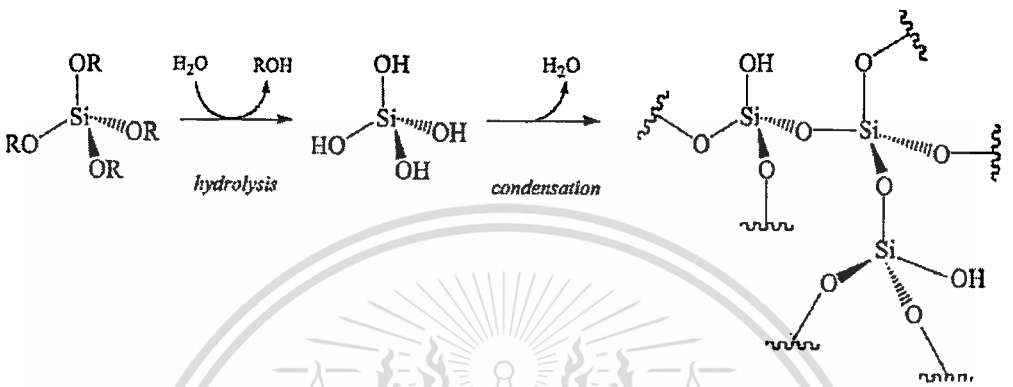

Figure 2.17 Basic steps of a typical sol-gel process from a metal alkoxide. Hydrolysis of alkylorthosilicates affords silicon hydroxides that undergo condensation reactions to form a silicate network

In the case of silicon alkoxides, hydrolysis occurs by the nucleophilic attack of the oxygen contained in water on the silicon atom and is most rapid and complete when acid (e.g. HCl, CH_3COOH, HF, ...) or basic (e.g. NH_3, KOH, amines, ...) catalysts are employed. Under acidic conditions, it is likely that an alkoxide group is protonated in a rapid first step. Electron density is withdrawn from silicon, making it more electrophilic and thus more susceptible to be attacked by water. Under basic conditions it is likely that water dissociates to produce nucleophilic hydroxyl anions in a rapid first step. The hydroxyl anion then attacks the silicon atom. Polymerization to form siloxane bonds occurs by either a water-producing condensation reaction or an alcohol-producing condensation reaction (see both condensation equations above). Depending on conditions, a complete spectrum of structures ranging from molecular networks to colloidal particles may result. Although the condensation of silanols can proceed thermally without involving catalysts, the use of acid or basic catalysts, similar to those used for hydrolysis, is often helpful and various mechanisms have been suggested to explain the role of the catalyst. An important advantage of sol-gel chemistry over conventional oxide preparation techniques is the possibility it offers to prepare mixed oxides, such as SiO_2-ZrO_2, SiO_2-Al_2O_3, SiO_2-TiO_2, ..., with

This material is reserved for educational use only, not allowed for commercial use.
Forbidden to modify the content, and cite the document when use.

an excellent control of mixing because of its ability to adjust the relative precursor reactivity. Mixed oxides are interesting catalysts or catalyst supports because they often display acid strengths that are significantly higher than either of the component oxides. In a mixed oxide MO_x-$M'O_y$, the acidic properties are related to the homogeneous mixing of the two component oxides in terms of the number of available M-O-M' linkages. The key condition to obtain molecularly homogeneous mixed oxides is to adjust the relative reactivity of the precursors in such a way that they have similar rates of hydrolysis and/or condensation. The matching of precursor reactivity can be accomplished using various strategies including the use of a precursor containing a different alkoxy group **[65]**, the prehydrolysis of a less reactive precursor, the slowing down of a more reactive precursor by replacing some of its alkoxy groups with different ligands or by stabilizing it by using an appropriate solvent, and the modification of synthesis temperature **[65]**. In a recent paper, *Rupp et al.,* **[66]** prepared SiO_2-TiO_2 mixed oxides with low titania crystallization tendency by using single-source precursors containing both -$Si(OR)_3$ and -$Ti(OR)_x$ (x = 2 or 3) moieties linked by an organic group. From the hydrolysis and condensation reactions presented above as starting point, various theories corresponding to various physico-chemical mechanisms have been suggested to explain the formation of the wet gel. According to several authors who investigated how inorganic polymer systems, such as SiO_2, TiO_2 and ZrO_2 are formed, the materials are obtained *via* the formation of elementary building blocks that, in a secondary stage, aggregate until the resulting clusters fill the space. This is the *aggregation* theory. According to that theory, the large variety in structures results from differences in the details of the building blocks and in their aggregation mechanism, which are governed by the nature of the precursor and by the synthesis conditions **[67]**. It must be noted that the building block notion is sometimes confusing in literature since it designates now a monomer molecule, now a silica, alumina, titania, ... article of about several tens nanometer, that is a large macromolecule. However, the aggregation mechanism implies most often first the formation of inorganic particles by polycondensation followed by their aggregation. On the other hand, in some cases, a *phase separation* mechanism, which is often proposed to explain the formation of organic gels (see Section 8.2.1.2. below), agrees better with experimental results. If the initial homogeneous solution is separated into two immiscible continuous and interconnected liquid phases, the phase separation is named *spinodal phase separation* or *spinodal decomposition*. The two phases are an oligomer-rich or polymer-rich phase which, after polycondensation, will constitute the porous inorganic skeleton of the gel, and a solvent-rich phase. Let us mention that

Forbidden to modify the content, and cite the document when use.

both clusters formation followed by aggregation and phase separation mechanisms can take place simultaneously and competitively [100].

2.5.3 Gelation and Aging

The gel point is defined as the time when an infinite, spanning polymer or aggregate first appears. For aqueous systems, It can be observed the formation of three dimensional gel networks below pH 7 or 7–10 with salts present **(Figure 2.18)** and attributed gelation to what is now known as ballistic cluster–cluster aggregation.

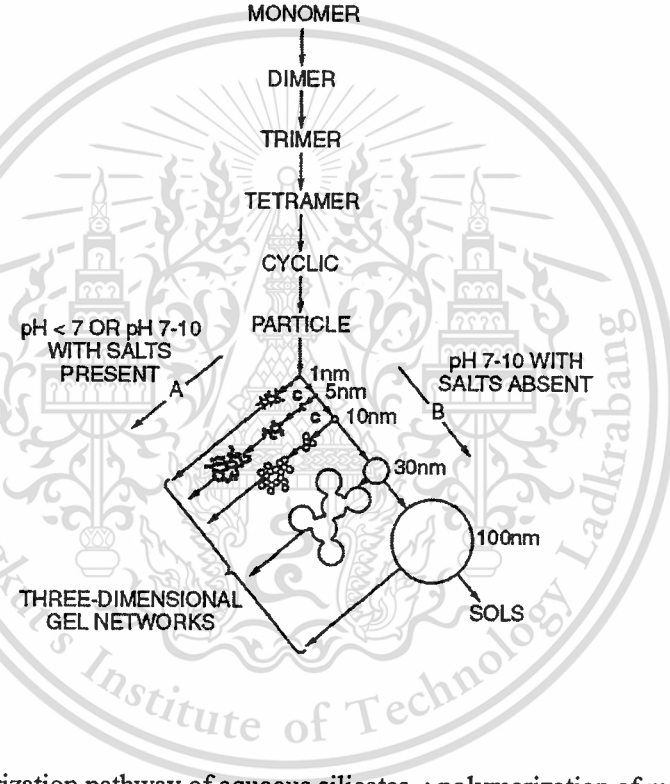

Figure 2.18 Polymerization pathway of aqueous silicates. : polymerization of monomer to form particles, growth of particles, and linking of particles together into branched chains, networks and finally, gels.

As discussed later, gelation in both aqueous and alkoxide derived sols is consistent with a percolative process involving cluster–cluster aggregates. The physical and chemical changes that occur after gelation but before complete drying are referred to as aging. The first theory that attempted to derive the divergences in cluster mass and average radius accompanying gelation is that of Flory and Stockmayer. In their model, bonds are formed at random between adjacent nodes on an infinite Cayley tree or Bethe lattice (see **Figure 2.19**).

This material is protected by copyright and is allowed for commercial use.
Forbidden to modify the content, and cite the document when use.

The Flory–Stockmayer (FS) model is qualitatively successful because it correctly describes the emergence of an infinite cluster at some critical extent of reaction and provides good predictions of the gel point. Although the polymerization of silicon alkoxides under acid-catalyzed conditions appears to produce molecular networks analogous to the organic polymers for which the FS model was developed, two inherent problems are encountered when adapting the FS approach to describe silicate polymers and gels. (1) Because of the nature of the Cayley tree, cyclic species are excluded, yet cyclic species are very prevalent in acid-catalyzed silicate sols (see **Figure 2.18**). (2) Because cyclic configurations are avoided, the purely branched clusters formed on the Cayley tree are predicted to have a fractal dimension of 4; a divergent density for large clusters results (M_ r4). Because of problems with the FS approach, Stauffer and de Gennes advanced bond percolation as a desription of polycondensation (see **Figure 2.19**). In the percolation model, bonds are formed at random between adjacent nodes on a regular or random d-dimensional lattice. In this approach, cyclic molecules are allowed and excluded volume effects are directly accounted for.

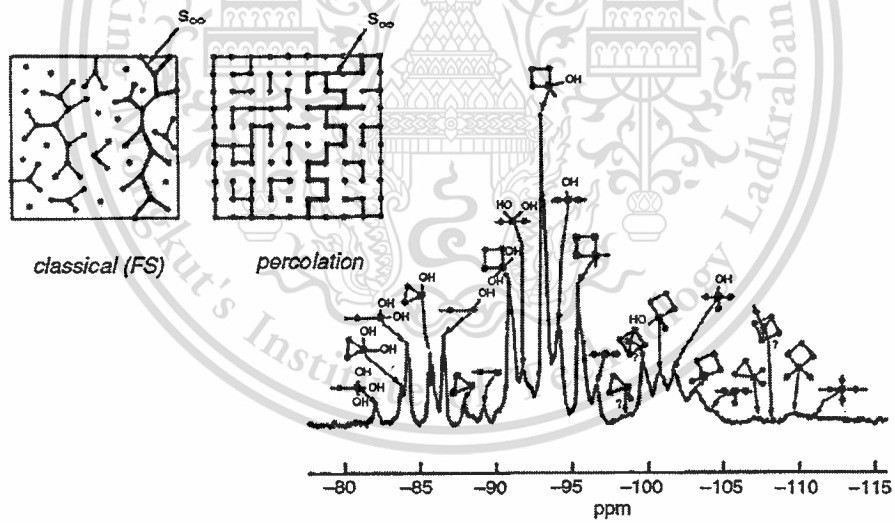

Figure 2.19 Illustrations of gelation according to the classical Flory–Stockmayer model and the percolation model.

To incorporate more of the reactants in the gel network and thus impart strength and stiffness, gels are often aged prior to drying in either the mother liquor or other liquid. The aging process comprises (1) continued polymerization; (2) syneresis; (3) coarsening; (4) phase separation; and in some cases (5) hydrolysis and esterification. Polymerization continues both between monomers

This material is reserved for educational use only, not allowed for commercial use.
Forbidden to modify the content, and cite the document when use.

or polymers and the spanning network and within the network itself as reactive terminal groups diffuse into close proximity. This process appears to promote syneresis (sometimes called macrosyneresis) , the shrinkage of the gel network, resulting in expulsion of liquid from the pores. This has been stated that the kinetics of syneresis depend on the driving force (polymerization), the mobility of the gel network, and the rate of fluid flow through the contracting network. Iler's view of aging is represented schematically in **Figure 2.20.**

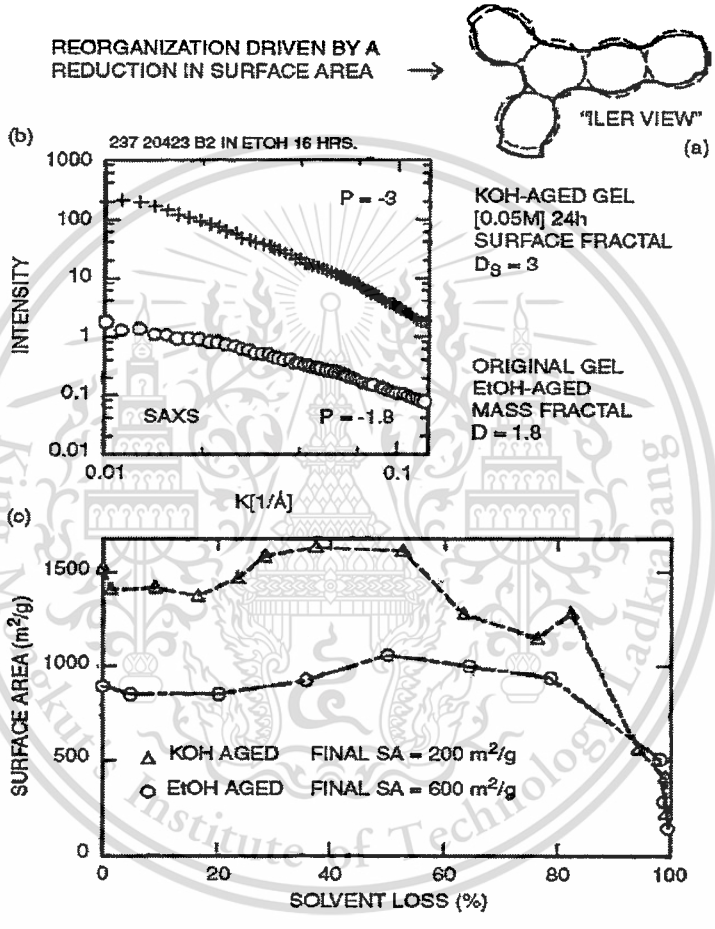

Figure 2.20 (a) coarsened structure that results from aging a network of particles under conditions in which there is partial solubility of the condensed phase. Material is removed from surfaces with positive curvatures and deposited at interparticle contacts that have negative curvatures; "neck" formation results. (b) Porod plots obtained by SAXS for an alkoxide-derived gel prepared at neutral pH in a 90% ethanol– 10% water solvent (original gel EtOH-aged) and a similar gel aged for 24 h in 0.05 M KOH in ethanol (KOH-aged gel). (c) surface areas of EtOH- and KOH-aged gels as a function of percent solvent loss during drying; data

This material is reserved for educational use only, not allowed for commercial use.
Forbidden to modify the content, and cite the document when use.

obtained by proton spin relaxation methods. Final surface areas (SA) of fully dried gels were measured by using N_2 BET method.

The higher solubility of surfaces with positive curvatures causes dissolution there and reprecipitation on interparticle contacts that have negative curvatures and lower solubilities. This coarsening process, which is driven by a reduction in the solid–liquid interfacial energy, builds necks between particles that significantly strengthen the gel network. **Figure 2.20b** shows that aging an alkoxide-derived gel under basic conditions, where coarsening is enhanced, causes reorganization of a mass fractal (D = 1.8) into a surface fractal (Ds = 3) accompanied by an increase in the solid–liquid interfacial area from about 900 to 1500 m^2/g **(Figure 2.20c),** as measured in situ by proton spin-relaxation techniques. Although coarsening occurs under these conditions, apparently the dissolution–reprecipitation process creates a microporous "skin" at the solid–liquid interface that accounts for the unexpected increase in surface area. As discussed later, this microporous layer collapses during drying because of capillary forces, and the dry gel (xerogel) surface area is less for the base-aged sample than the original sample aged in mother liquor, consistent with Iler's original view **(Figure 2.20a)**.

2.5.4 Drying

Drying is generally accomplished by evaporation to form a xerogel (from the prefix xero, meaning dry). Scherer divides the evaporative drying process into several stages (see **Figure 2.21**) In the first stage, or constant rate period, the body shrinks to accommodate the liquid lost by evaporation, and the liquid–vapor interface remains at the exterior surface. The second stage begins when the body is too stiff to shrink, so the liquid recedes into the gel interior. Initially, a continuous liquid film remains that supports flow to the exterior, where evaporation continues to occur (first falling rate period). Eventually the liquid becomes isolated into droplets, so evaporation of liquid in the gel and diffusion of vapor to the exterior (second falling rate period) is required.

This material is reserved for educational use only, not allowed for commercial use.
Forbidden to modify the content, and cite the document when use.

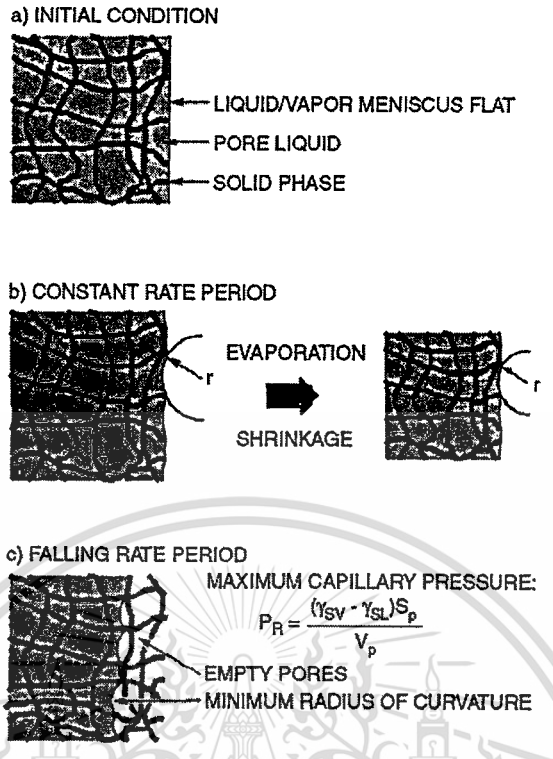

Figure 2.21 Illustration of drying process. Capillary tension develops in liquid as it "stretches" to prevent exposure of the solid phase by evaporation, and the network is drawn back into liquid (a). The network is initially so compliant that little stress is needed to keep it submerged, so the tension in the liquid is low, and the radius of the meniscus (rc) is large (b). As the network stiffens, the tension rises as rc decreases. At the critical point, the radius of the meniscus becomes equal to the pore radius; the constant rate period ends and the liquid recedes into the gel (c).

In gels, the first stage of drying, where the liquid– vapor interface (meniscus) remains at the exterior surface, continues while the body shrinks to as little as one-tenth of its original volume. The most important pressure contributing to this shrinkage is the capillary pressure (Pc) that results from the radius of curvature (r_c) of the meniscus **[68]**:

$$P_c = 2\,\gamma_{LV}\cos(\theta)/r_c$$

where γ_{LV} is the liquid–vapor interfacial energy (surface tension) and θ is the contact angle. Before evaporation begins, the meniscus is flat and $P_c = 0$. Capillary pressure ($P_c > 0$) develops in

This material is reserved for educational use only, not for commercial use.
Forbidden to modify the content, and cite the document when use.

the liquid at it "stretches" to prevent exposure of the solid phase by evaporation. At the initial stage of drying the gel is quite compliant and the network shrinks in response to this tension, so r_c remains large. However, shrinkage is accompanied by continued polymerization reactions within the network. As the network stiffens, r_c decreases and P_c increases. The maximum capillary pressure (P_R) is attained when r_c is equal to the hydraulic radius of the pore ($2V_P/S_P$, where V_P is the pore volume and S_P is the surface area) **[68]**:

$$P_R = \gamma_{LV}\cos(\theta)\, S_P / V_P = (\gamma_{SV} - \gamma_{SL})\, S_P / V_P$$

Any further drying causes the meniscus to recede into the gel interior. Because the pore radius may approach molecular dimensions in some alkoxide-derived gels, P_R is an enormous tension, often exceeding several hundred megapascals. This tension is balanced by a compressive stress in the network that causes shrinkage. Despite the large magnitude of P_R, if P_R were uniform throughout the body, cracking would not be a major problem **[68]**. Unfortunately, because of the low permeability of the network, it is difficult to draw liquid from the gel interior, so a pressure gradient develops. As the pressure gradient increases, so does the variation in free strain rate, with the surface tending to contract faster than the interior. The spatial variation in strain (or strain rate) causes the stress that leads to fracture **[68]**. Several strategies reduce the tendency of gels to crack during drying **[68]**. Very slow drying reduces the gradient in strain by allowing the surface and interior to shrink at comparable rates. Aging strengthens the network and in some cases increases the pore radius, consequently reducing P_R. The use of surfactants or so-called drying control chemical additives (DCCA) or, for example, the replacement of water with alcohol, reduces the pore fluid surface tension (or increases the contact angle), also reducing P_R. Supercritical drying **[69]** avoids liquid– vapor interfaces altogether and therefore capillary pressure. Supercritical drying (also referred to as hypercritical drying) was first used by Prassas and Hench to produce large silica monoliths without cracking. It involves the extraction of solvent above its critical point, where there is no distinction between liquid and vapor and, hence, no liquid–vapor interfacial energy ($\gamma_{LV} = 0$, so according to Equation, $P_R = 0$). In some cases drying is accomplished with no measurable shrinkage of the network. The resulting dry gels are called aerogels, because air may constitute over 99% of the volume. Whereas Iler referred to xerogels as "a contracted and distorted version of the gel originally formed in solution", aerogels should more closely represent the structure of the original gel. In support of this idea, *Schneider*

This material is reserved for educational use only, not for commercial use.
Forbidden to modify the content, and cite the document when use.

M et al., [70] found that the mechanical properties of aerogels are reasonably consistent with percolation theory; for example, the Young's modulus (E) varies with density (ρ) as follows: $E \alpha \rho^{3.7\pm0.3}$

2.5.5 Calcination of Inorganic Gels in an Oxidative Atmosphere

Even when thoroughly dried, gels still contain a significant amount of residues that block up part of the porosity of the catalyst support. In order to burn off any residual organics (alcohol, ligands, ...) present in dried inorganic gels and to convert organic precursors of the active metal into metal oxide or to burn off organic parts of alkoxysilane-functionalized complexes and produce metal oxide in cogelled catalysts, samples are calcined at high temperature (e. g. 400–500°C) in flowing air or oxygen. The calcination temperature should be high enough to ensure the complete removal of all organic parts but not higher than necessary to avoid sintering of the support (micropore closing) and/or of the metal compound. The metals act as oxidation catalysts because oxidation occurs at lower temperature when these ones are present in the gel. In cogelled materials, calcination results in a considerable increase of the support surface area corresponding to the unblocking of micropores that were completely filled with residues which makes active metal precursors (in the form of oxides) accessible

2.5.6 Sol-gel methods for preparing supported metal oxide catalysts

The common industrially important preparation methods of supported metal oxide catalysts are multisteps processes consisting of: (a) preparation of the support; (b) distribution of the active component precursor over the support surface (by impregnation, ion exchange, anchoring, ...); (c) drying, calcination or pyrolysis and possibly reduction of the catalyst to obtain the active species (often metal or metal oxide nanoparticles) dispersed in the porosity of the support. An important advantage of sol-gel process over traditional methods for the preparation of catalysts is the possibility its offers to prepare a solid from a homogeneous solution which includes not only the support precursor(s), but also the metal(s) precursor(s). Steps (a) and (b) corresponding to classical methods are then gathered in one single step. Although the present review is mainly focused on one-step synthesis methods, the two-steps method, which consists in preparing a xerogel or aerogel support which will be next loaded with one or several metal(s) processor(s), is briefly presented below.

This material is reserved for educational use only, not allowed for commercial use.
Forbidden to modify the content, and cite the document when use.

2.5.6.1 Two-Steps Method

Although sol-gel process is particularly attractive in catalyst preparation because it allows the preparation of both support and active sites in one single-step, the two steps method consisting in dispersing the active metal(s) precursor(s) in the porosity of a xerogel or aerogel support prepared in advance leads in some particular cases to catalysts with higher performances than one-step made catalysts. Indeed, while it often results in highly dispersed supported metal catalysts, the one-step method leads also sometimes to poor dispersion of metallic species. Furthermore, depending on the conditions of catalyst preparation and/or operation such as temperature, pressure or composition of gaseous atmosphere, there is a risk of active metal occlusion in the bulk of the support of one-step-made catalysts which would make it partly or completely inaccessible for the reactants in a catalytic process. Such an occlusion has been observed in a Pd-Ag/SiO_2 aerogel **[48]**, in Pt/SiO_2 xerogels, in Ru/SiO_2 xerogels, in Pd/SiO_2 xerogels, as well as in Ni/C aerogels. It must be however mentioned that, while leading to a loss of active metallic surface, partial occlusion can be beneficial when it corresponds to a partial burying of metal particles in the support. Indeed, such more strongly anchored metal particles are more resistant to sintering, which makes the catalyst more stable at high temperature. In consequence, it is sometimes preferable to use the sol-gel method in a two steps process rather than in a one-step one in order to obtain an efficient catalyst. Due to their particularly high specific surface area and porous volume, sol-gel materials are attractive candidates as catalysts supports. Conventional methods such as impregnation and ion exchange have been used to introduce one or several metal(s) precursor(s) into a xerogel or aerogel support. For example, such methods have been applied to Pt/SiO_2 aerogels, Pd/SiO_2 xerogels and aerogels, Ru/SiO_2 xerogel, Co/Al_2O_3 xerogels, Pt/ZrO_2 aerogel, Fe/TiO_2 and Fe/Al_2O_3 xerogels, Pt/TiO_2 xerogels, Rh/SiO_2-TiO_2 aerogels, Ni/SiO_2-TiO_2 aerogels, Ni/Al_2O_3-TiO_2 xerogels, Co-Mo/SiO_2 xerogels, Ag-Co/Al_2O_3 xerogels, Ru/C aerogels, Pt/C aerogels, and Pd-Ag/C xerogels. In the case of inorganic supports, it is important to calcine xerogel and aerogel supports in an oxidizing atmosphere (most often in air) at high temperature (e.g. 400°C) before impregnation. Indeed, such a calcination increases drastically the microporosity, and thus the specific surface area, of the support because its allows to burn the many organic residues which block the pores, and particularly the micropores, in xerogels and aerogels just dried. In the case of carbon supported catalysts, the organic gel, most often obtained from aqueous poly-condensation of resorcinol and formaldehyde, is, after drying, pyrolyzed at high temperature (e.g. 800–1000°C) in an inert

This material is reserved for educational use only, not allowed for commercial use.
Forbidden to modify the content, and cite the document when use.

atmosphere to be converted into a high surface area carbon support. The two-steps method has also been combined with a one-step method (described below) to synthesize bimetallic catalysts. In those cases, monometallic samples prepared by a one-step method have been impregnated with a solution of a second metal. With the aims to avoid the formation of Pt-Sn alloys and to promote the formation of 'tin-aluminate' compounds in order to obtain a Pt-Sn/Al_2O_3 bimetallic catalyst with high performance in the reforming of naphta, tetrabutyltin was added to a homogeneous solution containing aluminum tri-sec-butoxide to form a Sn/Al_2O_3 gel, which, after drying and calcination, was impregnated with an hexachloroplatinic acid solution. A second example concerns a comparison of different preparation methods of Fe-Mo/Al_2O_3 sol-gel catalysts for the synthesis of single wall carbon nanotubes (SWNTs). In that study, catalysts prepared by the impregnation of the molybdenum containing dried gel, prepared in one single step, with the methanolic solution of the $Fe(NO_3)_3.9H_2O$ were particularly selective in SWNTs in comparison with bimetallic catalysts prepared in one step only (Fe and Mo precursors both dissolved in the precursory sol-gel solution).

2.5.6.2 One-Step Method

Other than the convenience of saving a step, this feature allows to prepare supported metal catalysts with unique structures that are inaccessible with other preparation methods. Often, supported catalysts prepared by one-step sol-gel methods exhibit higher dispersion than those prepared by impregnation. Stronger anchoring of metal particles in the porosity of the support is also often observed and this may benefit a higher stability at high temperature. Moreover, the ability to introduce all components into solution during the sol-gel step makes this approach especially attractive for the preparation of multimetallic catalysts supported on single or mixed oxides as well as on carbon.

- Dissolution of Metal Salts in the Precursory Sol-Gel Solution

Since the synthesis of a support by the sol-gel method starts with a homogeneous solution of precursors of that support, the idea of dissolving an adequate precursor of the active species in that solution comes naturally to the mind. Many catalysts have been synthesized in that way. Pd/SiO_2 xerogels, Pt/SiO_2 xerogels, Ru/SiO_2 xerogels, Fe/SiO_2 xerogels, Ni/SiO_2 xerogels, Co/SiO_2 xerogels, Pd/Al_2O_3 aerogels, Pt/Al_2O_3 aerogels and xerogels, Pd-Sn/SiO_2 xerogels, Co-Mo/SiO_2 xerogels , Co-Fe/SiO_2, Co-Ni/SiO_2, and Fe-Ni/SiO_2 xerogels The underlying purpose is to try to include the active metal precursor in the porous growing gel network without making it inaccessible in the final catalyst. An essential condition to obtain a final catalyst in which the

This material is reserved for educational use only, not allowed for commercial use.
Forbidden to modify the content, and cite the document when use.

metal is highly dispersed is to maintain the metal precursor in solution throughout the sol-gel step, which is sometimes difficult with noble metals which are easily reduced and then precipitate. In a study of the synthesis of transition metal doped carbon xerogels by solubilization of metal salts in resorcinol-formaldehyde aqueous solution. Indeed, some salts can be dissolved easily and kept dissolved during the gel synthesis (nickel acetate for example). But in many cases, theaddition of a complexing agent proved to be essential for two reasons: i) some salts are not very soluble in the resorcinolformaldehyde aqueous solution: the addition of a complexing agent improves their solubility. In particular, many metal ions (Fe^{3+}, Cu^{2+}, for instance) precipitate as hydroxides under the pH conditions chosen; ii) formaldehyde is a powerful reductant and often causes the metal to precipitate under metallic state before gelation, leading to non homogeneous gels and metal agglomerates. In that study, Ni/C, Fe/C and Pd/C xerogel samples were prepared. As significant amounts of nickel acetate tetrahydrate can be dissolved in resorcinol-formaldehyde aqueous solutions without precipitation, Ni/C samples were prepared by simple addition of nickel acetate tetrahydrate. The Fe/C samples were synthesized using iron acetate and hydroxyethyl-ethylenediaminetriacetic acid (HEDTA) as complexing agent to increase the solubility of the metal salt. The Pd/C xerogels were prepared with palladium acetate. Again, significant amounts of palladium acetate cannot be dissolved without additional complexing agent. Preliminary results showed that though HEDTA improves palladium acetate dissolution, this complexing agent cannot prevent the reduction of palladium cations during gelation. HEDTA was then replaced by diethylenetriaminepentaacetic acid (DTPA). Unfortunately, despite those precautions, the study showed that nickel, iron and palladium are under metallic state after drying without needing further reduction treatment, which indicates that the metal complexes are not stable throughout the polymerization reaction. Though the xerogels seem homogeneous, the transition metals are reduced by formaldehyde and precipitate locally. As a result, the metal particles obtained are rather big (15–20 nm and more) in the final catalysts. Investigations have therefore to be conducted to improve the preparation method.

In another study, Cr, Mo and W oxides loaded carbon aerogel catalysts have been prepared by *Cotton F.A. et al.*, **[56]** by dissolving metal salts in aqueous solutions of resorcinol and formaldehyde. According to X-ray diffraction results, the metal oxide or carbide was well dispersed inside the organic matrix. In the case of metals supported on inorganic gels, it is sometimes possible to find a salt of the desired metal which is soluble in the initial sol-gel solution whose solvent most often is an alcohol. It is also possible to realize a dissolution of the

This material is reserved for educational use only, not allowed for commercial use.
Forbidden to modify the content, and cite the document when use.

metal salt in an adequate solvent and to add that metal precursor solution to the sol-gel solution. The preliminary dissolution of the metal salt in the water which will be used to hydrolyze the support precursor alkoxyde is often encountered. Unlike the cogelation method which is presented below, metal precursors in the dissolution method do not participate directly in the sol-gel chemistry involving the oxide precursors which are usually alkoxides. In the dissolution method, the metal precursor is often simply encapsulated in a growing gel network, but its presence can still indirectly influence the sol-gel process **[65]** and leads to modifications in the structure of the final catalyst. For example, in a study of spectroscopic characterization of Pd/SiO_2 xerogel catalysts prepared by hydrolysis and polycondensation of tetraethoxysilane ($Si(OC_2H_5)_4$) in a solution containing $PdCl_2$. The result showed that the preparation method leads to the formation of [SiO_2 -[PdCl -OH] surface species with an unusual interaction detected by UV-VIS and FT-IR spectroscopies. The interaction of palladium with the silica gel has an important effect on the specific surface of the final catalyst: whereas the SiO_2 support prepared without palladium shows an area of 110 m^2/g only, the Pd/SiO_2 catalysts exhibit an much higher area which decreases from 889 m^2/g down to 630 m^2/g when the metal loading increases from 0.1 to 3 wt.%. In another study on the synthesis of Ni/C, Fe/C and Pd/C xerogels, it was observed that the solubilization of transition metal salts in the resorcinol-formaldehyde initial aqueous solution does not prevent the texture regulation, even though this texture control is influenced: the limits of the pH interval leading to micro-mesoporous carbon materials can slightly differ when a metal salt and/or a complexing agent are added. The pH range shift depends mainly on the amount and nature of the complexing agent, but also slightly on the nature of the metal ion. A serious drawback that can arise with the one-step dissolution method is the possible partial occlusion of the active metal in the bulk of the support leading to a loss of metallic surface available for the catalytic reaction. Cases in which that problem occurred have been devoted to the two-steps method which represents a possible alternative to avoid occlusion. However, because of the above mentioned advantages of the one-step methods, it is really worth to try to solve the problem of metal occlusion by improving the one-step methods. In the following Section, a second one-step method that allows to avoid occlusion and leads to unique structural characteristics is presented.

- *Cogelation of Metal Chelates with Support Precursors*

Since the eighties, a particularly attractive method to prepare nanometer-sized uniform metal particles in a silica matrix by sol-gel processing of metal complexes has been developed. Numerous metals and alloys supported on SiO2 including Ag, Co, Cu, Ni, Pd, Pt, Cu-

This material is reserved for educational use only, not allowed for commercial use.
Forbidden to modify the content, and cite the document when use.

Ru, Pd-Ni, Cu-Ni, and Pt-Cu were prepared. That method has been applied to prepare Pd/SiO2, Ag/SiO_2, Cu/SiO_2, $Pd\text{-}Ag/SiO_2$ and $Pd\text{-}Cu/SiO_2$ xerogel and aerogel catalysts for various applications. The method consists in using an alkoxysilane-functionalized ligand of the type $(RO)_3Si\text{-}X\text{-}L$ in which the ligand L, able of forming a complex - LNM with a metal M (M = Pd, Ni, Ag, Cu, etc.), is connected to the alkoxide moiety $(RO)_3Si$- via an inert and hydrolytically stable tethering organic group X. The concomitant hydrolysis and condensation of such molecules with a network-forming reagent such as $Si(OC_2H_5)_4$ (TEOS), i.e. their *cogelation*, result in materials in which the catalytic metal is anchored to the SiO_2 matrix **[64]**.

2.6 PHYSICAL PROPERTIES OF BUTYRALDEHYDE

n-Butyraldehyde, also known as butanal, is an organic compound with the formula $CH_3(CH_2)_2CHO$. This compound is the aldehyde derivative of butane. It is a colourless flammable liquid that smells like sweaty feet. It is miscible with most organic solvents.

Figure 2.22 Molecular and ball & stick structure of n-butyraldehyde

Table 2.6 Properties of n-butyraldehyde **[26]**

Properties	
Molecular formula	C_4H_8O
CAS number	123-72-8
Molar mass	72.11 g/mol
Density	0.817 g/ml (25 °C)
Melting point	-99 °C
Boilng point	74.8 °C
Solubility in water	7.6 g/100 ml (20 °C)

This material is reserved for educational use only, not allowed for commercial use.
Forbidden to modify the content, and cite the document when use.

Ru, Pd-Ni, Cu-Ni, and Pt-Cu were prepared. That method has been applied to prepare Pd/SiO2, Ag/SiO_2, Cu/SiO_2, $Pd\text{-}Ag/SiO_2$ and $Pd\text{-}Cu/SiO_2$ xerogel and aerogel catalysts for various applications. The method consists in using an alkoxysilane-functionalized ligand of the type $(RO)_3Si\text{-}X\text{-}L$ in which the ligand L, able of forming a complex - LNM with a metal M (M = Pd, Ni, Ag, Cu, etc.), is connected to the alkoxide moiety $(RO)_3Si$- via an inert and hydrolytically stable tethering organic group X. The concomitant hydrolysis and condensation of such molecules with a network-forming reagent such as $Si(OC_2H_5)_4$ (TEOS), i.e. their *cogelation*, result in materials in which the catalytic metal is anchored to the SiO_2 matrix **[64]**.

2.6 PHYSICAL PROPERTIES OF BUTYRALDEHYDE

n-Butyraldehyde, also known as butanal, is an organic compound with the formula $CH_3(CH_2)_2CHO$. This compound is the aldehyde derivative of butane. It is a colourless flammable liquid that smells like sweaty feet. It is miscible with most organic solvents.

Figure 2.22 Molecular and ball & stick structure of n-butyraldehyde

Table 2.6 Properties of n-butyraldehyde **[26]**

Properties	
Molecular formula	C_4H_8O
CAS number	123-72-8
Molar mass	72.11 g/mol
Density	0.817 g/ml (25 °C)
Melting point	-99 °C
Boilng point	74.8 °C
Solubility in water	7.6 g/100 ml (20 °C)

This material is reserved for educational use only, not allowed for commercial use.
Forbidden to modify the content, and cite the document when use.

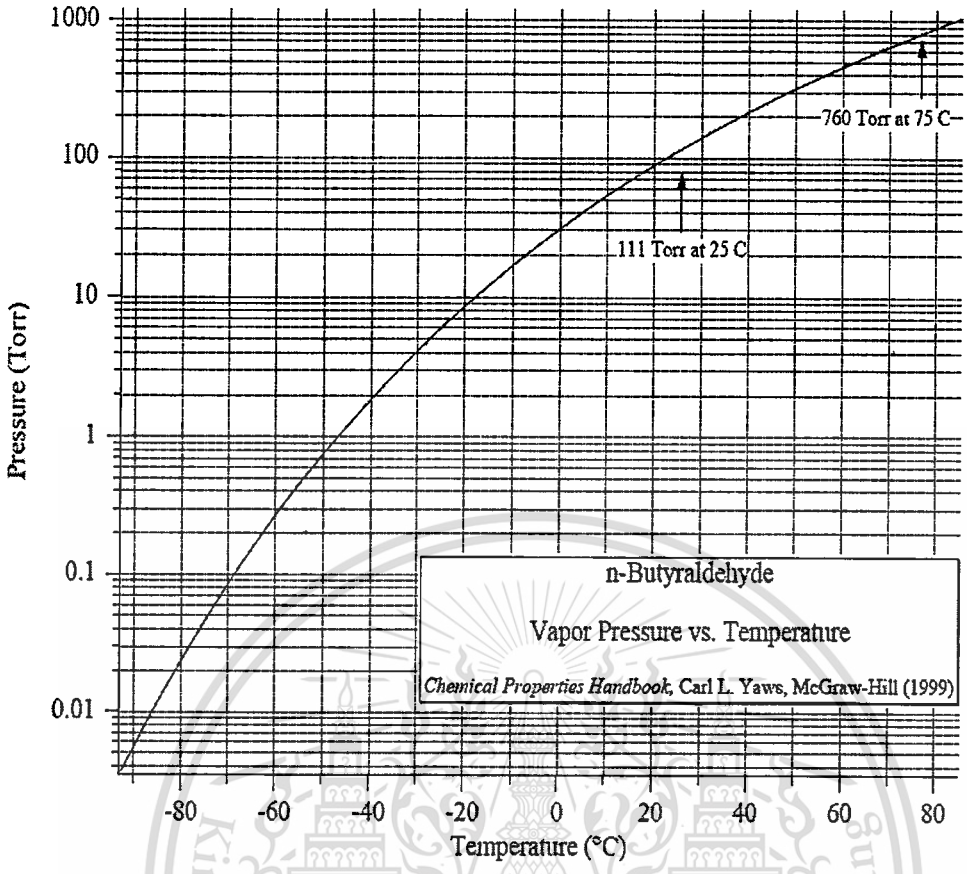

Figure 2.23 Vapor pressure of n-butyraldehyde at different temperature

n-Butyraldehyde can be produced by the catalytic dehydrogenation of *n*-butanol. At one time, it was produced industrially by the catalytic hydrogenation of crotonaldehyde, which is derived from acetaldehyde. Upon prolonged exposure to air, n-butyraldehyde oxidizes to form butyric acid.

This material is reserved for educational use only, not allowed for commercial use.
Forbidden to modify the content, and cite the document when use.

2.7 LITERATURE REVIEWS

Molybdenum (VI) oxides produced by the sol–gel method were reported previously [71]. In all cases, hydrolysis of the precursors resulted in rapid precipitation of amorphous molybdenum (VI) oxide. Amorphous xerogel powders were produced which, upon heating, led to various molybdenum (VI) oxides, including MoO_3 [73], Mo_8O_{23} and Mo_3O_5 [72]. The only molybdenum (VI) oxide aerogel reported to date is MoO_2 which exhibited surface areas as high as 170 m^2/g [74]. In the study by *Yanovskaya et al.,* [73], it was proposed that the presence of terminal oxygen atoms when molybdenum alkoxides are hydrolyzed is the main obstacle for sol–gel methods to form a 3D gel network. In the spectroscopic study, it was conclusively shows that Mo=O bonds are being successfully suppressed through the gelation, aging, and drying processes. As-prepared aerogels are hydrated amorphous molybdenum (VI) oxides possessing density 0.15–0.3 g/cm^3 and surface area 150–200 m^2/g. Crystallization from the amorphous to the orthorhombic phase occurs between 350 and 400 °C.

Juarez et al., [75] have recently demonstrated that β-MoO_3 can be obtained free from the α-phase by vacuum drying the molybdic acid solution. However, this method has a disadvantage of slowness in the drying process: it required 36 hours to dry the solution in a 50 cm^3 vessel. *Mizushima et al.,* [76] developed a new synthesis route of β-MoO_3 with a high purity. As a result, they found that an addition of a small amount of nitric acid to the molybdic acid solution before a simple evaporation into dryness led to a selective formation of the β -form of molybdenum (VI) oxide.

The effect of the impregnation pH on the adsorption of the molybdenum species and the final structure of the MoO_3, catalysts has been examined in various studies [77,78]. In spite of the experimental simplicity of the TPR technique it has not been used to examine systematically the effect of the impregnation pH on the structure of MoO_3/Al_2O_3 catalysts. *Lopez Corder R et al.,* [79] reported a comparative study of the effect of the impregnation pH on the structure of MoO_3 supported on Al_2O_3 by a combined use of temperature programmed reduction (TPR), X-ray diffraction (XRD), and zeta potential measurements. They concluded that at pH ≤ 3 and high concentration of molybdenum in the impregnating solution, although the adsorption of the

This material is reserved for educational use only, not allowed for commercial use.
Forbidden to modify the content, and cite the document when use.

predominant $Mo_7O_{24}^{6-}$ species **[80]** is favoured, a considerable amount of molybdenum remains in the solution since its concentration is relatively high. Consequently, when the solvent is removed the unadsorbed $Mo_7O_{24}^{6-}$ species will precipitate and/or polymerize, and upon drying and calcinations, they will form a heterogeneous deposit of polymeric molybdenum species on the $A1_2O_3$.In the preparations at pH $>$ 5 the solutions contain predominantly MoO_4^{2-}species. At these pH values, the alumina is negatively charged and therefore no adsorption of anions occurs. Thus the unadsorbed species deposited on the alumina after drying will be essentially MoO_4^{2-}. This then leads to a minor proportion of molybdenum in polymeric form or as MoO_3 crystallites.

Slurry impregnation is a special case of equilibrium adsorption impregnation method. The maximum amount of MoO_3 that can be deposited by slurry impregnation corresponds to the formation of a saturated adsorption monolayer. *Ma X. Ma et al.,* **[81]** reported the benefits brought by slurry impregnation methodology via comparing the performances of catalysts prepared by conventional impregnation. Three catalyst systems, MoO_3/γ-Al_2O_3, MoO_3/C and MoO_3/SiO_2 were prepared by both the slurry and the conventional impregnation. These catalysts were tested in transesterification of dimethyl oxalate (DMO) and phenol. The dependence of catalytic activities on Mo loadings for the slurry prepared catalysts was similar to those of the samples prepared by the conventional impregnation method with ammonium heptamolybdate (AHM). The activities of the slurry impregnation MoO_3/γ-Al_2O_3 catalysts were the same as those of the corresponding catalysts prepared conventionally. The slurry preparation method for carbon support overcame the problem of oxidative damage of active carbon at high calcination temperature and provided MoO_3/C catalysts with relatively high transesterification activity. Moreover, slurry impregnation MoO_3/SiO_2 catalysts performances for transesterification of DMO were better than conventional impregnation ones.

Although, most of the researchers **[82,83]** use impregnation method but some groups report the use of the sol–gel method as an alternative and superior route to the impregnation method for preparing well dispersed MoO_3/SiO_2 catalysts. *Smith et al.,* **[84]** has reported the effect of the nature of surface species on the activity and selectivity of MoO_3/SiO_2 catalysts for the partial oxidation of methane to formaldehyde. *Amol P et al.,* **[85]** have prepared MoO_3/SiO_2 composites

This material is reserved for educational use only, not for commercial use.
Forbidden to modify the content, and cite the document when use.

by sol–gel method, and applied in anisole condensation with paraformaldehyde as a liquid phase reaction in the absence of the solvent. The condensation of anisole with paraformaldehyde catalyzed by MoO_3/SiO_2 composite prepared by sol–gel method gave mainly 4,4' dimethoxydiphenyl methane (4,4'-DMDPM). The activity of MoO_3/SiO_2 catalyst has been compared with the known catalysts like p-TSA and WO_x/ZrO_2. Under the similar reaction conditions, synthesized 10% MoO_3/SiO_2 500 °C was found to be the best among the catalysts studied, which is attributed to its highest acidity and uniform distribution of MoO_3 species on silica support.

Shubhangi B. U et al., **[86]** have successfully established the synthesis of mesoporous MoO_3/SiO_2 solid acid catalyst by sol–gel technique without using any surfactant template and the catalyst has been found to be very active for acid catalyzed organic reactions such as nitration of benzene and cumene, transesterification of diethyl oxalate to diphenyl oxalate **[87]** and Beckmann rearrangement **[88]**. In continuation of their efforts, MoO_3/SiO_2 catalysts prepared by sol–gel techniques were used successfully for acetalization of glycerol with various aldehydes. High conversion up to 78% was obtained for aliphatic aldehydes. Very high selectivity (up to 100%) for six-membered acetal was obtained at lower conversions (10%) ; however, up to 70% selectivity for six-membered acetal was obtained at 70% conversion for *o*-chloro benzaldehyde. MoO_3/SiO_2 catalysts with 20 mol% Mo loading were found to be most acidic and highly active catalyst in the series. The extensive characterization of the catalysts showed presence of various well dispersed entities like silicomolybdic acid (SMA), polymolybdate species or molybdenum (VI) oxide nanoparticles depending on the Mo loading. It has been shown that SMA, at low Mo loading was not formed during the sol–gel process but by the rehydration of the calcined catalyst due to the presence of nanosize molybdenum oxo species supported on high surface mesoporous silica support. The presence of a well dispersed surface polymolybdate is observed. It has also been shown that the formation of aggregates of α-MoO_3 particles at high Mo loadings originated from the AHM precipitation during the sol–gel preparation. But intermediately β-MoO_3 nanoparticles are stabilized even after calcination at 500 °C.

However, few papers reported that MoO_3/SiO_2 was used as a catalyst in the liquid phase epoxidation of propylene with cumene hydroperoxide (CHP) **[89]**. *Miao. Y. et al.,* **[90]** modified base-catalyzed sol–gel method was used to prepare the MoO_3/SiO_2 catalyst for the liquid phase

This material is reserved for educational use only, not allowed for commercial use.
Forbidden to modify the content, and cite the document when use.

epoxidation of propylene by CHP without any depressor or additives. A variety of molybdenum-containing species can be formed on silica support, including highly dispersed polymolybdate, α-MoO_3 , β-MoO_3, monomeric species, and a small amount of SMA that was formed due to exposure to air. The presences of small size (below 5 nm) of β-MoO_3 and monomeric molybdenum species are in favor of an increase in the catalytic performance of MoO_3/SiO_2. Using 1,2-propanediol as a solvent instead of de-ionized water and adopting appropriate sequence of feeding, the MoO_3/SiO_2 catalyst with the β-MoO_3 species and monomeric molybdenum species can be prepared and behaves very high catalytic activity. At 80 °C and 2.2 MPa for 4 hours, the conversion of CHP and selectivity to propylene oxide for CHP over the MoO_3/SiO_2 catalyst can reach >99% and 85.3%, respectively.

Since β-MoO_3 is a metastable phase of molybdenum (VI) oxide, the formation of β-MoO_3 on supported catalysts was detected under the limited conditions such as the reaction of methanol to formaldehyde. Therefore, it is of interest to apply the new synthesis method to the preparation of supported catalyst for understanding the catalysis of β-MoO_3. Additionally, *Deltcheff et al.,* **[91]** pointed out that the molybdic acid was the effective precursor for the synthesis of SMA. This means that the anchored SMA by the reaction with Si–O species of supports can be prepared and the desired Mo species, either SMA or β-MoO_3 can consequently be obtained by use of the molybdic acid solution. *Kido et al.,* **[92]** successfully synthesized formaldehyde from methane on SiO_2-supported SMA catalysts at temperatures of 873 K under the presence of water vapor. They supposed that the presence of β-MoO_3 was indispensable for the regeneration of a high catalytic activity for the partial oxidation of methane (POM). It is believed that at high temperature SMA decomposes to SiO_2 and molybdenum (VI) oxide. But in the presence of water, SMA regenerated reaction occurs **[93]**.

In the last decades, several research groups **[94, 95]** published that silica-supported Mo catalysts have high catalytic activities for alcohol synthesis and photochemical reactions. In these reactions the reactivity is reported to be very sensitive to the structure and valence of the supported Mo species. *Ono et al.,* **[96]** reported that at low loadings most of the supported Mo atoms are in tetrahedral coordination and these Mo ions play a significant role in the

This material is reserved for educational use only, Forbidden to modify the content, and cite the document when use.

photoreaction, but the octahedrally coordinated Mo ions, which are formed at high loadings, are not active in this reaction. From Raman spectral study by *Jeziorowski H et al.,* **[97]** observed the existence of two molybdenum (VI) oxide species; an "interaction species" at low loadings and a "free MoO_3" at high loadings. The former is supposed to be a polyanion chemically interacting with the support surface and the latter a small MoO_3 crystallite still having a weak interaction with the support. Raman spectral obtained after the calcinations confirmed that the spectrum is identical with that of MoO_3 but EXAFS spectra clearly indicate that not all species formed at high loadings are MoO_3 crystallites. The contradiction between the results derived from these two methods is discussed in relation with a possible catalyst structure. Both *Knozinger et al.,* **[97]** and *Cheng et al.,* **[98]** observed the formation of "free MoO_3 " or " MoO_3 phase". Raman spectra obtained indeed support the existence of MoO_3, crystallite, but the analysis of EXAFS spectra gives a contradictory result; not all the species formed are MoO_3, crystallite, because of the Mo-Mo coordination number being much smaller in the catalyst. This cannot, however, explain the small coordination number of Mo-Mo observed by EXAFS, because the coordination number in this model is 6, which is the same as that of bulk. The physical mixture of the same Mo contents was used for Raman measurement. The peak intensity of the 822 cm^{-1} band of MoO_3, is about 7 times stronger than that of the 946 cm^{-1} band of ammonium heptamolybdate. The result indicates that the polymolybdate species should be detectable with 20 wt % catalyst by Raman spectroscopy if the X-ray amorphous oxides, which account for about 80% of the supported Mo, exist as one kind of oxide such as heptapolyanion. At low loadings, the "interaction species" is formed already in the dried stage and it is stable and does not change by calcining at 773 K. At high loadings, free heptamolybdate is formed first and many kinds of Mo oxides exist after calcination at 773 K. One is MoO_3, crystallites and the others are the various kinds of octahedrally coordinated Mo oxide clusters.

Desikan. A. N. et al., **[99]** suggested the nature of oxygen chemisorption sites on supported molybdena catalysts has been the subject of controversy. The group of *Hall et al.,* **[100]** suggests that O_2 chemisorption on MoO_3/Al_2O_3 occurs on sites with at least two missing oxygen atom. *Peri J. P. et al.,* **[101]** indicate that on MoO_3/SiO_2 adsorption occurs on Mo^{5+} sites. The concensus

This material is reserved for educational use only, not allowed for commercial use.
Forbidden to modify the content, and cite the document when use.

seems to be that chemisorption sites on reduced MoO_3/Al_2O_3 are multiply coordinatively unsaturated. From the limiting stoichiometry of one oxygen atom per molybdenum atom, the results here indicate that oxygen chemisorption occurs on Mo^{4+} centers.

Several mechanisms accounting for the reduction of MoO_3 to MoO_2 have been proposed in the literature. According to *Ressler et al.,* **[102]** revealed that the reduction pathway, precisely the formation or not of intermediate species, depends on the reduction temperature. Below 698 K, MoO_3 would reduce directly to MoO_2 without any intermediate species. But above 698 K, the MoO_2 resulting from the direct reduction of MoO_3 would react in situ with the "not yet reduced" remaining fraction of MoO_3, so leading to the formation of a third phase with a more distorted structure, namely Mo_4O_{11}. *Dury. F. et al.,* **[103]** developed a parallel approach, namely the use of "probe reactions" that allow to monitor the properties of the catalysts through the distribution of the reaction products. Precisely, this work envisaged the potentiality of the deoxygenation of benzoic acid as a probe of the presence and the mutual organization of oxygen vacancies at the surface of Mo suboxide catalysts. Mo_8O_{23} undergoes a reduction to MoO_2 in the course of the deoxygenation of benzoic acid in the presence of hydrogen. The phenomenon is temperature dependent. Below 698 K, Mo_8O_{23} reduces directly to MoO_2. But, above 698 K, the reduction proceeds through the formation of Mo_4O_{11}as an intermediate phase. Measuring the performances of the phases involved in this reduction pathway reveals that Mo_4O_{11} mainly produces benzene, Mo_8O_{23} mainly produces toluene and MoO_2 mainly produces benzaldehyde.

Most of the previous TPR studies addressed the influences of the preparation method **[104]** and of the pH of the impregnating AHM solution on the structure of highly loaded MoO_3/SiO_2 catalysts **[104, 105]**. Moreover, as a result of different conditions adopted for catalyst pretreatment, contradictory conclusions were achieved **[106]**. *Arena. F. et al.,* **[107]** provided basic insights into the surface structures of MoO_3/SiO_2 catalysts shedding light on the influences of thermal treatments, oxide loading, and preparation method on reduction pattern. In particular, the main results of this work can be summarized as follows: (1) Irrespective of the preparation method and silica carrier, molybdenum(VI) oxide stabilizes three defined surface structures on the silica support having a progressively lower reducibility : polymolybdates > MoO_3 crystallites

This material is used for educational use only, not allowed for commercial use.
Forbidden to modify the content, and cite the document when use.

> isolated molybdates ; (2) The formation of polymolybdates occurs reversibly at ambient conditions upon the adsorption of water from the atmosphere disappearing upon calcination at $T \geq 400$ °C ; (3) Polymolybdates are reduced to Mo^0 in a single step at $T < 500$ °C, (4) Modeling of TPR spectra allows evaluation of the influences of loading and calcination treatments on the related distribution of the above surface species in MoO_3/SiO_2 catalysts

The production of 2-ethyl-2-hexenal (2E2H) via self-condensation of n-butyraldehyde has been studied over various catalysts **[108-110]**. *Ko A.N. et al.,* **[111]** performed low-pressure one-step synthesis of 2-ethyl hexanal (2EH) from n-butyraldehyde and hydrogen by designing bifunctional catalysts capable of proceeding aldol condensation, dehydration and selective hydrogenation. With a palladium catalyst, saturated aldehydes can be produced from the corresponding unsaturated aldehydes at high yields **[112]**. The optimum reaction conditions for the synthesis of 2EH are 0.5% Pd/KXU, 150 °C, B/H 1 and W/F 22.2 g.h/mol. The main reaction path starts from self-condensation of n-butyraldehyde to 2-ethyl-3-hydroxyhexanal, followed by dehydration to 2-ethyl-2-hexenal, and finally hydrogenation to 2-ethyl- hexanal.

This material is reserved for educational use only, not allowed for commercial use.
Forbidden to modify the content, and cite the document when use.

CHAPTER 3

EXPERIMENTAL DETAILS

3.1 CHEMICAL REAGENTS

Chemical reagents	Grade of purity	Manufacturers
1. Ammonium heptamolybdate $((NH_4)_6Mo_7O_{24}.4H_2O)$	99.9 %	APS AJAX FINE CHEM
2. Air zero	High purity	TIG
3. Ammonia in helium gas	10% NH_3/He	TIG
4. Butyraldehyde	GC	FLUKA CHEMIKA
5. Deionized water		
6. Hydrogen gas	High purity	TIG
7. Hydrogen in argon gas	10% H_2/Ar	TIG
8. Helium gas	High purity	TIG
9. *i*-propanol	Analytical	LAB-SCAN
10. Liquid Nitrogen	High purity	TIG
11. Liquefied petroleum gas	Commercial	SIAM GAS
12. Nitrogen gas	High purity	TIG
13. precipitated silica	99.9 %	CARLO ERBA
14. Tetraethyl orthosilicate ($C_8H_{20}O_4Si$, TEOS)	GC	FLUKA CHEMIKA

3.2 APPARATUS AND INSTRUMENTS

1. Catalytic testing rig
2. Clamp
3. Gas adsorption analyzer (Autosorb-1C, Quantrachrome)
4. Gas chromatograph (Model 910, Buck scientific)
5. Heating mantle & stirrer
6. Heating Tape with a programmable temperature controller
7. Laboratory glassware
8. Laboratory plasticware

This material is restricted for educational use only, not allowed for commercial use.
Forbidden to modify the content, and cite the document when use.

9. Magnetic stirrer
10. Mass flow controller
11. Oven
12. Sieve (U.S.A standard sieve, AASHO N-92)
13. Tube furnace with a programmable temperature controller
14. Temperature programmed reduction (TPR) system
15. Temperature programmed deduction (TPD) system
16. Water circulator
17. Scanning Electron Microscope/energy dispersive spectroscopy (SEM-EDS) (LEO 1455VP, LEO Electron Microscopy, Scientific Service Centre, KMITL)
18. X-ray Powder Diffractometer (D8 Advance, Bruker AG, Scientific Instrument Service Centre, KMITL)
19. Gas Chromatograph/Mass spectrometer (6890N/5973N, Agilent, Scientific Instrument Service Centre, KMITL)
20. Inductively coupled plasma/atomic emission spectroscopy (ICP-Plasma-1000, Perkin Elmer, Scientific and Technology Research Equipment Centre, Chulalongkorn University)
21. Transmission Electron Microscope (JEM-2100, JEOL, Scientific and Technology Research Equipment Centre, Chulalongkorn University)
22. Diffused reflectance ultraviolet spectrophotometer (SolidSpec-3700/3700DUV, Shimadzu, Department of science service, Ministry of science and technology)

3.3 PROCESS OF STUDY

A process of the study on the preparation of the catalysts with different surface molybdenum oxide species and catalytic activity comprises the following stages:

3.3.1 Synthesis and modification of catalysts

3.3.1.1 Synthesis of molybdenum oxide supported silica catalysts (MoO_3/SiO_2) with different MoO_3 loadings (1-20 mol %) by sol-gel method.

3.3.1.2 Preparation of molybdenum oxide supported silica catalysts (MoO_3/SiO_2) with different MoO_3 loadings (3 and 20 mol %) by incipient wetness

This material is reserved for educational use only, not allowed for commercial use.
Forbidden to modify the content, and cite the document when use.

impregnation method.

3.3.1.3 Modification of the catalysts obtained in 3.3.1.1 and 3.3.1.2 by heat treatment with different temperature (500, 600 and 700 °C)

3.3.2 Characterization of catalysts

3.3.2.1 Determine chemical composition of the catalysts using inductively coupled plasma/atomic emission spectroscopy (ICP-AES).

3.3.2.2 Investigate the catalysts structure by X-ray diffractometer (XRD).

3.3.2.3 Investigate the surface morphology by scanning electron microscopy (SEM).

3.3.2.4 Determine the surface area and pore size distribution by gas adsorption analysis (Autosorb-1C).

3.3.2.5 Investigate cluster size and size distribution of active sites by transmission electron microscopy (TEM).

3.3.2.6 Investigate active sites by diffuse reflectance ultraviolet spectroscopy (DR-UV).

3.3.2.7 Investigate reducibility of the active sites by H_2-Temperature programmed reduction (TPR).

3.3.2.8 Determine the acidity of the catalysts by NH_3-Temperature programmed desorption (TPD).

3.3.3 Catalytic testing

3.3.3.1 Investigate the product distribution.

3.3.3.2 Investigate the effect of MoO_3 loading on support.

3.3.3.3 Investigate the effect of calcination temperature.

3.3.3.4 Investigate the effect of preparation method

3.3.3.5 Investigate the effect of reaction temperature.

This material is reserved for educational use only, not allowed for commercial use.
Forbidden to modify the content, and cite the document when use.

3.3.4 Analysis of products

3.3.4.1 Determine the amount of product on-line by gas chromatograph equipped with a flame ionization detector (GC-FID)

3.3.4.2 Determine the qualitative of product by gas chromatograph-mass spectrometer (GC-MS).

3.4 SYNTHESIS AND MODIFICATION OF CATALYSTS

3.4.1 Synthesis of molybdenum oxide supported silica catalysts (MoO_3/SiO_2) with different MoO_3 loadings (1-20 mol %) by sol-gel method.

A series of MoO_3/SiO_2 catalysts with varying molybdenum oxide molar concentrations (1, 3, 5, 7, 10, 15 and 20 mol%) were prepared by sol–gel method. The molar composition of catalysts is shown in Table 3.1. Ammonium heptamolybdate ($(NH_4)_6Mo_7O_{24}.4H_2O$), tetraethyl orthosilicate ($C_8H_{20}O_4Si$, TEOS) and *i*-propanol were used as molybdenum, silica source and solvent, respectively. In a typical procedure, 1 mol% MoO_3/SiO_2 catalyst was synthesized by dissolving 0.1765 grams of ammonium heptamolybdate in 20 grams of distilled water at 80 °C. This hot solution was immediately added to the 15.7 grams of *i*-propanol solution of tetraethyl orthosilicate (21.021 grams) with constant stirring. After complete addition, the stirring was continued for 10 hours. The resultant greenish gel was dried in oven at 80 °C for 12 hours. The obtained solid was calcined in a horizontal tube furnace under a flow of air zero (60 ml/min) at different calcination temperature (500, 600 and 700 °C) by a heating rate of 1 °C/min. and hold at those temperature for 8 hours. After that, the sample was pressed, crushed and sieved into 600-850 micron. Similarly, the catalysts with 3, 5, 7, 10, 15 and 20 mol% molybdenum oxide loadings were also prepared. The chemical composition of the catalysts were determined by inductively coupled plasma/atomic emission spectroscopy.

This material is reserved for educational use only, not allowed for commercial use.
Forbidden to modify the content, and cite the document when use.

Table 3.1 The molar composition of catalysts prepared by sol–gel method.

Molar ratio / Catalyst	MoO_3	SiO_2	Alcohol (*i*-propanol + ethanol[a])	H_2O
1%mol MoO_3/SiO_2	0.0101	1	2.6394 + 4.0000[a]	11.2232
3 %mol MoO_3/SiO_2	0.0309	1	2.6930 + 4.0000[a]	11.4546
5 %mol MoO_3/SiO_2	0.0526	1	2.7497 + 4.0000[a]	11.6957
7 %mol MoO_3/SiO_2	0.0752	1	2.8089 + 4.0000[a]	11.9473
10 %mol MoO_3/SiO_2	0.1111	1	2.9025 + 4.0000[a]	15.4311
15 %mol MoO_3/SiO_2	0.1764	1	3.0733 + 4.0000[a]	19.6082
20 %mol MoO_3/SiO_2	0.2500	1	3.2653 + 4.0000[a]	27.7775

[a]Mole of ethanol from hydrolysis reaction of TEOS

3.4.2 Preparation of molybdenum oxide supported silica catalysts (MoO_3/SiO_2) with different MoO_3 loadings (3 and 20 mol %) by incipient wetness impregnation method.

The wetness impregnation method was also applied for preparation of MoO_3/SiO_2 catalysts. In a typical procedure, 3 mol% MoO_3/SiO_2 catalyst was prepared by dissolving ammonium heptamolybdate in distilled water (MoO_3/H_2O molar ratio is equal to 3 mol% catalyst prepared by sol-gel method) at 80 °C. The Mo precursor solution was elaborately dropped into silica support (MoO_3/H_2O/ SiO_2) molar ratio is equal to 3 mol% catalyst prepared by sol-gel method) until wet. The process was repeated until all Mo precursor solution is consumed. The mixture was then dried in oven at 80 °C for 12 hours. The obtained solid was in a horizontal tube furnace under a flow of air zero (60 ml/min) at different calcination temperature (500, 600 and 700 °C) by a heating rate of 1 °C/min. and hold at those temperature for 8 hours. After that, the sample is pressed, crushed and sieved into 600-850 micron. Similarly, the catalysts 20 mol% molybdenum oxide loadings will be also prepared.

This material is reserved for educational use only, not allowed for commercial use.
Forbidden to modify the content, and cite the document when use.

3.5.8 Temperature programmed desorption

Ammonia is probably the most frequently used probe molecule for acidity assessment. Its small molecular size allows one to probe almost all acid sites of both micro- and mesoporous materials NH_3-temperature-programmed desorption (NH_3-TPD) experiments were carried out using a TCD detector. Before adsorption, the samples (0.05 g) were heated to its calcination temperature in air zero for 1 hour (30 ml/min) and cooled to 50 °C. Adsorption of 10% NH_3/He was performed at 50 °C. After saturation, the samples were flushed with He at this temperature for 2 hours. TPD measurements were done from 50 to 900 °C with a heating rate of 10 °C/min, using He as a carrier gas.

3.6 CATALYTIC TESTING

Gas phase catalytic conversion of butyraldehyde can be investigated at atmospheric pressure in a continuous fixed bed down flow reactor made with quartz tube (8 mm O.D.). The catalyst bed was packed by quartz wool in the middle of the reactor. The reactor was installed onto the catalytic test rig which was located inside a temperature-controlled electrical furnace. The gas flows was controlled by mass flow controllers and checked by bubble flow meter. Before activity testing, the catalyst was activated by heating at 1° C/min to its calcination temperature and hold at that temperature for 1 hour under the stream of air zero (30 ml/min). The reactor was cooled to the reaction temperature (300-500 °C) under a flow of N_2 and then purged with carrier gas (30 ml/min of H_2) for half an hour prior to the reaction.

In each run, butyraldehyde vapour saturated at -1.12 °C was passed through the catalyst bed by a 30 ml/min flow of H_2.The catalytic test was continued for at least 10 hours on stream. The reacted gaseous mixture was flowed out of the reactor passing a gas sampling loop. In order to prevent condensation of products, the line after reactor was heated by heating tape. The product effluents were trapped at -70 ° C (vapor of liquid N_2). Description of the reactor set up and the reaction conditions are summarized in **Table 3.2**. The schematic diagram of the experimental setup is shown in **Figure 3.1**.

This material is reserved for educational use only, not allowed for commercial use.
Forbidden to modify the content, and cite the document when use.

Table 3.2 Description of the reactor set up and the reaction conditions

Parameters	Value
Reactor inside diameter (mm)	6
Reactor outside diameter (mm)	8
Total flow (ml/min)	~30
Bed length (mm)	~20
Catalyst weight (g)	0.1608
Contact time : W/F ($g.h.mol^{-1}$)	10-60
Catalyst size (μm)	600-850
Catalyst activation (before reaction)	Heating rate : 1°C/min Heat treatment : 500-700°C hold for 1 hour Gas : air zero (30 ml/min)
Carrier gas	H_2
Reaction temperature	300-500 °C
Reaction total pressure	Atmospheric pressure (~1 atm)

This material is reserved for educational use only, not allowed for commercial use.
Forbidden to modify the content, and cite the document when use.

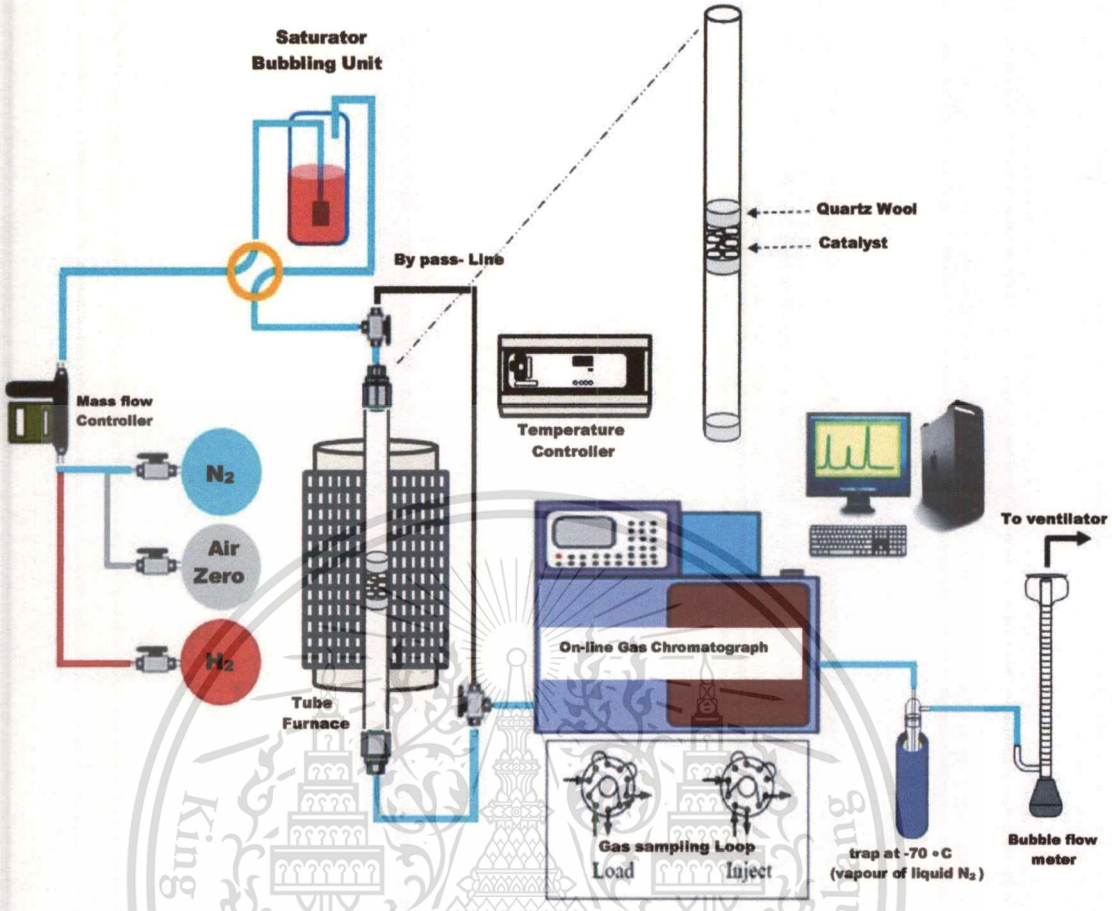

Figure 3.1 The schematic diagram of the catalytic testing rig

3.7 PRODUCTS ANALYSIS

The product analysis was generally performed using an on-line gas chromatograph. The gas sample is collected in gas sampling loop, then periodically injected into GC column (HP-5 capillary column for oxygenated compounds and HP-PLOT for light hydrocarbon compounds) connected to flame ionized detectors. The components were separated as they pass through the column with an inert carrier gas and their presence in the effluent will was and recorded as a chromatogram. The peak area from the chromatogram was measured and calculated as the peak area percentage. Then the unknown peak was identified using standard and the composition of

This material is reserved for educational use only, not allowed for commercial use.
Forbidden to modify the content, and cite the document when use.

product was determined by the normalization method. Then the unknown products were identified by gas chromatograph-mass spectrometer (GC-MS) technique.

This material is reserved for educational use only, not allowed for commercial use.
Forbidden to modify the content, and cite the document when use.

CHAPTER 4

RESULTS AND DISCUSSION

4.1 Characterization of MoO_3/SiO_2 Catalysts

4.1.1 Elemental Analysis and gas adsorption characteristics

The molybdenum oxide content of the catalysts was determined by inductively coupled plasma/atomic emission spectroscopy (ICP/AES) and X-ray fluorescence spectroscopy (XRF). The samples are designated as xMoSiy(z) when x is the loading of molybdenum oxides on silica support, y is the calcination temperature and z is the preparation method. The molybdenum oxide content, surface area, average pore diameter and average pore volume of the catalysts are given in **Table 4.1.**

Table 4.1 The molybdenum oxide content and gas adsorption characteristics of MoO_3/SiO_2 catalysts

Catalyst	Preparation method	MoO_3 loading (mol%)	Calcination temperature ($^{\circ}C$)	Elemental analysis (mol% of MoO_3)	BET surface area (m^2/g)	Average pore diameter (Å)	Pore volume (cc/g)
1MoSi500(s)	Sol-gel	1	500	1.04[a]	722	26.4	0.76
1MoSi600(s)			600	1.04[a]	487	63.09	0.67
1MoSi700(s)			700	1.04[a]	423	76.6	0.45
3MoSi500(s)		3	500	3.16[a]	657	29.9	0.71
3MoSi600(s)			600	3.16[a]	426	67.8	0.44
3MoSi700(s)			700	3.16[a]	294	165.8	0.23
5MoSi500(s)		5	500	5.09[a]	604	33.1	0.56
7MoSi500(s)		7	500	6.94[a]	497	31.1	0.52
10MoSi500(s)		10	500	9.71[a]	367	54.8	0.45
15MoSi500(s)		15	500	14.82[a]	267	100.7	0.39

This material is reserved for educational use only, not allowed for commercial use.
Forbidden to modify the content, and cite the document when use.

20MoSi500(s)		20	500	19.31[a]	214	122.6	0.21
3MoSi500(i)	Incipient wetness impregnation	3	500	3.32[b]	378	148.9	0.57
3MoSi600(i)			600	3.32[b]	324	228.6	0.25
3MoSi700(i)			700	3.32[b]	289	287.3	0.29
20MoSi500(i)		20	500	21.07[b]	159	278.9	0.16

[a] Elemental analysis by inductively coupled plasma/atomic emission spectroscopy (ICP/AES)

[b] Elemental analysis by X-ray fluorescence spectroscopy (XRF)

The catalysts prepared by sol–gel method exhibit very high surface area and micro-mesoporous nature of the silica support. Upon increasing the MoO_3 loading the surface area of the catalysts decreased gradually. It can be suggested that, as MoO_3 loading is increased, the crystalline molybdenum oxide clusters are formed on the amorphous silica support, reducing the total surface area of the catalyst. However, the catalysts prepared by sol–gel method show a very high surface area as compared to the catalysts prepared by impregnation method.

4.1.2 Structure and morphology of MoO_3/SiO_2 catalysts

The diffraction pattern of catalysts was obtained by X-ray powder diffraction technique (XRD). The CuKα was used as radiation source. The 2θ angle of the catalysts diffraction pattern was compared with 2θ angle of the reference diffraction pattern to identify their crystal structure. Crystalline phase structure of MoO_3/SiO_2 catalysts prepared by sol–gel method and calcined at 500 °C were characterized and identified by X-ray diffraction is shown in **Figure 4.1**. For comparison, the XRD pattern of pure silica is also included in the Figure.

This material is reserved for educational use only, not allowed for commercial use.
Forbidden to modify the content, and cite the document when use.

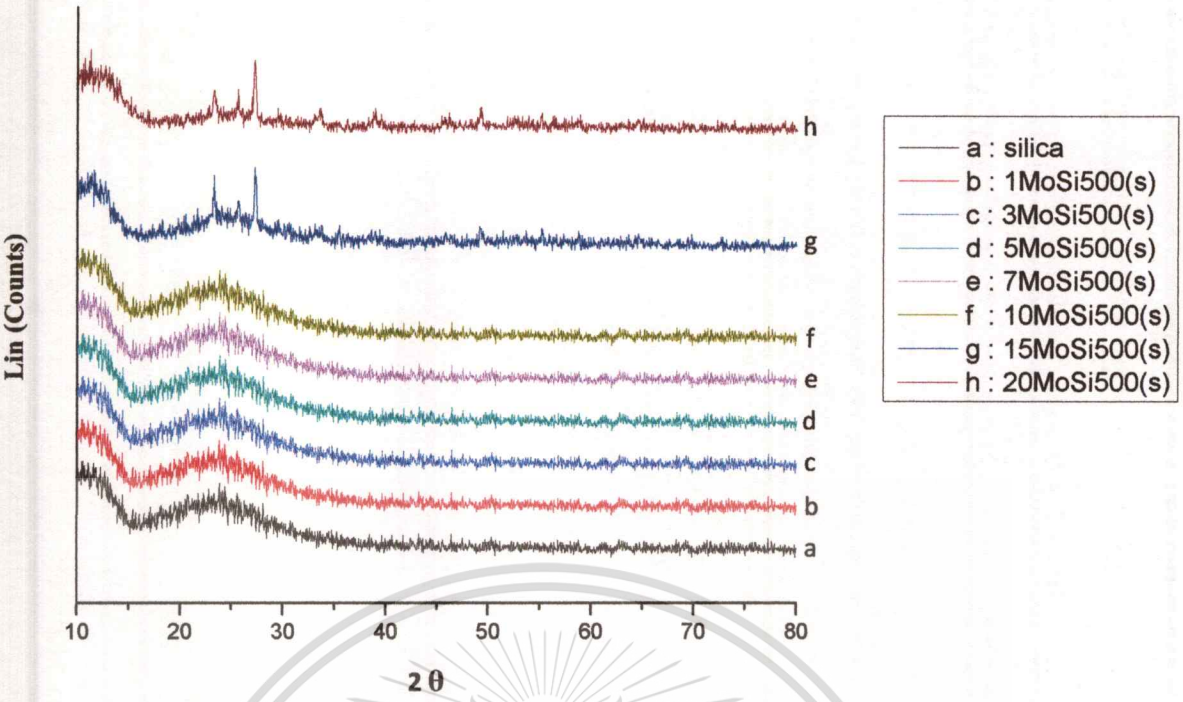

Figure 4.1 XRD patterns of silica (a) and MoO_3/SiO_2 : (b) 1MoSi500(s), (c) 3MoSi500(s) (d) 5MoSi500(s), (e) 7MoSi500(s), (f) 10MoSi500(s), (g) 15MoSi500(s) and (h) 20MoSi500(s)

From XRD analysis, the amorphous nature of the catalyst can be obtained up to 10 mol% MoO_3 loading **(Figure 4.1b-f)**. In consistent with the observed lower surface area, catalysts with 15 and 20 mol% MoO_3 loading **(Figure 4.1g-h)** show crystalline nature with intensed peaks at 23.4° , 25.8° and 27.4° corresponding to α-MoO_3 in the orthorhombic phase. No β -MoO_3 phase is observed in the structure because the samples were calcined at 500 °C, a temperature at which β -MoO_3 phase is not stable.

In a support manner, crystalline phase of α-MoO_3 can be observed from scanning electron micrographs **(Figure 4.2)** only at higher MoO_3 loading. The amorphous nature of the silica support can be seen at lower MoO_3 loading, leading to the high surface area of the catalysts. This suggests that a high dispersion of MoO_3 particle in the silica support can be obtained from sol-gel synthesis even at moderate molybdenum oxide loading (10 mol %).

This material is reserved for educational use only, not allowed for commercial use.
Forbidden to modify the content, and cite the document when use.

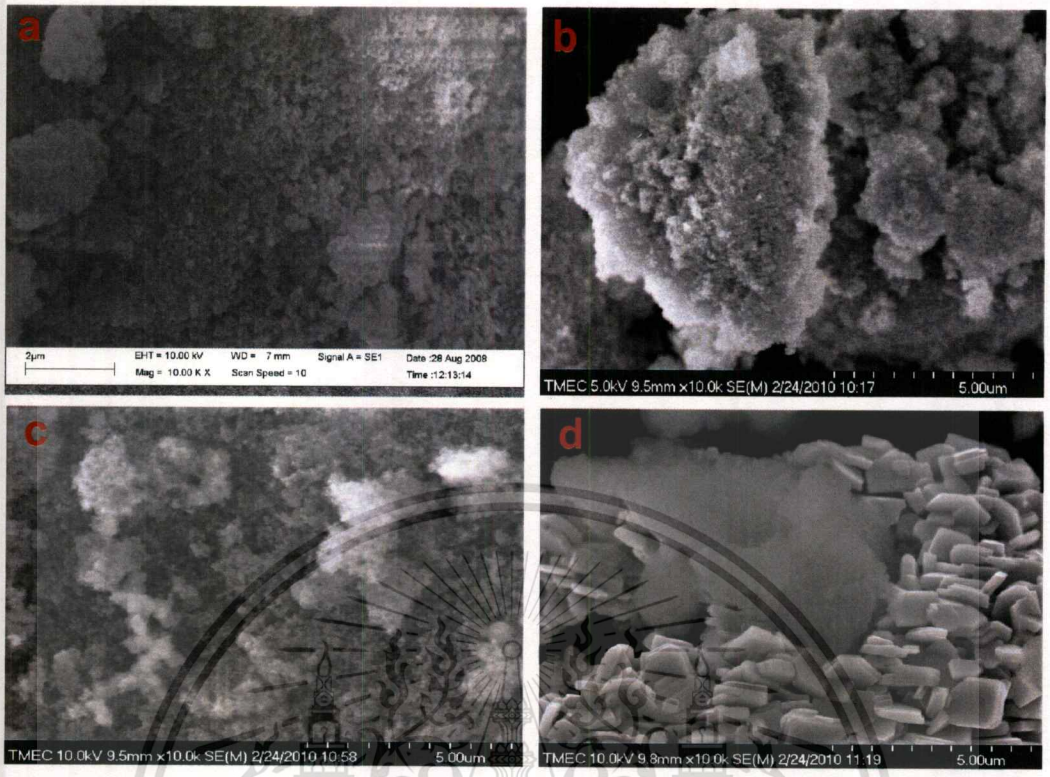

Figure 4.2 SEM micrographs of MoO_3/SiO_2 : (a) 1MoSi500(s), (b) 3MoSi500(s), (c) 10MoSi500(s) and (d) 20MoSi500(s)

However, TEM analysis **(Figure 4.3)** reveals high dispersion of MoO_3 nano-cluster. It was reported that the isolated MoO_3 species in tetrahedral coordination (MO_4) and some of oligomeric species are predominant on the silica support for the catalysts prepared by sol-gel method with low MoO_3 content **[113]**. 1MoSi500(s) **(Figure 4.3a)** shows high dispersion of isolated MoO_3 species, with a size comprised between 2 and 3 nm. The particle size of nano MoO_3 is found to be increase when increasing the MoO_3 loading as seen in the TEM image **(Figure 4.3b)** of the 3MoSi500(s). Moreover, the lower dispersion of MoO_3 species can be observed for 3MoSi500(s) as compared to 1MoSi500(s).

This material is reserved for educational use only, not allowed for commercial use.
Forbidden to modify the content, and cite the document when use.

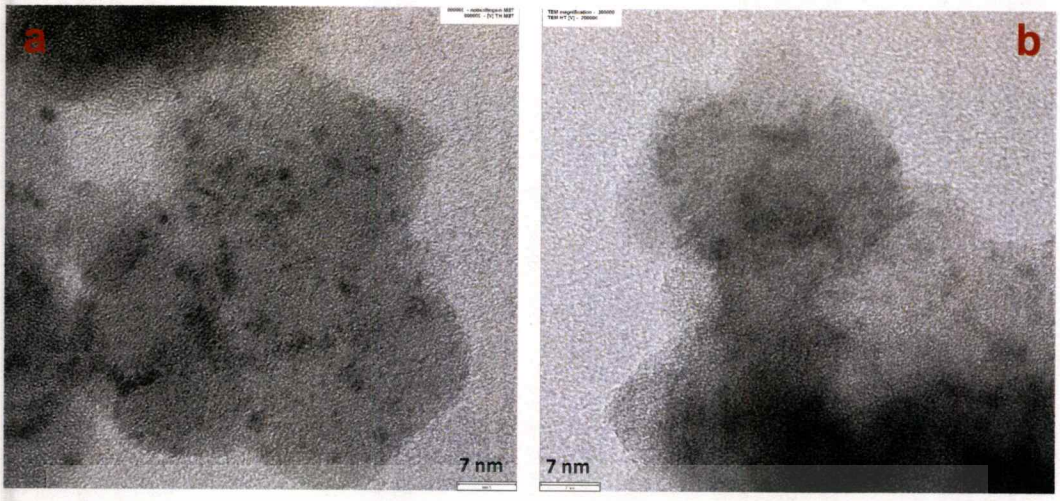

Figure 4.3 TEM micrographs of MoO_3/SiO_2 : (a) 1MoSi500(s) and (b) 3MoSi500(s)

It can be suggested that at all of molybdate ion precursors are completely incorporated to the silicon alkoxide sol network during hydrolysis and condensation step. Moreover, the appropriate pH (~ 5.5) at above isoelectric point of colloidal silicon alkoxide (IEP~ 2-3) in the sol allows the strong electrostatic interaction between silicon alkoxide network and molybdate ion precursors during polymerization step. This leads to the difficulty for the molybdate ion precursors to aggregate and agglomerate, because they are all surrounded by silicon alkoxide network. After the calcination process, molybdate precursor transformed to the isolated MoO_3 species in tetrahedral coordination (MO_4) and some of oligomeric species bound on the silica surface. However, the different molybdenum oxo species on the silica surface can be generated depending on MoO_3 content, calcination temperature and preparation method as will be further discussed.

The energy dispersive analysis of the catalysts also shows the dispersion of molybdenum oxide **(Figure 4.4)**. At the same MoO_3 content, it can be seen that the catalysts obtained from impregnation method exhibited the non-uniformly dispersed molybdenum on silica surface. This indicates that the dispersion and interaction between molybdenum oxide and silica support are relatively low. Meanwhile, the catalysts obtained from sol-gel method have good dispersion and strong interaction of molybdenum oxide particle with the silica support.

This material is reserved for educational use only, not allowed for commercial use.
Forbidden to modify the content, and cite the document when use.

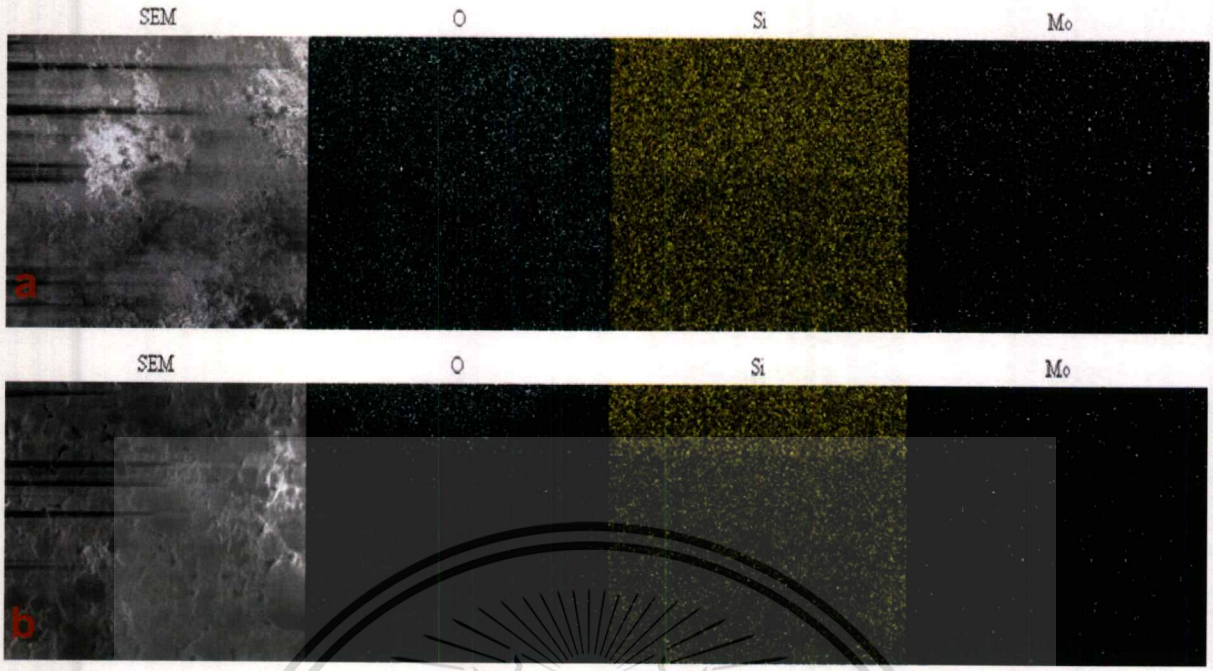

Figure 4.4 SEM-EDX images of MoO_3/SiO_2 : (a) 3MoSi500(s) and (b) 3MoSi500(i)

For both catalysts prepared by sol-gel and impregnation method, the crystalline species are not formed at the low MoO_3 content for all calcinations temperature **(Figure 4.5).**

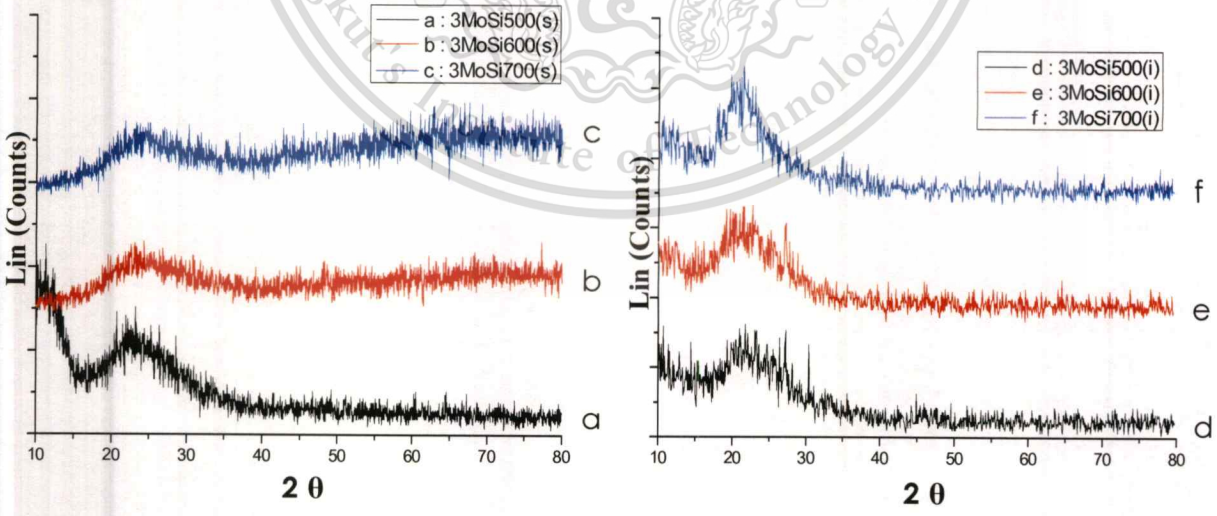

Figure 4.5 XRD patterns of MoO_3/SiO_2 : (a) 3MoSi500(s), (b) 3MoSi600(s), (c) 3MoSi700(s), (d) 3MoSi500(i), (e) 3MoSi600(i) and (f) 3MoSi700(i)

This material is reserved for educational use only, not allowed for commercial use.
Forbidden to modify the content, and cite the document when use.

Hence, XRD analysis is applicable for phase determination only at high concentration of molybdenum oxide (15-20 mol % MoO_3). However, at the high molybdenum oxide content (i.e. 20 mol % MoO_3), the catalyst prepared by impregnation method, XRD pattern show higher crystallinity as compared to that prepared by sol-gel method, as seen in the **Figure 4.6**.

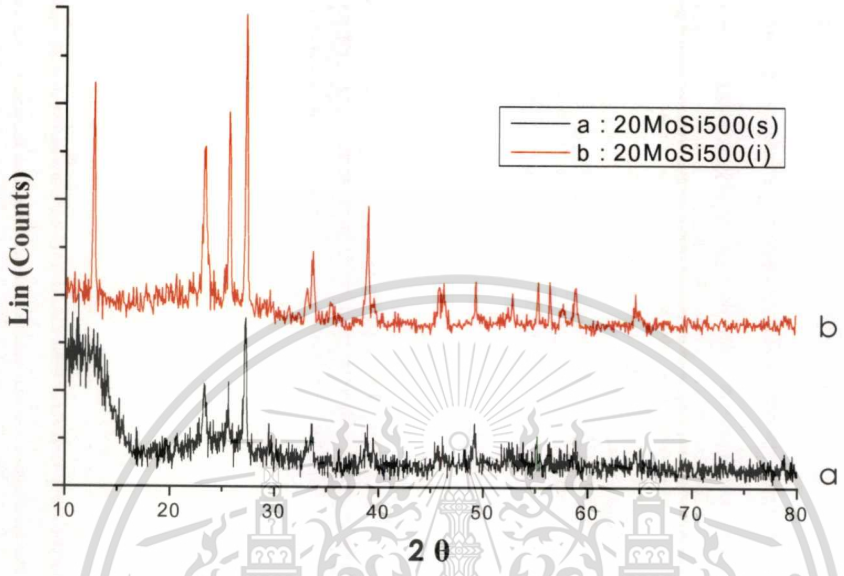

Figure 4.6 XRD patterns of MoO_3/SiO_2 : (a) 20MoSi500(s) and (b) 20MoSi500(i)

Figure 4.7 SEM micrographs of MoO_3/SiO_2 : (a) 20MoSi500(s) and (b) 20MoSi500(i)

In line with XRD results, the crystal of α-MoO_3 on the silica surface of 20 mol% MoO_3/SiO_2 catalysts can be observed from SEM micrographs **(Figure 4.7)**. It can be seen that, the average α-MoO_3 crystal size of the catalyst obtained from sol-gel method is smaller than that obtained from impregnation method. It can be suggested that, α-MoO_3 prepared by sol-gel method possess the

This material is reserved for educational use only, not allowed for commercial use.
Forbidden to modify the content, and cite the document when use.

stronger interaction with silica surface leading to a better in dispersion as discuss earlier **(Figure 4.3)**.

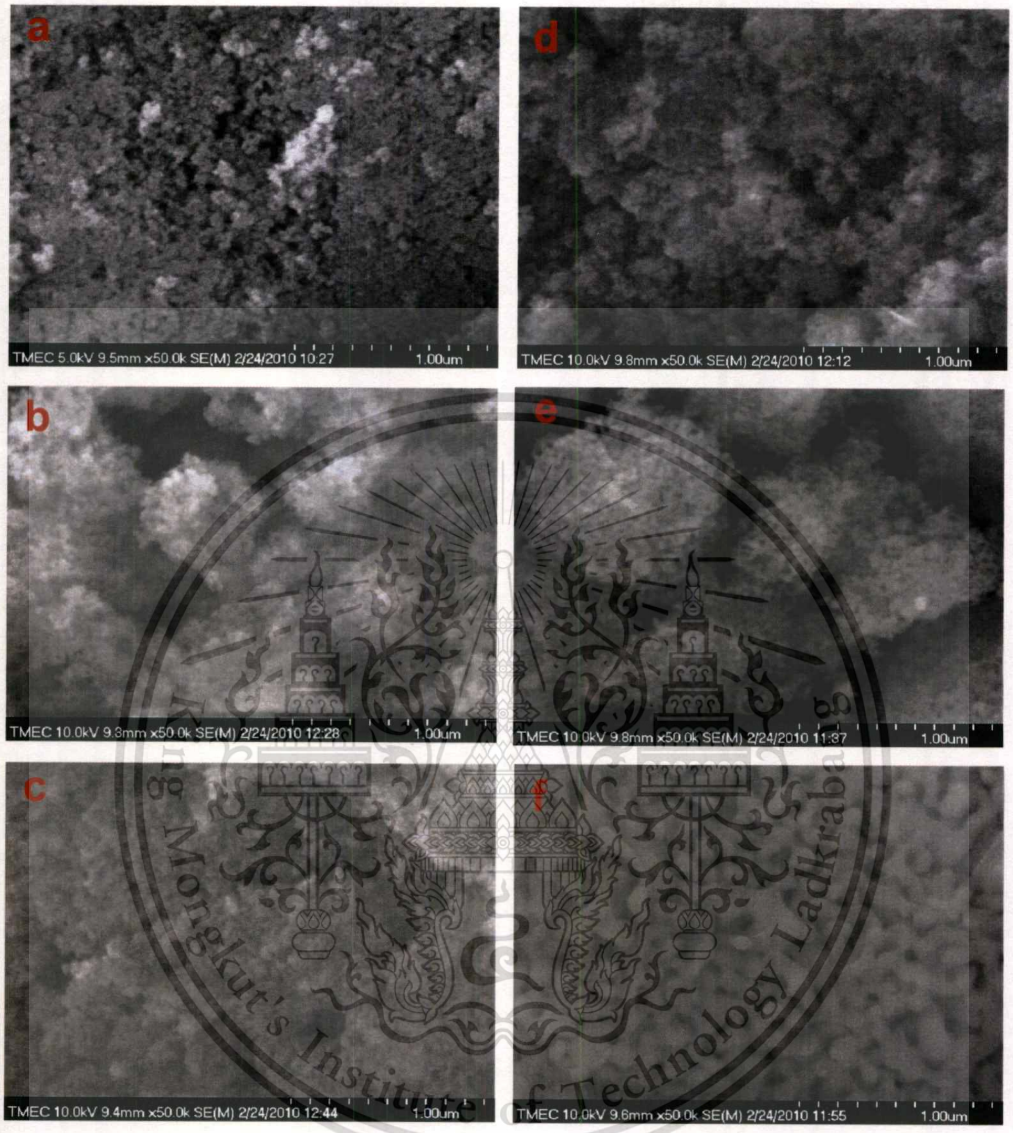

Figure 4.8 SEM micrographs of MoO_3/SiO_2 : (a) 3MoSi500(s), (b) 3MoSi600(s), (c) 3MoSi700(s), (d) 3MoSi500(i), (e) 3MoSi600(i) and (f) 3MoSi700(i)

For the samples with low molybdenum oxide loading, SEM analysis**(Figure 4.8)** reveals a significant difference in the surface morphology of the catalysts obtained from different preparation method and calcination temperature (600-700 °C). Although, XRD analysis **(Figure 4.5)** does not show the difference in the crystallinity for both catalysts, it can be seen that at higher calcination temperature (i.e.700 °C), the silica support of the catalysts obtained from impregnation method are sintered. This leads to an increase in average grain size and a dramatic

This material is reserved for educational use only, not allowed for commercial use.
Forbidden to modify the content, and cite the document when use.

decrease in surface area, as given in the **Table 4.1**. Meanwhile, the catalysts prepared by sol-gel method exhibit a higher stability of the silica support. This is because the silica support obtained from sol-gel synthesis exhibits the large chain network in three dimensions via siloxane bonds from polymerization process. This leads to the transcendent thermal stability. In contrast, the commercial silica used for impregnation process was obtained from precipitation method which exhibit the small aggregate of silica network. Hence, the fused and dense structure from sintering process is obtained for this silica.

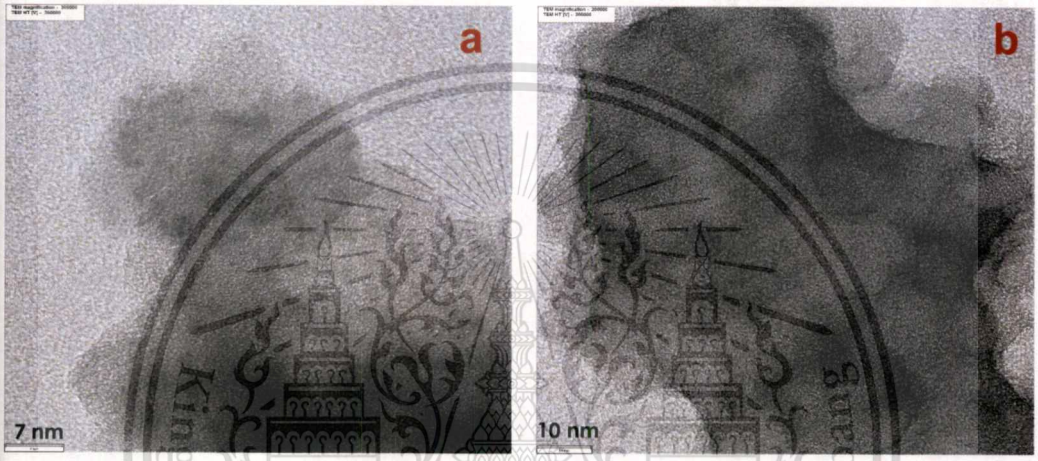

Figure 4.9 TEM micrographs of MoO_3/SiO_2 : (a) 3MoSi500(s), (b) 3MoSi700(s)

Although, no significant different in morphology can be observed for the catalyst obtained from sol-gel method at high calcination temperature, the calcination temperature readily effects the dispersion of molybdenum species as seen by TEM analysis **(Figure 4.9)**. However, the low dispersion of MoO_3 species can be observed for 3MoSi700(s) as compared to 3MoSi500(s). This is because at high calcination temperature, the isolated and oligomeric MoO_3 species tend to agglomerate to polymeric and bulk MoO_3 crystalline phase.

This material is reserved for educational use only, not allowed for commercial use.
Forbidden to modify the content, and cite the document when use.

4.1.3 The active species of MoO_3/SiO_2 catalysts

The nature and surface distribution of the molybdenum species present on silica support can be validated by H_2- temperature programmed reduction (H_2-TPR).

The H_2-TPR profiles of the catalysts prepared by sol-gel method with different molybdenum oxide loading are comparatively shown in **Figure 4.10**

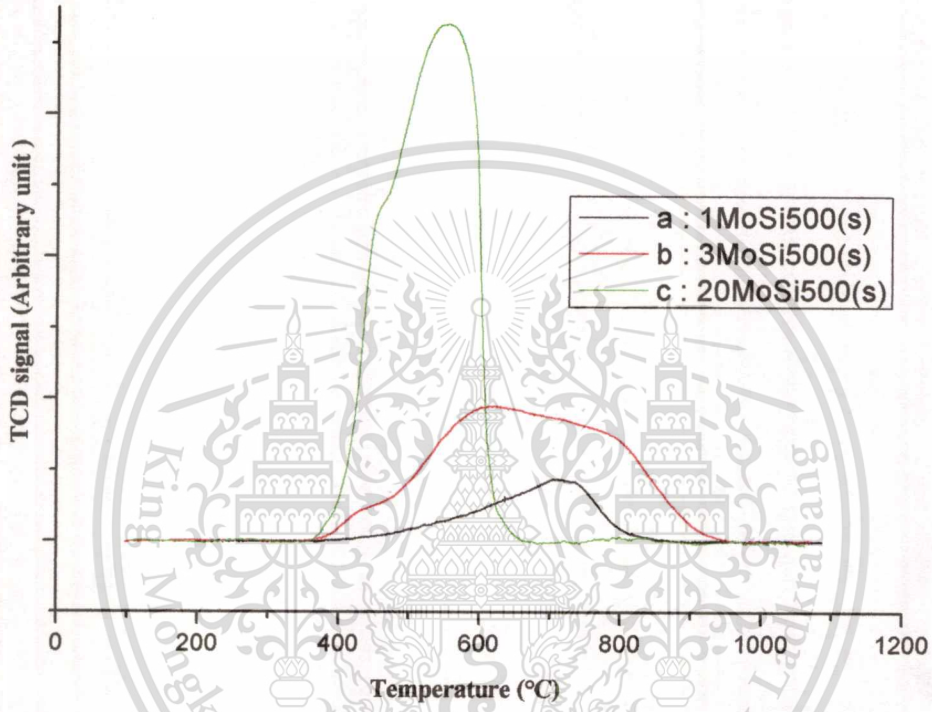

Figure 4.10 H_2-TPR profiles of MoO_3/SiO_2: (a) 1MoSi500(s), (b) 3MoSi500(s) and (c) 20MoSi500(s)

In **Figure 4.10**, the TPR profiles of 20MoSi500(s) show the higher amount of H_2 consumption as compared to those with low MoO_3 loading. Moreover, the differences in reduction temperature are observed for different MoO_3 loading. It can be seen that, the increase in MoO_3 loading from 1 to 20 mol % causes a marked shift to lower reduction temperature. This indicates that the catalyst with high MoO_3 loading particularly provides the species that exhibit a weak interaction with the silica support. However, using a least-squares fitting program, such spectra have been resolved into the discrete Gaussian-shaped peaks. It can be suggested that all catalysts contain multi-species components. The deconvoluted TPR profiles for 1MoSi500(s), 3MoSi500(s) and 20MoSi500(s) are shown in **Figure 4.11.**

This material is reserved for educational use only, not allowed for commercial use.
Forbidden to modify the content, and cite the document when use.

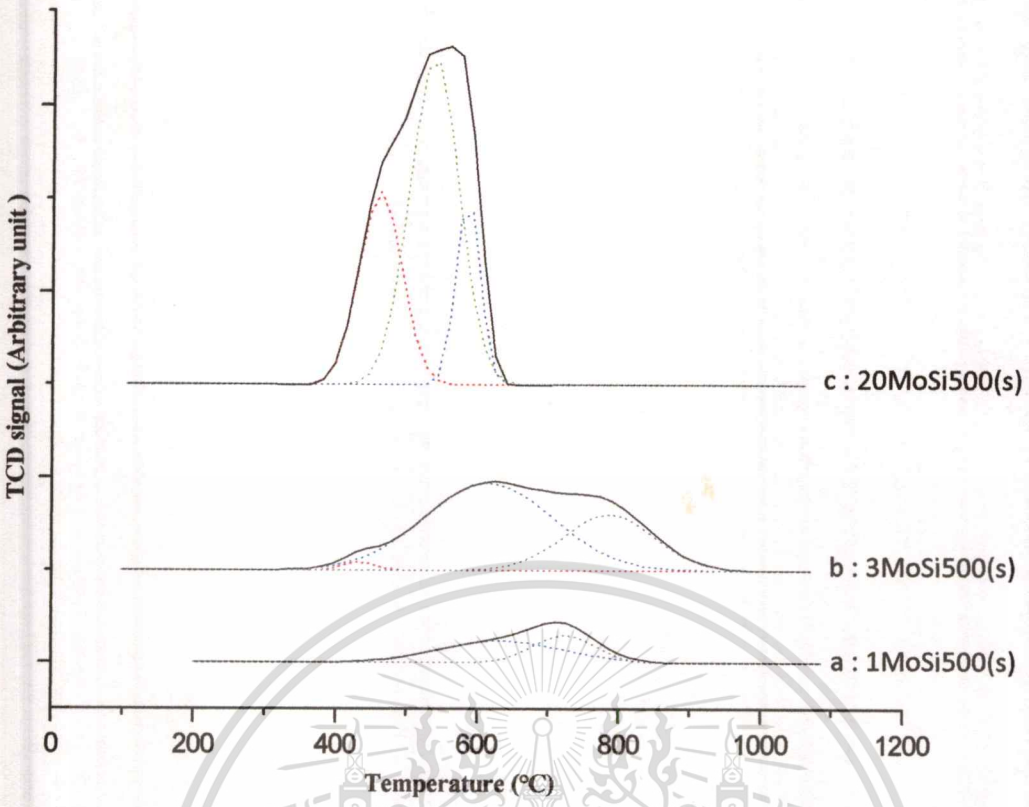

Figure 4.11 H_2-TPR profiles with the Gaussian deconvolution of MoO_3/SiO_2 : (a) 1MoSi500(s), (b) 3MoSi500(s) and (c) 20MoSi500(s)

The fitting parameters of TPR profile, types of species, the temperature of peak maxima (T_{Mi}), and percentage peak area (A_i) are summarized in **Table 4.2**.

Table 4.2 Influence of MoO_3 loading on H_2-TPR of MoO_3/SiO_2: types of species, the temperature of peak maxima (T_{Mi}) and percentage peak area (A_i)

Species / Catalyst	Polymeric MoO_3 *Pm*		Crystalline MoO_3 *Mc*		Oligomeric MoO_3 *Om*		Isolated MoO_3 *Im*	
	T_{M1} (°C)	A_1 (%)	T_{M2} (°C)	A_2 (%)	T_{M3} (°C)	A_3 (%)	T_{M4} (°C)	A_4 (%)
1MoSi500	-	-	-	-	633	61.21	723	38.79
3MoSi500	432	1.63	-	-	614	67.64	784	30.73
20MoSi500	460	28.51	535	55.78	583	15.71	-	-

This material is reserved for educational use only, not allowed for commercial use.
Forbidden to modify the content, and cite the document when use.

From the deconvoluted TPR profiles, several species of MoO_3 can be observed in **Figure 4.11**. For the sample with high molybdenum oxide loading (20 mol %), it can be suggested that the first peak (T_{M1}) at low reduction temperature (T_{M1} ~ 460 °C) refers to the reduction of polymeric MoO_3 species (*Pm*) which is the precursor of the crystalline MoO_3 (*Mc*).

The crystalline MoO_3 (*Mc*) species can be reduced at relatively higher temperature ~ 535 °C (T_{M2}). On the other hand, the third reduction temperature (T_{M3} ~ 583 °C) reveals the peak of oligomeric MoO_3 (*Oc*) species that possess a stronger interaction with the silica support as compared to the polymeric (*Pm*) and crystalline MoO_3 (*Mc*) species **[114]**. It can be suggested that crystalline MoO_3 is predominant for the catalyst with high molybdenum oxide loading, which exhibits a "weak type" interaction between MoO_3 and SiO_2 surface.

In the case of low MoO_3 loading (1 and 3 mol %), it can be seen that crystalline MoO_3 (*Mc*) species cannot be observed. On the other hand, oligomeric MoO_3 (*Oc*) species: (T_{M3} ~ 610-630 °C) and the well- dispersed isolated MoO_3 species (*Im*) : (T_{M4} ~ 720-780 °C) are the main species for these samples. The well- dispersed isolated MoO_3 species (*Im*) is defined as the single molybdate species in tetrahedral coordination (MO_4) which can be reduced only at high temperature (~ 720-780 °C) due to the strong interaction with the silica support. Nevertheless, some of polymeric species (*Pm*): (T_{M1} ~ 432 °C) can be revealed for 3MoSi500(s).

From a systematic inspection of the fitting parameters **(Table 4.2)**, it can be seen that oligomeric MoO_3 species can be revealed for all catalysts whereas crystalline MoO_3 species can be observed only for the catalyst with high molybdenum oxide loading. In contrast, isolated MoO_3 species can be observed only for the catalyst with low molybdenum oxide loading (i.e. 1-3 mol %).

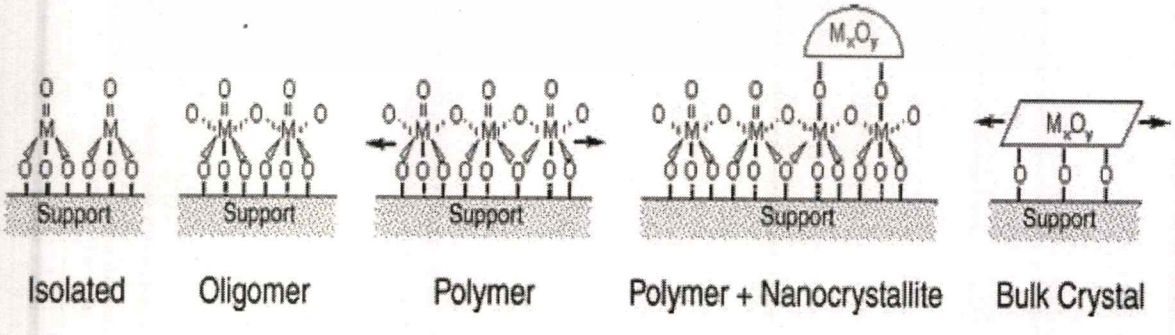

Figure 4.12 As describe previously in **Figure 2.13**

This material is reserved for educational use only, not allowed for commercial use.
Forbidden to modify the content, and cite the document when use.

In a support manner, DR-UV analysis **(Figure 4.13)** of MoO_3/SiO_2 samples exhibit an absorption band in the range of 200–400 nm. The catalysts with low MoO_3 loading (1MoSi500(s) and 3MoSi500(s)) exhibit the absorption bands around 240 and 290 nm which the former band (240 nm) is attributed to MoO_3 species in tetrahedral coordination and the latter band (290 nm) is assigned to the electrons transitions caused by Mo–O–Mo bonds in the polymeric MoO_3 species. It can be seen that an increase in the MoO_3 loading, the ratio of the intensity of the absorbance at 290 nm to 240 nm is increased. This indicates that the isolated MoO_3 species tend to aggregated to oligomeric or polymeric species on the silica surface. However, an increase in the absorption band at over 320 nm which attributed to the electron transition in the dense phase of MoO_3 **[115]** is observed for the catalysts with high MoO_3 loading (i.e., 20MoSi500(s)).

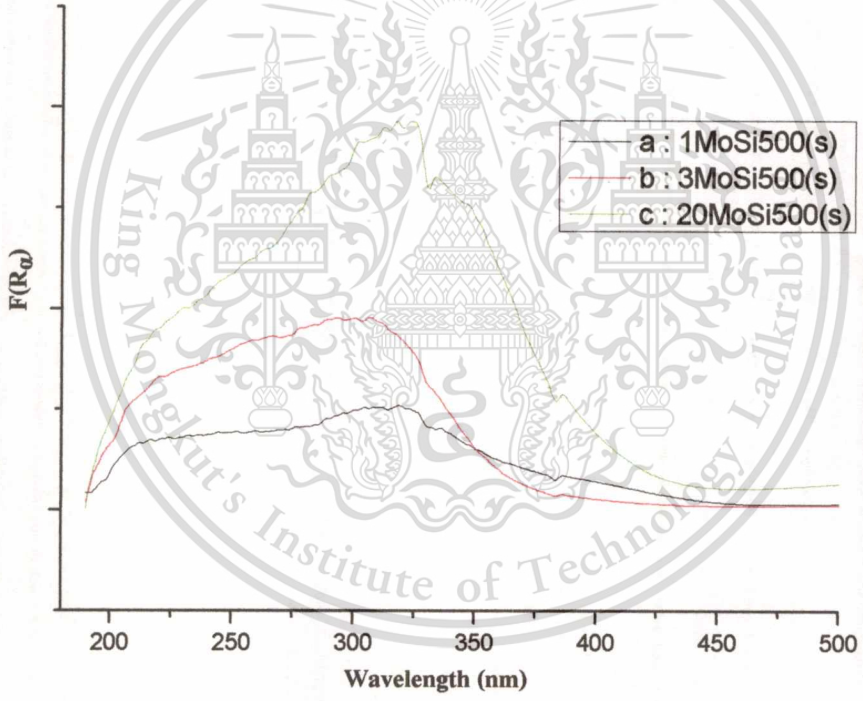

Figure 4.13 DR-UV profiles of MoO_3/SiO_2: (a) 1MoSi500(s), (b) 3MoSi500(s) and (c) 20MoSi500(s)

This material is reserved for educational use only, not allowed for commercial use.
Forbidden to modify the content, and cite the document when use.

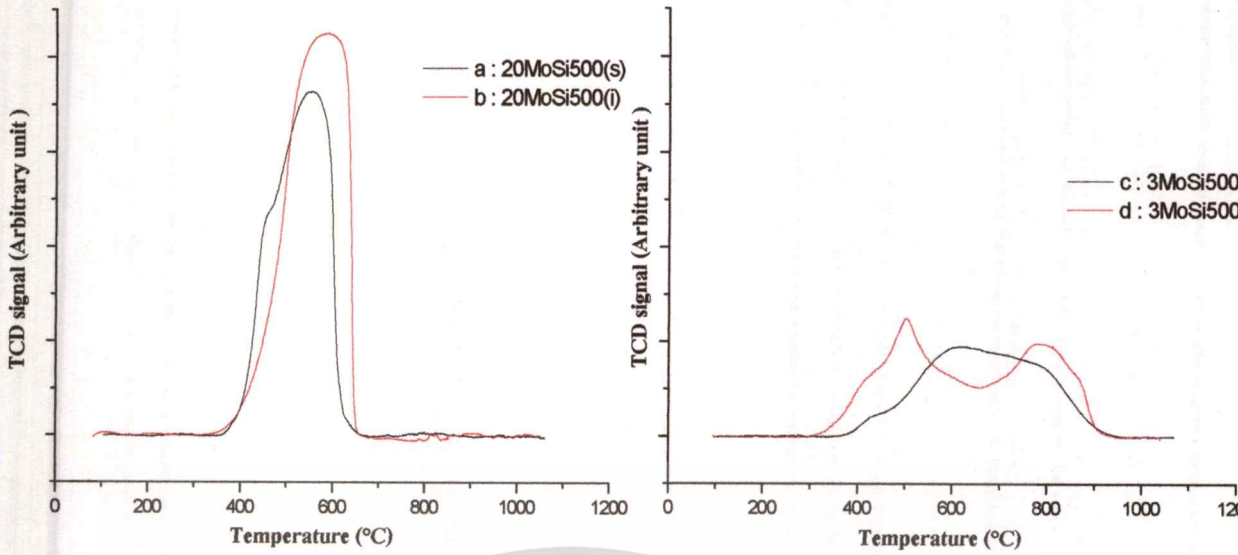

Figure 4.14 H_2-TPR profiles of MoO_3/SiO_2: (a) 20MoSi500(s), (b) 20MoSi500(i), (c) 3MoSi500(s) and (d) 3MoSi500(i)

Figure 4.14 shows the TPR profiles of the MoO_3/SiO_2 catalysts prepared from different preparation method. For the high MoO_3 loading catalyst (20 mol %), it can be seen that there is no significant different in reducibility of MoO_3 species for both preparation methods. This suggests that both catalysts possess the crystalline α-MoO_3 as the active species as evidenced by XRD analysis **(Figure 4.6)**. However, the catalyst obtained from impregnation method shows the higher amount of H_2 consumption as compared to that obtained from sol-gel method. This is due to the fact that α-MoO_3 obtained from impregnation method exhibits weak interaction with silica support as described earlier **(Figure 4.7)**.

In consistent with the XRD analysis **(Figure 4.6)** of 20MoSi500(s) and 20MoSi500(i), catalyst prepared by impregnation method exhibits higher crystallinity as compared to that prepared by sol-gel method. Moreover, SEM analysis also **(Figure 4.7)** clearly shows that the average α-MoO_3 crystal size of the catalyst obtained from impregnation method is larger than that obtained from sol-gel method. In the case of low MoO_3 loading (3 mol %), the catalyst prepared by impregnation method shows the distinct peak at about 400-600 °C which reveals the existence of polymeric and crystalline MoO_3 species. However, it can be seen that the higher extent of H_2 consumption for these species can be obtained over 3MoSi500(i). It is suggested that polymeric and crystalline MoO_3 species are predominant for the catalyst prepared by impregnation method at low MoO_3 loading (3 mol %). In contrast, the isolated MoO_3 is the main species only for the

This material is reserved for educational use only, not allowed for commercial use.
Forbidden to modify the content, and cite the document when use.

catalyst prepared sol-gel method. This is in line with the energy dispersive analysis **(Figure 4.4)** of 3MoSi500(s) and 3MoSi500(i) reveal that the catalyst obtained from sol-gel method have good dispersion of molybdenum oxide. This result supports the formation of isolated MoO_3 species in tetrahedral coordination (MO_4) for the catalysts prepared by sol-gel method with low MoO_3 content as discussed in **Figure 4.3**. Despite, XRD analysis **(Figure 4.5)** cannot show the different in phase structure as it is applicable for phase determination only at high concentration of molybdenum oxide (15-20 mol % MoO_3).

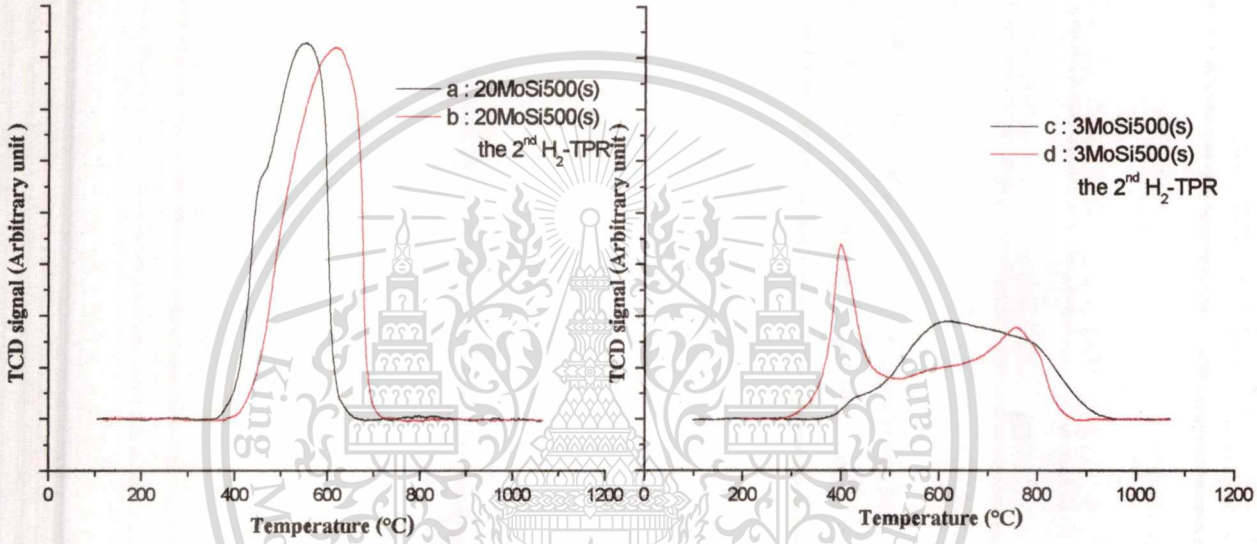

Figure 4.15 H_2-TPR profiles of MoO_3/SiO_2 : (a) 20MoSi500(s), (b) 20MoSi500(s) : the 2nd H_2-TPR, (c) 3MoSi500(s) and (d) 3MoSi500(s) : the 2nd H_2-TPR

To investigate the change in the nature of molybdenum oxide species caused by reduction/oxidation, the secondary H_2-TPR was performed. After the primary H_2-TPR, the samples were slowly cooled down to 50°C under a flow of N_2. Then, they were re-calcined under a flow of air zero in order to recover the molybdenum oxide species. The re-calcination was carried out at 500 °C using a heating rate of 1°C /min for 2 hours.

From **Figure 4.15**, the secondary H_2-TPR profiles show that crystalline α-MoO_3 was recovered for the high MoO_3 loading catalyst (20 mol %) as indicated by the similar H_2 consumption at about 500-600 °C. Interestingly, the peak is shifted to the higher reduction temperature. This suggests that the larger crystal of α-MoO_3 was formed after re-calcination. Hence, the higher temperature was required for the reduction. Formation of the large crystal of α-

This material is reserved for educational use only, not allowed for commercial use.
Forbidden to modify the content, and cite the document when use.

MoO_3 was attributed from sintering of MoO_3 species during the primary H_2-TPR. Hence, when this species was re-oxidized in air zero, the larger crystal of α-MoO_3 was generated. In the case of low MoO_3 loading (3 mol %), the higher extent of H_2 consumption at about 400-500 °C can be observed in the secondary H_2-TPR. It can be suggested that the isolated MoO_3 species tend to agglomerate to polymeric species after the first reduction/oxidation process.

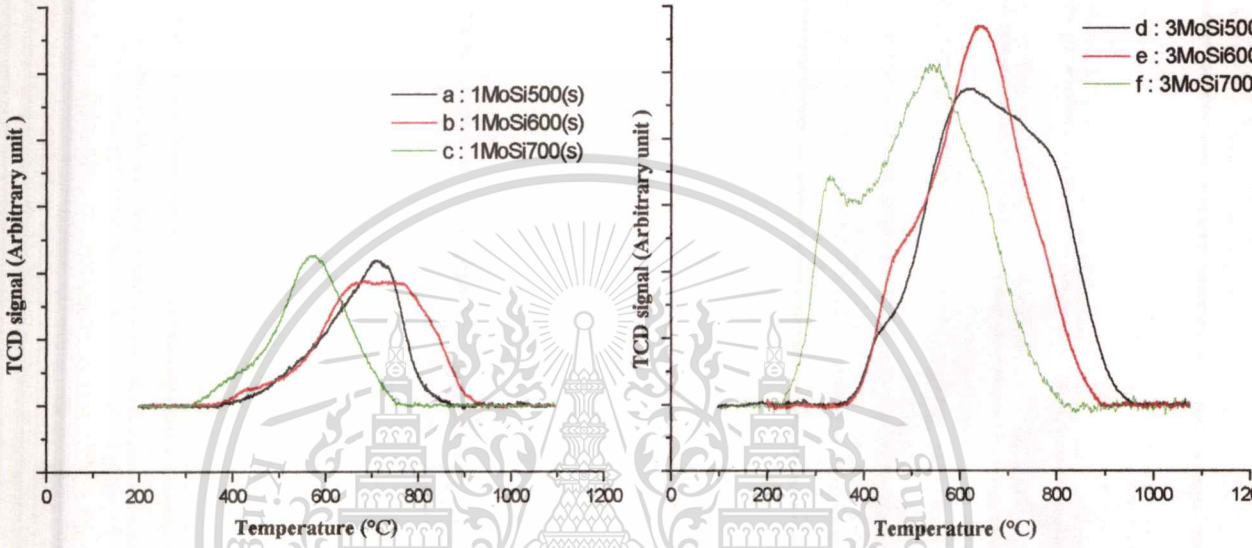

Figure 4.16 H_2-TPR profiles of MoO_3/SiO_2: (a) 1MoSi500(s), (b) 1MoSi600(s), (c) 1MoSi700(s), (d) 3MoSi500(s), (e) 3MoSi600(s) and (f) 3MoSi700(s)

Figure 4.16 show the TPR profiles of 1 and 3 mol% MoO_3/SiO_2 catalysts prepared by sol-gel method with different calcination temperature. For 1 mol% MoO_3/SiO_2 catalysts, it can be seen that there is no significant change can be observed when increasing calcination temperature from 500 to 600 °C. In contrast, the increase in calcination temperature from 500 to 700 °C causes a marked shift of the reduction temperature to lower temperature. It can be suggested that the isolated and oligomeric MoO_3 species tend to agglomerate to polymeric and crystalline MoO_3 at high temperature (700 °C). A similar phenomenon is also observed for 3 mol% loading. Although, XRD analysis of 3 mol% MoO_3/SiO_2 catalysts **(Figure 4.5)** do not show the difference in the crystallinity, it can be seen the significant different in reducibility of MoO_3 species for different calcination temperature as a manner similar to 1 mol% loading. Moreover, it is obvious that 3MoSi700(s) possess the two distinct peaks at about ~300-400 °C and 500-600 °C.

This material is reserved for educational use only, not allowed for commercial use.
Forbidden to modify the content, and cite the document when use.

This suggests that the formation of polymeric and crystalline MoO_3 were attributed from sintering of MoO_3 species after calcined at 700 °C.

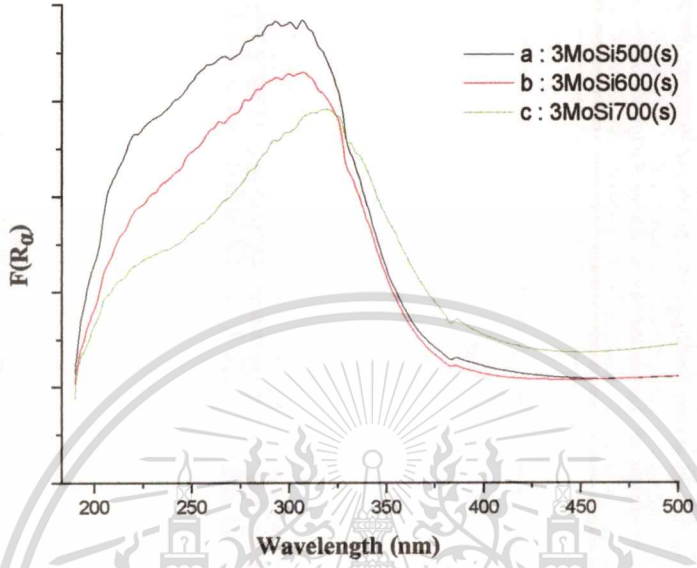

Figure 4.17 H_2-TPR profiles of MoO_3/SiO_2: (a) 3MoSi500(s), (b) 3MoSi600(s), and (c) 3MoSi700(s)

In consistent with the TPR results **(Figure 4.16)**, DR-UV analysis **(Figure 4.17)** shows that the increase in the calcination temperature give a higher ratio of the intensity of the absorbance at 290 nm (polymeric MoO_3 species) to 240 nm (isolated MoO_3 species). This suggests that the isolated MoO_3 species tend to aggregate to polymeric species on the silica surface. In particular, an increase in the absorption band at over 320 nm (crystalline MoO_3 species) is observed for the catalyst with high calcinations temperature (i.e., 3MoSi700(s)).

This material is reserved for educational use only, not allowed for commercial use.
Forbidden to modify the content, and cite the document when use.

4.2 Study of butyraldehyde conversion

4.2.1 Products distribution of butyraldehyde conversion

Products distribution is studied in the butyraldehyde conversion over 3MoSi500(s) catalyst with various contact time (W/F of 10-60 g.h.mol^{-1}). The catalytic performance is observed by the conversion and yield as shown in **Figure 4.18**

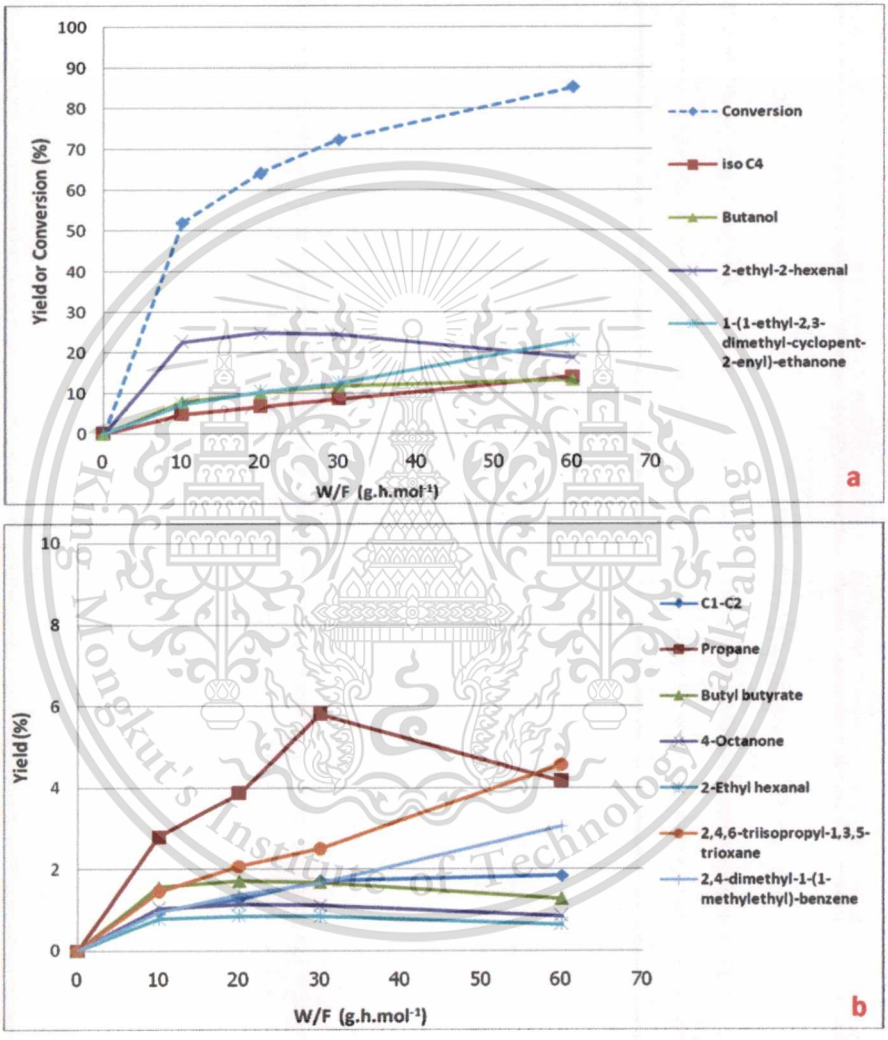

Figure 4.18 Conversion and product yield over 3MoSi500(s) catalyst as function of contact time : (a) major products and (b) minor products

** Reaction conditions; Catalyst:3MoSi500(s), Carrier gas:H_2, Temperature:500 °C, Flow rate of saturated vapour of feed plus Carrier gas:30 ml.min^{-1}, Pressure:1 atm, The results collect from initial state.*

This material is reserved for educational use only, not allowed for commercial use.
Forbidden to modify the content, and cite the document when use.

It can be seen that the conversion of butyraldehyde is increased to 85.17% when using contact time up to 60 g.h.mol^{-1}**(Figure 4.18a)**. This result is generally expected since increasing contact time which allows a better chance for the reactant to interact with the catalyst active sites. From the products distribution results, it can be seen that the major products for this catalyst comprise iso C4 hydrocarbon, butanol, 2-ethyl-2-hexenal and 1-(1-ethyl-2,3-dimethyl-cyclopent-2-enyl)-ethanone. In addition, the minor products comprise C1-C2 hydrocarbon, propane, butyl butyrate, 4-octanone , 2-Ethyl hexanal, 2,4,6-triisopropyl-1,3,5-trioxane and 2,4-dimethyl-1-(1-methylethyl)-benzene.

Considering the major products yield, it is observed that the iso C4 compounds and butanol yield are increased together with an increase in contact time, as well as the reaction conversion. This indicates that iso C4 compounds and butanol yield are generated in parallel. It is known that butanol is generated via hydrogenation of butyraldehyde. Consequently, butanol may undergo dehydration and subsequent isomerization to iso C4 hydrocarbon as shown below **(Figure 4.19)**.

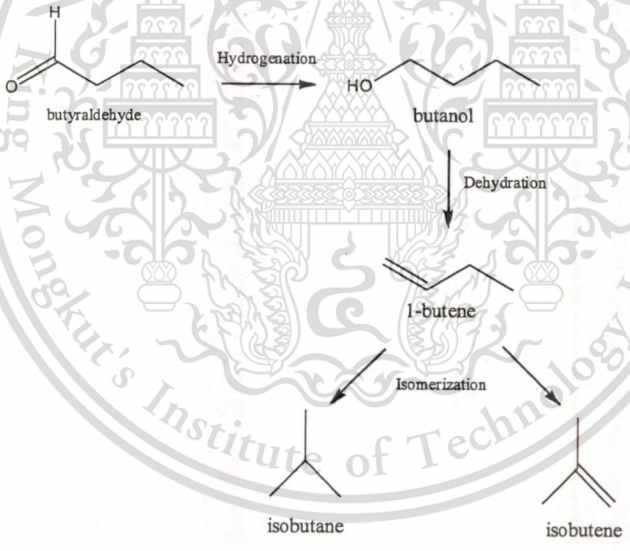

Figure 4.19 Formation of butanol and iso C4 hydrocarbon

The formation of 2-ethyl-2-hexenal (major of dimer product) can also take place via acid-catalyze condensation reaction **[110-112]**. However, it can be seen that the 2-ethyl-2-hexenal yield is continuously decreased while the 1-(1-ethyl-2,3-dimethyl-cyclopent-2-enyl)-ethanone (major of trimer product) yield appears to be increased, when increase contact time from 30 to 60 g.h.mol^{-1} This suggests that 1-(1-ethyl-2,3-dimethyl-cyclopent-2-enyl)-ethanone is formed by secondary reaction of 2-ethyl-2-hexenal **(Figure 4.18)**. As contact time increase, 2-ethyl-2-

This material is reserved for educational use only, not allowed for commercial use.
Forbidden to modify the content, and cite the document when use.

hexenal can undergo oligomerization and decarbonylation, leading to the increase in 1-(1-ethyl-2,3-dimethyl-cyclopent-2-enyl)-ethanone yield as shown in **Figure 4.18a**.

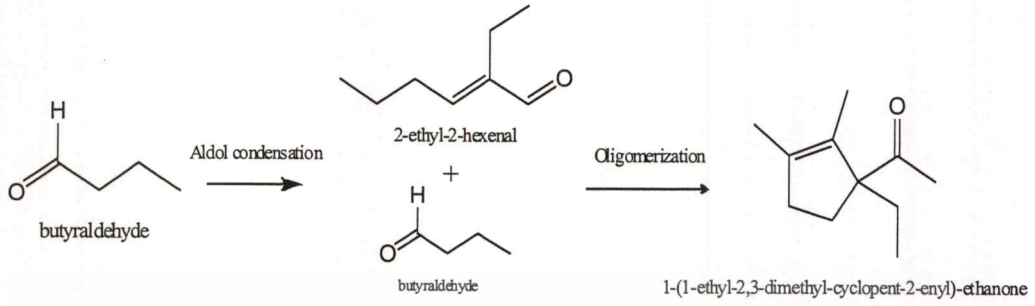

Figure 4.20 Formation of 2-ethyl-2-hexenal and -(1-ethyl-2,3-dimethyl-cyclopent-2-enyl)-ethanone

In addition to the major products discussed earlier, the minor product is also considered. It can be observed that the formation of propane (C3) indicates the decarbonylation activity of the catalyst.

Figure 4.21 Formation of propane

Moreover, C1-C2 hydrocarbon can be generated via cracking reaction of C3 and iso C4 compounds. It can be seen the slightly increase in C1-C2 yield while increasing in contact time **(Figure 4.18b)**. This suggests that the cracking reaction is increased when increasing in active site. However, it can be seen that the other trimer products (2,4,6-triisopropyl-1,3,5-trioxane and 2,4-dimethyl-1-(1-methylethyl)-benzene) yield is dramatically increased while the other dimer products (Butyl butyrate, 4-Octanone and 2-Ethyl hexanal) yield appears to be decreased, when increase the amounts of catalyst from 30 to 60 g.h.mol^{-1} **(Figure 4.18a).** This suggests that trimer products are formed by secondary reaction of dimer products. As contact time increase, dimer product can undergo condensation, leading to the increase in trimer product yield. The overall

This material is reserved for educational use only, not allowed for commercial use.
Forbidden to modify the content, and cite the document when use.

reaction pathways for butyraldehyde conversion over MoO_3/SiO_2 catalyst can be illustrated as shown in **Figure 4.22.**

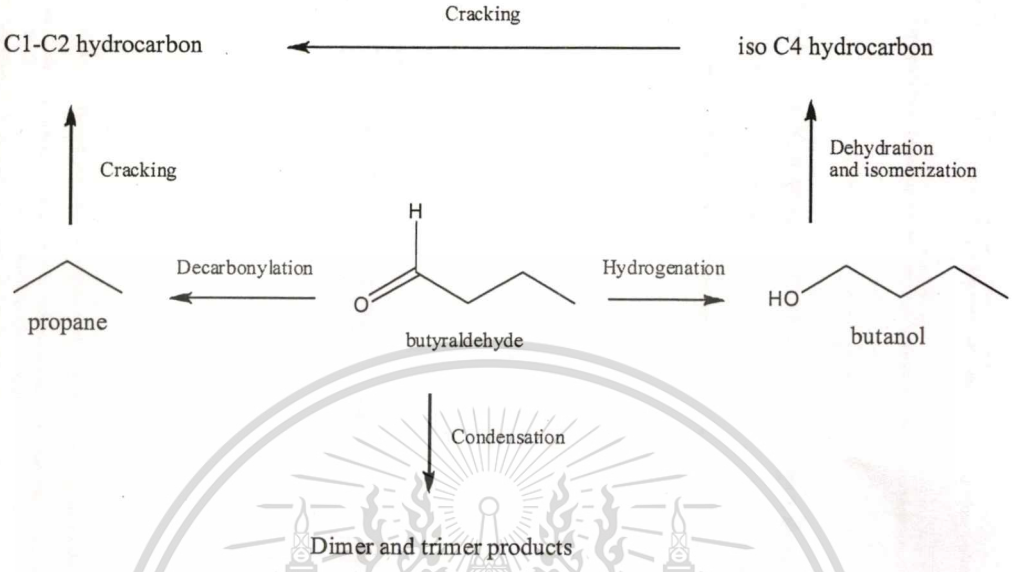

Figure 4.22 The overall reaction pathways for butyraldehyde conversion over MoO_3/SiO_2 catalyst

This material is reserved for educational use only, not allowed for commercial use.
Forbidden to modify the content, and cite the document when use.

4.2.2 Influence of MoO_3 content

The effect of MoO_3 content on butyraldehyde conversion was investigated over 1MoSi500(s), 3MoSi500(s) and 20MoSi500(s) catalysts. The results are shown in **Table 4.3**.

Table 4.3 The butyraldehyde conversion over 1MoSi500(s), 3MoSi500(s) and 20MoSi500(s) catalysts

Catalyst / Activity results		1MoSi500(s)	3MoSi500(s)	20MoSi500(s)
Conversion (%)		30.17 (61.46)[i]	54.67 (72.36)[i]	86.15 (98.21)[i]
Yield (%)				
C1-C2 compounds		0.34 (0.76)[i]	1.15 (1.71)[i]	2.71 (3.15)[i]
Propane		0.29 (0.57)[i]	3.61 (5.81)[i]	18.13 (30.91)[i]
iso C4		0.81 (1.62)[i]	5.26 (8.46)[i]	11.40 (19.44)[i]
Butanol		1.87 (3.61)[i]	8.08 (11.75)[i]	18.39 (16.94)[i]
Condensation products	*Dimer*	25.51 (48.84)[i]	29.64 (28.04)[i]	25.66 (19.19)[i]
	Trimer	1.34 (6.07)[i]	6.92 (16.60)[i]	9.86 (8.58)[i]
Selectivity (%)				
C1-C2 compounds		1.14 (1.24)[i]	2.11 (2.36)[i]	3.14 (3.21)[i]
Propane		0.95 (0.93)[i]	6.61 (8.03)[i]	21.04 (31.47)[i]
iso C4		2.69 (2.62)[i]	9.63 (11.68)[i]	13.24 (19.79)[i]
Butanol		6.21 (5.87)[i]	14.78 (16.24)[i]	21.35 (17.25)[i]
Condensation products	*Dimer*	84.56 (79.46)[i]	54.21 (38.75)[i]	29.78 (19.54)[i]
	Trimer	4.45 (9.87)[i]	12.66 (22.94)[i]	11.45 (8.74)[i]

** Reaction conditions; Catalyst: 1MoSi500(s),3MoSi500(s)and 20MoSi500(s), Contact time: 30 g.h.mol^{-1}, Carrier gas: H_2, Temperature: 500 °C, Flow rate of saturated vapour of feed plus Carrier gas: 30 ml.min^{-1}, Pressure:1 atm, The results average between fifth and seventh hour on stream (steady state), [i] The results collect from initial state*

This material is reserved for educational use only, not allowed for commercial use.
Forbidden to modify the content, and cite the document when use.

Considering the product selectivity, it can be seen from **Table 4.3** that a higher in condensation products selectivity is observed over 1MoSi500(s) and 3MoSi500(s), respectively. This can be described that acid-catalyzed condensation activity is promoted over the catalysts with low MoO_3 loading (1MoSi500(s) and 3MoSi500(s)), in which oligomeric MoO_3 (*Oc*) and the well- dispersed isolated MoO_3 species (*Im*) are predominant as described previously in **Table 4.2**. Hence, it can be suggested that the acid sites on oligomeric MoO_3 (*Oc*) and isolated MoO_3 species (*Im*) **[85]** prefer to promote condensation reaction. In contrast, 20MoSi500(s) exhibits the highest in propane selectivity. This suggests that decarbonylation activity prefers to promote over the polymeric (*Pm*) and crystalline MoO_3 (*Mc*) species which are the main species for the catalyst with high MoO_3 loading as described previously in **Table 4.2**. As the reaction is carried out under H_2 atmosphere at 500 °C, the surface of crystalline MoO_3 (*Mc*) species can be easily reduced and generating oxygen vacancy sites that are presumably active sites for decarbonylation reaction **[103]**. However, deactivation of the catalysts are observed as shown in **Figure 4.23**

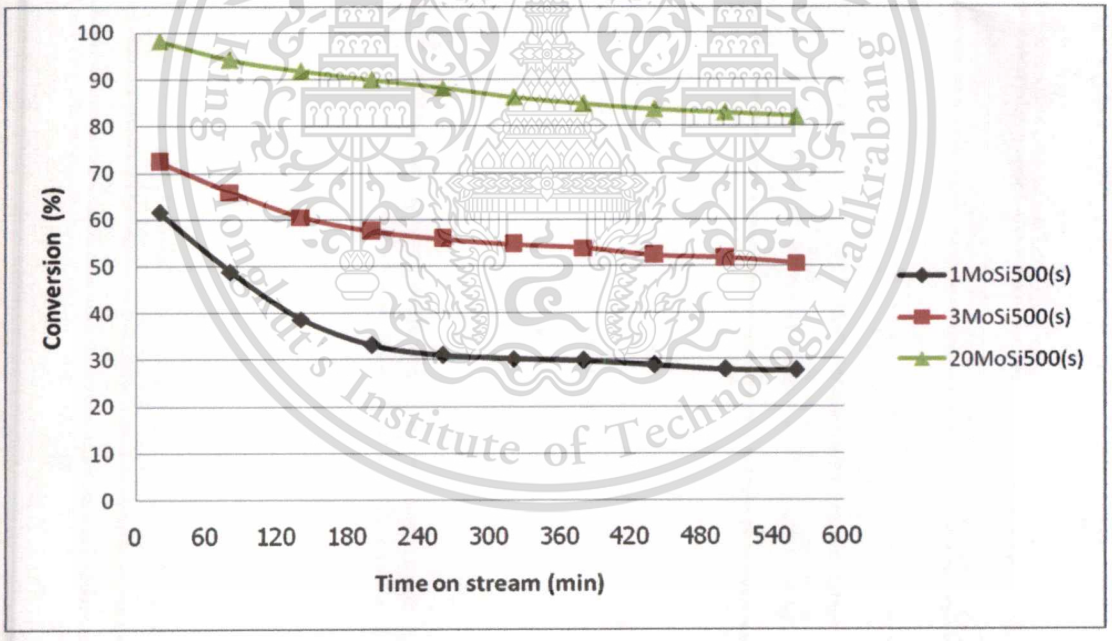

Figure 4.23 Conversion of butyraldehyde over MoO_3/SiO_2 catalyst with different MoO_3 loading as function of time on stream

* *The conditions are same as* ***Table 4.3***

It can be seen from **Figure 4.23** that the initial conversion of butyraldehyde is proportional to MoO_3 content of catalyst, which is consistently related to the amount of active site. The catalyst

This material is reserved for educational use only, not allowed for commercial use.
Forbidden to modify the content, and cite the document when use.

with low MoO_3 content (1MoSi500(s)) gives moderate conversion over 60% for the initial state. However, a rapid deactivation can be particularly observed in this catalyst. This is because 1MoSi500(s) prefers to promote condensation reaction. This can lead to the formation of high molecular weight molecules, causing active site blockage, and subsequent catalyst deactivation.

4.2.3 Influence of calcination temperature

The effect of calcination temperature on butyraldehyde conversion was investigated over 3MoSi500(s), 3MoSi600(s) and 3MoSi700(s) catalysts. The results are shown in **Table 4.4.**

Table 4.4 The butyraldehyde conversion over 3MoSi500(s), 3MoSi600(s) and 3MoSi700(s) catalysts

Catalyst / Activity results		3MoSi500(s)	3MoSi600(s)	3MoSi700(s)
Conversion (%)		54.67 (72.36)[i]	56.02 (74.98)[i]	79.23 (91.65)[i]
Yield (%)				
C1-C2 compounds		1.15 (1.71)[i]	1.24 (1.70)[i]	2.36 (2.92)[i]
Propane		3.61 (5.81)[i]	4.24 (6.77)[i]	12.08 (14.79)[i]
iso C4		5.26 (8.46)[i]	5.83 (9.31)[i]	12.30 (15.06)[i]
Butanol		8.08 (11.75)[i]	8.89 (13.83)[i]	14.43 (18.52)[i]
Condensation products	*Dimer*	29.64 (28.04)[i]	30.84 (24.23)[i]	20.87 (25.44)[i]
	Trimer	6.92 (16.60)[i]	4.98 (19.13)[i]	17.20 (14.92)[i]
Selectivity (%)				
C1-C2 compounds		2.11 (2.36)[i]	2.21 (2.27)[i]	2.98 (3.19)[i]
Propane		6.61 (8.03)[i]	7.57 (9.03)[i]	15.24 (16.13)[i]
iso C4		9.63 (11.68)[i]	10.41 (12.42)[i]	15.52 (16.43)[i]
Butanol		14.78 (16.24)[i]	15.87 (18.45)[i]	18.21 (20.21)[i]
Condensation products	*Dimer*	54.21 (38.75)[i]	55.05 (32.32)[i]	26.34 (27.76)[i]
	Trimer	12.66 (22.94)[i]	8.89 (25.51)[i]	21.71 (16.28)[i]

This material is reserved for educational use only, not allowed for commercial use.
Forbidden to modify the content, and cite the document when use.

** Reaction conditions; Catalyst: 3MoSi500(s),3MoSi600(s)and 3MoSi700(s), Contact time: 30 g.h.mol^{-1}, Carrier gas: H_2, Temperature: 500 ^{o}C, Flow rate of saturated vapour of feed plus Carrier gas: 30 ml.min^{-1}, Pressure:1 atm, The results average between fifth and seventh hour on stream (steady state), ^{i} The results collect from initial state*

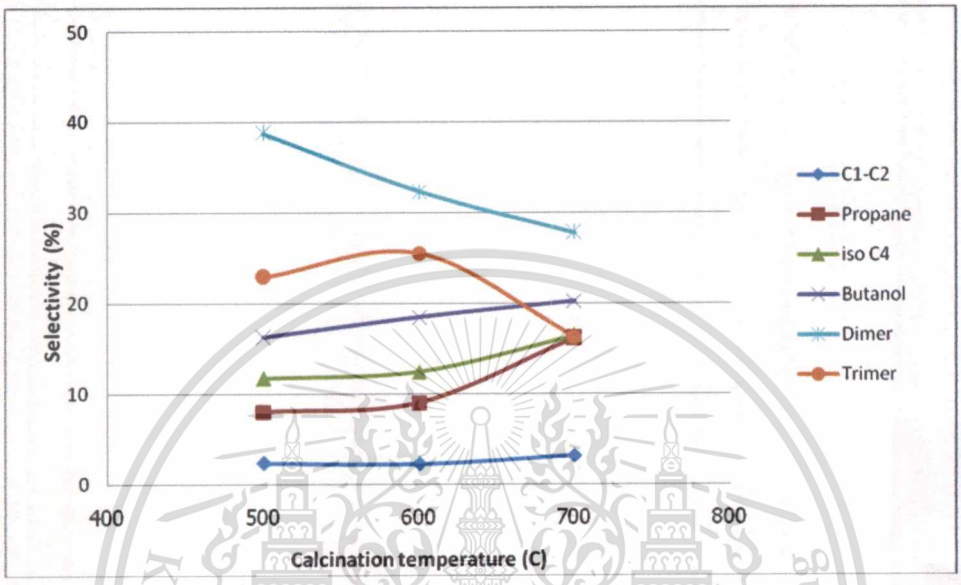

Figure 4.24 Product selectivity over MoO_3/SiO_2 catalyst with different calcinations temperature

** The conditions are same as **Table 4.4**, The results collect from initial state*

It can be seen from **Table 4.4** and **Figure 4.24** that the initial conversion of butyraldehyde is in the order of ; 3MoSi700(s) > 3MoSi600(s) ~ 3MoSi500(s). Moreover, the initial yield and selectivity of propane and condensation products are depend largely on the calcination temperature of catalyst, which is consistently related to species of active site. Considering the propane and condensation products selectivity, it can be seen that the increase in calcination temperature from 500 to 700 °C causes the increase in propane selectivity. This suggests that the isolated and oligomeric MoO_3 species tend to agglomerate to polymeric and crystalline MoO_3 at high calcination temperature (700 °C). This is consistent with the TPR analysis **(Figure 4.16)** of 3MoSi700(s) reveal that polymeric and crystalline MoO_3 are the major species that favor to promote the decarbonylation reaction as a manner similar to high MoO_3 content catalyst (20MoSi500(s)) as observed previously in **Table 4.3**. However, there is no significant different in decarbonylation activity between 3MoSi500(s) and 3MoSi600(s). This is due to the fact that the

This material is reserved for educational use only, not allowed for commercial use.
Forbidden to modify the content, and cite the document when use.

increase in calcination temperature from 500 to 600 °C causes no significant effect for those active species as shown by TPR analysis **(Figure 4.16)**.

In consistent with describe above, the lower in condensation products selectivity is observed over 3MoSi700(s). It can be suggested that the condensation activity is decreased. This is because the acid sites on oligomeric MoO_3 (*Oc*) and isolated MoO_3 species (*Im*) have been destroyed during the sintering process at 700 °C. This is in line with NH_3-TPD analysis **(Figure 4.25)** of 3MoSi500(s) and 3MoSi700(s). It is obvious that 3MoSi700(s) possess the lower acidity as compared to 3MoSi500(s). This leads to the decrease in condensation activity.

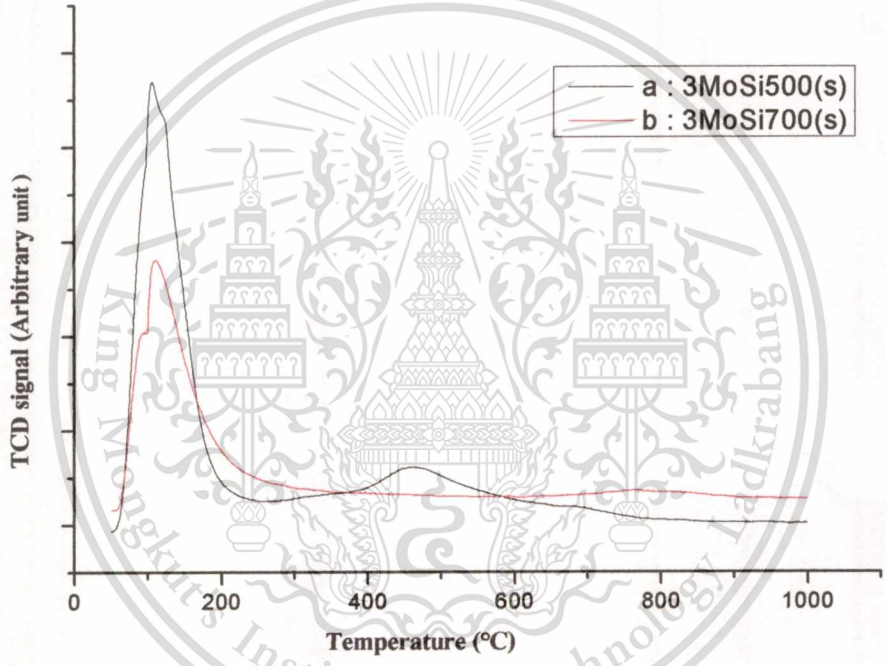

Figure 4.25 NH_3-TPD profiles of MoO_3/SiO_2: (a)3MoSi500(s) and (b)3MoSi700(s)

This material is reserved for educational use only, not allowed for commercial use.
Forbidden to modify the content, and cite the document when use.

4.2.4 Influence of preparation method

The effect of preparation method on butyraldehyde conversion was investigated over 3MoSi500(s), 3MoSi500(i), 20MoSi500(s) and 20MoSi500(i) catalysts. The results are shown in **Table 4.5**.

Table 4.5 The butyraldehyde conversion over 3MoSi500(s), 3MoSi600(s), 20MoSi500(s) and 20MoSi500(i) catalysts

Catalyst / Activity results		3MoSi500(s)	3MoSi500(i)	20MoSi500(s)	20MoSi500(i)
Conversion (%)		54.67 (72.36)^{i}	33.68 (95.98)^{i}	86.15 (98.21)^{i}	98.75(100)^{i}
Yield (%)					
C1-C2 compounds		1.15 (1.71)^{i}	17.70 (29.95)^{i}	2.71 (3.15)^{i}	7.18 (22.43)^{i}
Propane		3.61 (5.81)^{i}	8.85 (34.98)^{i}	18.13 (30.91)^{i}	70.21 (59.48)^{i}
iso C4		5.26 (8.46)^{i}	7.13 (28.16)^{i}	11.40 (19.44)^{i}	21.36 (18.09)^{i}
Butanol		8.08 (11.75)^{i}	0.00 (2.89)^{i}	18.39 (16.94)^{i}	0.00 (0.00)^{i}
Condensation products	*Dimer*	29.64 (28.04)^{i}	0.00 (0.00)^{i}	25.66 (19.19)^{i}	0.00 (0.00)^{i}
	Trimer	6.92 (16.60)^{i}	0.00 (0.00)^{i}	9.86 (8.58)^{i}	0.00 (0.00)^{i}
Selectivity (%)					
C1-C2 compounds		2.11 (2.36)^{i}	52.56 (31.21)^{i}	3.14 (3.21)^{i}	7.27(22.43)^{i}
Propane		6.61 (8.03)^{i}	26.28 (36.44)^{i}	21.04 (31.47)^{i}	71.10 (59.47)^{i}
iso C4		9.63 (11.68)^{i}	21.16 (29.34)^{i}	13.24 (19.79)^{i}	21.62 (18.09)^{i}
Butanol		14.78 (16.24)^{i}	0.00 (3.01)^{i}	21.35 (17.25)^{i}	0.00 (0.00)^{i}
Condensation products	*Dimer*	54.21 (38.75)^{i}	0.00 (0.00)^{i}	29.78 (19.54)^{i}	0.00 (0.00)^{i}
	Trimer	12.66 (22.94)^{i}	0.00 (0.00)^{i}	11.45 (8.74)^{i}	0.00 (0.00)^{i}

** Reaction conditions; Catalyst: 3MoSi500(s),3MoSi500(i), 20MoSi500(s)and 20MoSi500(i) Contact time: 30 g.h.mol^{-1}, Carrier gas: H_2, Temperature: 500 °C, Flow rate of saturated vapour of feed plus Carrier gas: 30 ml.min^{-1}, Pressure:1 atm, The results average between fifth and seventh hour on stream (steady state), ^{i} The results collect from initial state*

This material is reserved for educational use only, not allowed for commercial use.
Forbidden to modify the content, and cite the document when use.

For both catalysts with 3 and 20 mol% MoO_3 loading, a higher selectivity of propane and C1-C2 hydrocarbon is observed over the catalysts obtained from impregnation method (3MoSi500(i) and 20MoSi500(i)). In a different manner, the catalysts prepared by sol-gel method (3MoSi500(s) and 20MoSi500(s)) exhibit a higher in condensation products selectivity, as compared to those prepared by impregnation method. This is in line with the activity results as observed previously in **4.22** and **4.2.3** that decarbonylation reaction prefers to promote over the polymeric (*Pm*) and crystalline MoO_3 (*Mc*) species which are the main species for the catalysts obtained from impregnation method. On the other hand, the condensation reaction favor to promote over the catalysts which oligomeric MoO_3 (*Oc*) and the isolated MoO_3 species (*Im*) are the main species as described previously in **Figure 4.14**.

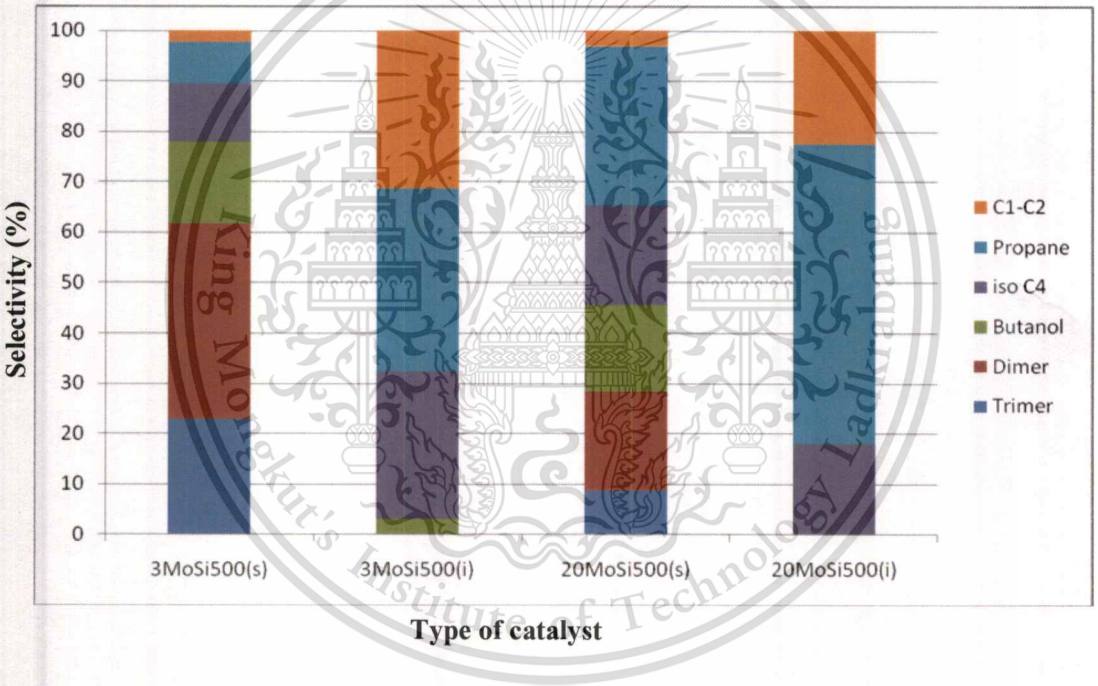

Figure 4.26 Product selectivity over 3MoSi500(s), 3MoSi500(i), 20MoSi500(s) and 20MoSi500(i) catalyst

* *The conditions are same as* ***Table 4.5****, The results collect from initial state*

Moreover, a higher propane selectivity is observed over 20MoSi500(i), as compared to 3MoSi500(i). This is due to the fact that the catalyst with high MoO_3 content would exhibit the higher amount of crystalline MoO_3 species which allows a better chance for the decarbonylation reaction. However, 3MoSi500(i) reveals higher C1-C2 yield and selectivity as compared to

This material is reserved for educational use only, not allowed for commercial use.
Forbidden to modify the content, and cite the document when use.

20MoSi500(i). This may be because the difference in dispersion of crystalline MoO_3 species as described previously in **Figure 4.5** and **4.6**.

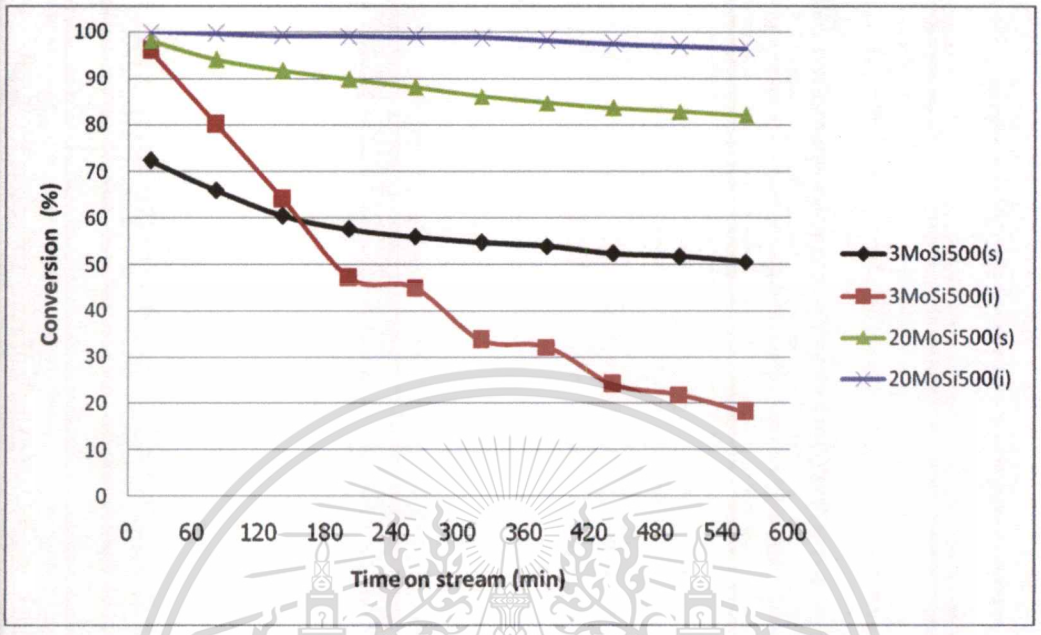

Figure 4.27 Conversion of butyraldehyde over MoO_3/SiO_2 catalyst with different preparation method as function of time on stream

** The conditions are same as **Table 4.5***

From **Figure 4.27**, it can be seen that the initial conversion of butyraldehyde over 3MoSi500(i), 20MoSi500(s) and 20MoSi500(i) have no significant difference. However, a slightly deactivation of 20MoSi500(s) can be observed while 20MoSi500(i) retains its stability. This is because 20MoSi500(i) possess an excess of crystalline MoO_3 species active sites leading to high decarbonylation activity which promotes only light hydrocarbon products. In contrast, some of condensation products can be generated over 20MoSi500(s). This can lead to the formation of high molecular weight molecules, causing active site blockage, and subsequent catalyst deactivation. Surprisingly, a rapid deactivation can be observed in 3MoSi500(i), despite the fact that condensation products cannot be observed over this catalyst. This is because a lower amount of oxygen vacancy sites that are presumably active sites for decarbonylation reaction. It can be suggested that oxygen vacancy sites are consumed incessantly as the reaction is carried out. Hence, a rapid deactivation can be observed only for 3MoSi500(i).

This material is reserved for educational use only, not allowed for commercial use.
Forbidden to modify the content, and cite the document when use.

4.2.5 Influence of reaction temperature

The effect of reaction temperature on butyraldehyde conversion was investigated over 3MoSi500(s) catalysts. The results are shown in **Table 4.6**.

Table 4.6 The butyraldehyde conversion over 3MoSi500(s) with different reaction temperature

3MoSi500(s)				
Calcination temperature (°C) / Activity results		300	400	500
Conversion (%)		32.60 (53.36)[i]	46.90 (59.67)[i]	54.67 (72.36)[i]
Yield (%)				
C1-C2 compounds		0.44 (0.47)[i]	0.85 (1.18)[i]	1.15 (1.71)[i]
Propane		0.37 (0.88)[i]	1.92 (3.34)[i]	3.61 (5.81)[i]
iso C4		0.54 (1.28)[i]	2.79 (4.87)[i]	5.26 (8.46)[i]
Butanol		1.62 (4.78)[i]	4.53 (7.42)[i]	8.08 (11.75)[i]
Condensation products	*Dimer*	26.36 (33.39)[i]	29.15 (29.89)[i]	29.64 (28.04)[i]
	Trimer	3.26 (12.57)[i]	7.65 (12.96)[i]	6.92 (16.60)[i]
Selectivity (%)				
C1-C2 compounds		1.36 (0.89)[i]	1.82 (1.98)[i]	2.11 (2.36)[i]
Propane		1.14 (1.64)[i]	4.09 (5.61)[i]	6.61 (8.03)[i]
iso C4		1.66 (2.39)[i]	5.96 (8.17)[i]	9.63 (11.68)[i]
Butanol		4.97 (8.95)[i]	9.65 (12.43)[i]	14.78 (16.24)[i]
Condensation products	*Dimer*	80.87 (62.57)[i]	62.16 (50.09)[i]	54.21 (38.75)[i]
	Trimer	9.99 (23.55)[i]	16.32 (21.72)[i]	12.66 (22.94)[i]

** Reaction conditions; Catalyst: 3MoSi500(s),Contact time: 30 g.h.mol^{-1}, Carrier gas: H_2, Temperature: 300-500 °C, Flow rate of saturated vapour of feed plus Carrier gas: 30 ml.min^{-1}, Pressure:1 atm, The results average between fifth and seventh hour on stream (steady state),*

[i] The results collect from initial state

This material is reserved for educational use only, not allowed for commercial use.
Forbidden to modify the content, and cite the document when use.

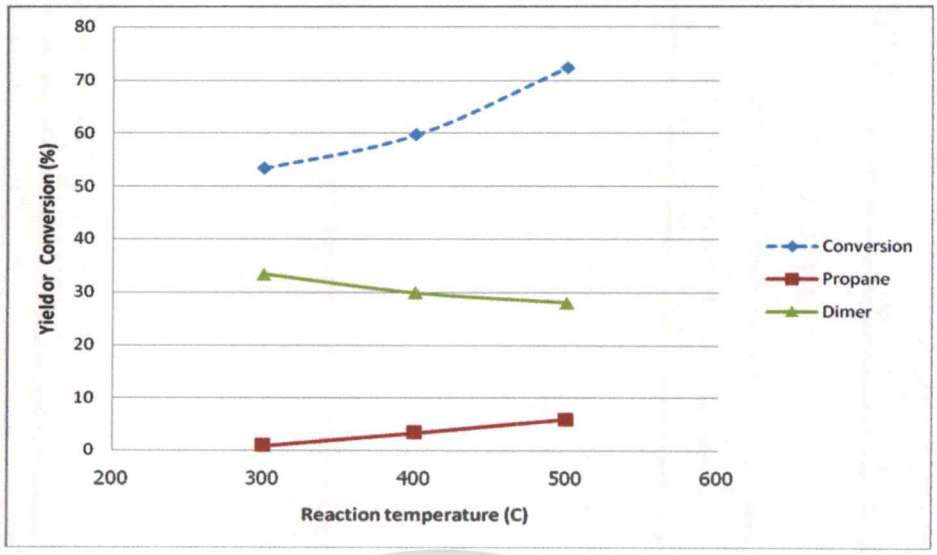

Figure 4.28 Yield and conversion of over 3MoSi500(s) catalyst

** The conditions are same as **Table 4.6***

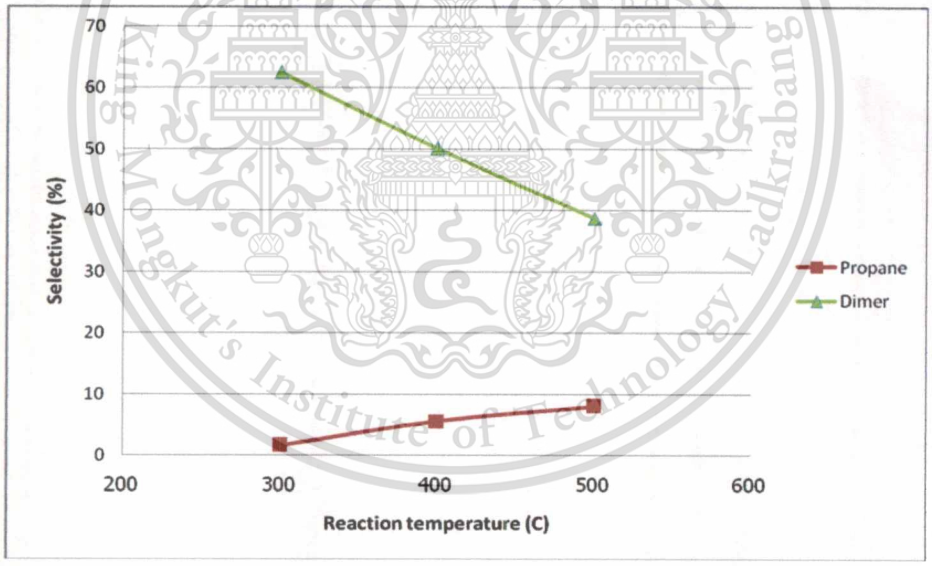

Figure 4.29 Product selectivity over 3MoSi500(s) catalyst

** The conditions are same as **Table 4.6***

It can be seen that raising reaction temperature (300–500 ^{o}C) increases the initial conversion of butyraldehyde **(Figure 4.28)**. Furthermore, it is also found that the yield and selectivity of propane **(Figure 4.28** and **(Figure 4.29))** is increased with the increase in temperature. This is

This material is reserved for educational use only, not allowed for commercial use.
Forbidden to modify the content, and cite the document when use.

because decarbonylation reaction is endothermic reaction, thus, high reaction temperature is preferred. While a marked drop in yield and selectivity of the dimer compounds **(Figure 4.28** and **(Figure 4.29))** as a function of temperature indicates that the condensation reaction does not thermodynamically favors at high temperature.

King Mongkut's Institute of Technology Ladkrabang

This material is reserved for educational use only, not allowed for commercial use.
Forbidden to modify the content, and cite the document when use.

CHAPTER 5

CONCLUSIONS AND SUGGESTIONS

5.1 CONCLUSIONS

This thesis has studied on the preparation method, MoO_3 loading and heat treatment that influence on the active surface structures of molybdenum oxide supported silica catalyst (MoO_3/SiO_2). The catalytic activity and selectivity of the obtained MoO_3 species were also investigated for the conversion of butyraldehyde. The results show that the catalysts prepared by sol–gel method exhibit very high surface area and uniformly micro-mesoporous nature of the silica support as compared to those obtained from impregnation method. Moreover, the silica support obtained from sol-gel synthesis exhibits the large chain network in three dimensions from polymerization process. This leads to the higher thermal stability as compared to the precipitated silica used for impregnation process. As increasing the MoO_3 loading and calcination temperature , the surface area of the catalysts decreases gradually. This is because the crystalline molybdenum oxide clusters are formed. However, at the same MoO_3 content, the catalysts prepared by sol–gel method reveals a higher dispersion of MoO_3 species as compared to those obtained from impregnation method. This suggests that MoO_3 species from sol–gel synthesis possess the stronger interaction with silica surface leading to a better dispersion.

The effects describe above also have an influence on the existence of the different MoO_3 species on the silica surface. The well-dispersed isolated MoO_3 (*Im*) and oligomeric MoO_3 (*Oc*) species are the main species for the catalysts prepared by sol–gel method with low MoO_3loading. On the other hand, the polymeric (*Pm*) and crystalline MoO_3 (*Mc*) species are predominant for the catalysts with high MoO_3loading. However, for the catalyst prepared by impregnation method, the polymeric (*Pm*) and crystalline MoO_3 (*Mc*) species can be observed for both low and high MoO_3loading. Heat treatment also plays a significant role on the structure of MoO_3 species. The significant different in MoO_3 species for different calcination temperature (500 and 700 °C) was observed at high calcination temperature (700 °C).The polymeric (*Pm*) and crystalline MoO_3 (*Mc*) species are also observed for the catalysts prepared by sol–gel method at low MoO_3loading (i.e., 1 and 3 mol %). This suggests that the formation of polymeric and crystalline MoO_3 were attributed from sintering of well dispersed MoO_3 species after calcined at 700 °C.

This material is reserved for educational use only, not allowed for commercial use.
Forbidden to modify the content, and cite the document when use.

The catalytic conversion of butyraldehyde reveals that the activity and selectivity are depend largely on the nature of the MoO_3 species. The acid sites on the oligomeric MoO_3 (*Oc*) and isolated MoO_3 species (*Im*) prefer to promote condensation reaction leading to the high molecular weight products (dimer and trimer products). In a different manner, decarbonylation activity prefers to be promoted over the oxygen vacancy sites of the polymeric (*Pm*) and crystalline MoO_3 (*Mc*) species causing in propane product. In addition, the hydrogenation and cracking products were also observed in this work.

5.2 SUGGESTIONS FOR FUTURE STUDIES

5.2.1 For improving the pore size distribution and dispersion of active sites, the combined sol–gel process with surfactant assisted template method should be studied.

5.2.2 The size and shape of the polymeric precursor have been shown to be dependent upon the hydrogen bonding and electrostatic interactions in the sol-gel system. Hence, the effect of water content, type of precursor and solvent should be investigated.

5.2.3 In order to probing surface composition, location and electronic structure of active surfaces and interfaces. EXAFS and XPS techniques should be also investigated for future study.

5.2.4 As the oxygen vacancy sites can be generated *in situ* during the reaction, the effect of type of carrier gas and H_2 partial pressure should be also studied.

5.2.5 For understand the effect of functional group, the catalytic nature of the catalysts in this work should be also tested with the other light oxygenated compound, i.e. butanol and butanoic acid.

This material is reserved for educational use only, not allowed for commercial use.
Forbidden to modify the content, and cite the document when use.

REFERENCES

[1] McDaniel M.P. **Advances in Catalysis.**, vol. 33, 1985. pp. 47.

[2] Burwell R.L., Haller G.L., Taylor K.C. and Read J.F. **Advances in Catalysis.**, vol. 20, 1969. pp.1.

[3] Mol J.C. and Mouljin J.A. "Catalysis – Science and Tèchnology", **Springer-Verlag Berlin.**, vol. 8, 1987. pp. 69.

[4] Grzybowska-Swierkosz B. and Haber J. "Vanadia Catalysts for Processes of Oxidation of Aromatic Hydrocarbons" , **Polish Scientific Publications.**, 1984.

[5] Bosch J. and Jansen F. **Catalysis Today.**, vol. 2, 1988. pp. 369.

[6] Liu H.F., Liu R.S., Liew K.Y., Johnson R.E., Lunsford J. H. and Am. **Journal of Chemical Society.**, vol. 106, 1984. pp. 4117.

[7] Iwasawa Y. and Tanaka H. "Proc. 8th Int", **Catal Berlin.**, vol. 4, 1984. pp. 381.

[8] Dury F., Misplon V. and Gaigneaux E.M. **Catalysis Today.**, vol. 91–92, 2004. pp.111–116

[9] Iwasawa Y. **Advances in Catalysis.**, vol 35, 1987. pp. 187.

[10] Smith M. R., Zhang L., Driscoll S.A. and Ozkan U. S. **Catalysis Letters.**, vol. 19, 1993. pp. 1

[11] Williams C. C., Ekerdt J. G., Jehng J.M., Hardcastle and Turek F. D. **Journal of Physical Chemistry.**, vol. 95,1991. pp. 8781.

[12] De Boer M., van Dillen A. J., Koninsberger D. C., Geus J. W.,Vuurman M. A. and Wachs I.E. **Catalysis Letters.**, vol. 11, 1991. pp. 227.

[13] Desikan L., Huang L. and Oyama S.T. **Journal of Physical Chemistry.**, vol. 95, 1991. pp. 10050.

[14] Smith M. R and Ozkan U. S. **Journal of Catalysis.**, vol. 142, 1993. pp. 124.

[15] Banares M. A., Rodriguez-Ramos I., Guerreor-Ruiz A. and Fierro J. L.G. **Proceedings of the10th International Congress on Catalysis.**, vol. B, 1993. pp. 1131.

[16] Yongxia M., Guanzhong L., Xiaohui L., Yanglong G., Yanqin W. and Yun G. **Journal of Molecular Catalysis A: Chemical.**, vol. 306, 2009. pp. 17–22.

[17] Mendez-Vivar J. **Materials Chemistry and Physics.**, vol. 43, 1996. pp. 140-144.

[18] Han O.H., Lin C. Y., Sustache N., McMillan M., Carruthers J. D., Zilm K.W. and Haller

This material is reserved for educational use only, not allowed for commercial use.

Forbidden to modify the content, and cite the document when use.

G.L. **Applied Catalysis A: General.**, vol. 98, 1993. pp. 195.

[19] Stencel J. M. "Raman Spectroscopy for Catalysis", **Van Nostrand–Reinhold.**, 1990. pp. 51.

[20] Francesco A. and Adolfo P. "Silica-Supported Molybdena Catalysts. Surface Structures, Reduction Pattern, and Oxygen Chemisorption", **Journal of Physical Chemistry.**, vol. 100, 1996. pp. 19994-20005.

[21] Harold H. K. "TRANSITION METAL OXIDES: Surface Chemistry and Catalysis", **Studies in Surface Science and Catalysis.**, vol. 45.

[22] Somorjai G. A. "Chemistry in Two Dimensions: Surfaces", **Cornell University.**

[23] Rhodin T. N. and Ertl G. "The Nature of Surface Chemical Bonds".

[24] Morrison S. R. "The Chemical Physics of Surfaces" . **Plenum Press.**, 1977.

[25] Ertl G. and Kuppers I. "Low Energy Electrons and Surface Chemistry".

[26] http://en.wikipedia.org/

[27] Wang D., Su D. S. and Schlögl R. "Electron Beam Induced Transformation of MoO_3 to MoO_2 and a New Phase MoO" , **Anorg. Allg. Chem.**, vol. 630, 2004. pp.1007-1014.

[28] Guo J.D., Zavalij P.Y. and Whittingham M.S. **European Journal of Solid State and Inorganic Chemistry.**, vol. 31, 1994. pp. 833

[29] Ressler T., Walter A., Huang Z.D. and Benschb W. **Journal of Catalysis.**, vol. 254, 2008. pp. 170–179.

[30] Hagg. G. and Magneli A. Mineral. Vol. 19, 1944

[31] Magneli A. **Acta Chem. Scand.**, vol. 2, 1948. pp. 501.

[32] Glemeer O. and Lutz G. Z. **anorg. U. allgem. Chem.**, vol. 263, 1950.

[33] Megneli A., Blomberg-Hansson B., Kihlborg L. and Sundkvist G. **Acta Chem. Scand.**, vol. 9, 1955.

[34] Kihlborg L. and Magneli A. **Acta Chem. Scand.** vol. 9, 1955.

[35] Magneli A. **Acta Cryst.** vol. 6, 1953.

[36] Magneli A., Andersson G., Blomberge B. and Kihlborg L. **Anal. Chem.**, vol. 24, 1952.

[37] Hegedus A. J., Sasvari K. and Neugebauer J. Z. **anorg. U. allgem. Chem.**, vol. 293, 1957

[38] Wachs I.E. "Raman and IR studies of surface metal oxide species on oxide supports: Supported metal oxide catalysts", **Catalysis Today.**, vol. 27(3–4), 1996. pp. 437–455.

This material is reserved for educational use only, not allowed for commercial use.
Forbidden to modify the content, and cite the document when use.

[39] Topsøe N. "Infrared study of sulfided Co-Mo-Al_2O_3 catalysts—The nature of surface hydroxyl-groups", **Journal of Catalysis.**, vol. 64(1), 1980. pp. 235–237.

[40] Diaz A.L. and Bussell M.E. "An infrared spectroscopy and temperature-programmed desorption study of CO on MoO3/Al2O3 catalysts: Quantitation of the molybdena overlayer", **Journal of Physical Chemistry.**, vol. 97(2), 1993. pp. 470–477.

[41] Scheithauer M., Cheung T.K., Jentoft R.E., Grasselli R.K., Gates B.C. and Knözinger H. "Characterization of WOx/ZrO2 by vibrational spectroscopy and n-pentane isomerization catalysis", **Journal of Catalysis.**, vol. 180(1), 1998. pp. 1–13.

[42] Gao X.T., Bare S.R., Fierro J.L.G., Banares M.A. and Wachs I.E. "Preparation and in situ spectroscopic characterization of molecularly dispersed titanium oxide on silica", **Journal of Physical Chemistry : B.**, vol. 102(29), 1998. pp. 5653–5666.

[43] Gao X.T., J.L. Fierro G. and Wachs I.E. "Structural characteristics and catalytic properties of highly dispersed ZrO_2/SiO_2 and $V_2O_5/ZrO_2/SiO_2$ catalysts", **Langmuir.**, vol. 15(9), 1999. pp. 3169–3178.

[44] Mestl G. and Knözinger H. "Vibrational spectroscopies", **Wiley-VCH.**, Vol. 2, 1997. pp. 539–574.

[45] Wachs I.E. "Molecular structures of surface metal oxide species: Nature of catalytic active sites in mixed metal oxides", **Taylor & Francis Group.**, 2006. pp. 1–30.

[46] Busca G. "Differentiation of mono-oxo and polyoxo and of monomeric and polymeric vanadate, molybdate and tungstate species in metal oxide catalysts by IR and Raman spectroscopy", **J. Raman Spectrosc.**, vol. 33(5), 2002. pp. 348–358.

[47] Horsley J.A., Wachs I.E., Brown J.M., Via G.H. and Hardcastle F.D., "Structure of surface tungsten oxide species in the WO3/Al2O3 supported oxide system from x-ray absorption near-edge spectroscopy and Raman spectroscopy", **Journal of Physical Chemistry.**, vol. 91(15), 1987. pp. 4014–4020.

[48] Barton D.G., Shtein M., Wilson R.D., Soled S.L. and Iglesia E. "Structure and electronic properties of solid acids based on tungsten oxide nanostructures", **Journal of Physical Chemistry : B.**, vol. 103(4), 1999. pp. 630–640.

This material is reserved for educational use only, not allowed for commercial use.
Forbidden to modify the content, and cite the document when use.

[49] Baertsch C.D., Komala K.T., Chua Y.H. and Iglesia E. "Genesis of Brønsted acid sites during dehydration of 2-butanol on tungsten oxide catalysts", **Journal of Catalysis.**, vol. 205(1), 2002. pp. 44–57.

[50] Liu H.C, Cheung P. and Iglesia E. "Effects of Al_2O_3 support modifications on MoO_x and VO_x catalysts for dimethyl ether oxidation to formaldehyde", **Phys. Chem.**, vol. 5(17), 2003. pp.3795–3800.

[51] Hu H.C. and Wachs I.E. "Catalytic properties of supported molybdenum oxide catalysts: In situ Raman and methanol oxidation studies", **Journal of Physical Chemistry.**, vol. 99(27), 1995. pp.10911–10922.

[52] Eberl. D.D., Drits V.A. and Srodon J. "Deducing growth mechanisms for minerals from the shapes of crystal size distributions", **Amer. J. Sci.**, vol. 298, 1998. pp. 499–533.

[53] Scheithauer M., Grasselli R.K. and Knözinger H. "Genesis and structure of WO_x/ZrO_2 solid acid catalysts", **Langmuir.**, vol. 14(11), 1998. pp. 3019–3029.

[54] Cullity B.D. and Stock S.R. "Elements of x-ray diffraction, Prentice Hall: Upper Saddle River", 2001. pp. 664.

[55] Wells A.F. "Structural inorganic chemistry, Oxford University: New York", 1984. pp. 1382.

[56] Cotton F.A. and Wilkinson G. "Advanced inorganic chemistry", **Wiley: New York.**, 1988. pp. 1455.

[57] Grzybowska B., Sloczynski J., Grabowski R., Wcislo K., Kozlowska A., Stoch J. and Zielinski J. "Chromium oxide alumina catalysts in oxidative dehydrogenation of isobutane", **Journal of Catalysis.**, vol. 178(2), 1998. pp. 687–700

[58] Sloczynski J., Grzybowska B., Grabowski R., Kozlowska A. and Wcislo K. "Oxygen adsorption and catalytic performance in oxidative dehydrogenation of isobutane on chromium oxide-based catalysts", **Phys. Chem. Chem. Phys.**, vol. 1(2), 1999. pp. 333–339.

[59] Bielanski A. and Haber J. "Oxygen in catalysis", **Dekker: New York.**, 1991.

[60] Kung H.H. "Oxidative dehydrogenation of light (C2 to C4) alkanes", **Adv. Catal.**, vol. 40, 1994. pp. 1–38.

[61] Davydov A. "Use of infrared spectroscopy in studies of catalysts based on molybdenum heteropolycompounds supported on oxides", **Usp. Chim. (in Russian); Russ. Chem.**, vol. 62, 1993. pp.105–120.

This material is reserved for educational use only, not allowed for commercial use.
Forbidden to modify the content, and cite the document when use.

[62] Pajonk G. M. "Catalytic Aerogels", **Catalysis Today.**, vol. 35, 1997. pp. 319–37.

[63] Thomas I. M. "Multicomponent Glasses from the Sol-Gel Process", **Noyes Publications.**, 1988. pp. 2–15.

[64] Watton S. P., Taylor C. M., Kloster G. M. and Bowman S. C. "Coordination Complexes in Sol-Gel Silica Materials", **Wiley, New York.**, 2003. pp. 333–420.

[65] Ward D. A. and Ko E. I. "Preparing Catalytic Materials by the Sol-Gel Method", **Ind. Eng. Chem. Res.**, vol. 34, 1995. pp. 421–33.

[66] Rupp W., Huesing N. and Schubert U. "Preparation of Silica-Titania Xerogels and Aerogels by Sol-Gel Processing of New Single-Source Precursors", **J. Mater. Chem.**, vol. 12, 2002. pp. 2594–96.

[67] Brinker C. J. and Scherer G. W. "Sol-Gel Science: The Physics and Chemistry of Sol-Gel Processing", **Academic Press, San Diego.**, 1990.

[68] Flory P. "Principles of Polymer Chemistry," **Cornell University Press, Ithaca**, 1971.

[69] Gommes C., Blacher S., Goderis B., Pirard R., Heinrichs B., Alié C. and . Pirard J.-P. "In Situ SAXS Analysis of Silica Gel Formation with an Additive", **Journal of Physical Chemistry : B.**, vol. 108, 2004. pp. 8983–91.

[70] Schneider M. and Baiker A. "Titania-Based Aerogels", **Catalysis Today.**, vol. 351, 997. pp. 339–65.

[71] Mendez-Vivar J., Campero A., Livage J. and Sanchez C. **J.Non-Cryst. Solids.**, vol. 121, 1990. pp. 26.

[72] Hollingshead J.A., Tyszkiewicz M.T. and McCarley R.E. **Chem. Mater.**, vol. 5, 1993. pp. 1600.

[73] Yanovskaya M.I., Obvintseva I.E., Kessler V.G., Galyamov B.Sh. , Kucheiko S.I., Shifrina R.R. and Turova N.Y., **J. Non-Cryst. Solids.**, vol. 124, 1990. pp. 155.

[74] Astier M., Bertrand A. and Teichner S.J. **Winny Dong Journal of Non-Crystalline Solids**, vol., 225, 1998. pp. 135–140.

[75] Juarez Ramirez I. and Martinez-de la Cruz A., **Mater. Lett.**, vol. 57, 2003. pp. 1034.

[76] Takanori M., Kazuya F., Huong T. M., Ohkita H. and Kakuta N. **Chemistry Letters.**, vol. 34, 2005.

[77] Wang L. and Hall,W. K. J., **Journal of Catalysis.**, vol. 66, 1980. pp. 251.

[78] Jeziorowski H. and Knijzinger H., **Journal of Physical Chemistry.**, vol. 83, 1979. pp. 1166.

This material is reserved for educational use only, not allowed for commercial use.
Forbidden to modify the content, and cite the document when use.

[79] Lopez Corder R., Gil Llambias F.J. and Lopez Agudo A., **Applied Catalysis.**, vol. 74, 1991. pp. 125-136.

[80] Luthra N.P. and Cheng W.C., **Journal of Catalysis.**, vol. 107, 1987. pp. 154.

[81] Ma X., Gong J., Yang X. and Wang S., **Applied Catalysis A: General,** vol. 280, 2005. pp. 215–223.

[82] Ma X., Gong J., Wang S., Gao N., Wang D., Yang X. and He F., **Catalysis Communication** ., 2004.

[83] Lietti L., Ramis G., Busca G., Bregani F. and Forzatti P, **Catalysis Today.**, 2000.

[84] Smith MR., Zhang L., Driscoll SA. and Ozkan US., **Catalysis Letter.**, 1993.

[85] Amol P., Lucas K., Palraj S. and Halligudi B., **Catalysis Letter**, vol. 126, 2008. pp. 286–292.

[86] Shubhangi B. U., Trupti V. K., Ankush V. B., Renu P., Jyoti C. and Mohan K. D., **Journal of Molecular Catalysis A: Chemical.**, vol. 310, 2009. pp. 150–158.

[87] Ma X., Gong J., Wang S., Gao N., Wang D., Yang X. and He F., **Catalysis Communication** ., vol. 5, 2004. pp. 101–106.

[88] Dongare M.K., Bhagwat V.V., Ramana C.V. and Gurjar M.K., **Tetrahedron Letter.**, vol. 45, 2004. pp. 4759–4762.

[89] Brgeault J.M., **Dalton Transaction.** vol. 17, 2003. pp. 3289.

[90] Miao Y., Lu G., Liu X., Guo Y., Wang Y. and GuoY., **Journal of Molecular Catalysis A: Chemical.**, vol. 306, 2009. pp. 17–22.

[91] Deltcheff C.R., Fournier M., Franck R. and Thouvenot R., **Inorg. Chem,** vol. 22, 1983. pp. 207.

[92] Kido A., Iwamoto H., Azuma N. and Ueno A., **Catal. Surv. Jpn.** vol. 6, 2002. pp. 45.

[93] Kazstelan S., Payen E. and Moffat J.B., **Journal of Catalysis,** vol. 112, 1988. pp. 320.

[94] Tatsumi T., Muramatsu A. and Tominaga H., **Chem. Lett**, 1984. pp. 685.

[95] Ogata A., Kazusaka A. and Enyo M., **Journal of Physical Chemistry.**, vol. 90, 1986. pp. 5201.

[96] **Ono** T., Anpo M. and Kubokawa Y., **Journal of Physical Chemistry.**, vol. 90 ,1986. pp. 5201.

[97] Jeziorowski H., Knozinger H. and Grange., **Journal of Physical Chemistry.**, vol. 84, 1980. pp. 1825.

This material is reserved for educational use only, not allowed for commercial use.
Forbidden to modify the content, and cite the document when use.

[98] Cheng C. P. and Schrader G. L., **Journal of Catalysis**, vol. 60, 1979. pp. 276.

[99] Desikan A. N., Huang L. and Oyama S. T., **Journal of Physical Chemistry.**, vol. 95, 1991. pp. 24.

[100] Hall W. K. and Millman W. S., **Journal of Catalysis.**, vol. 59, 1979. pp. 311.

[101] Peri J. P., **Journal of Physical Chemistry.**, vol. 6, 1982 . pp. 1615.

[102] Ressler T., Jentoft R.E., Wienold J., Gunter M.M. and Timpe O., **Journal of Physical Chemistry : B.**, vol.104, 2000. pp. 6360.

[103] Dury F., Misplon V. and Gaigneaux E.M., **Catalysis Today**, vol. 91–92, 2004. pp. 111–116.

[104] Cordero R. L., Gil Lambias F. J. and Lo´pez Agudo., **A. Appl. Catal.**, vol. 74, 1991. pp. 125.

[105] Liu T. C., Rau J. J. and **Chin J., Inst. Chem. Eng.**, vol. 20, 1989. pp. 269.

[106] Smith M. R., Zhang L., Driscoll S. A. and Ozkan U. S., **Catalysis Letters.**, vol. 1, 1993.

[107] Francesco A. and Adolfo P., **Journal of Physical Chemistry.**, vol. 100, 1996. pp. 19994-20005.

[108] Morris D.L., **US Patent 4 316 990**, 1985.

[109] Tsuji H., Yagi F., Hattori H. and Kita H., **Journal of Catalysis.**, vol. 148, 1994. pp. 759.

[110] Zhang G., Hattori H. and Tanabe K., **Chem. Soc. Jpn.**, vol. 62, 1989. pp. 2070.

[111] Ko An-Nan., Hao Hu Chih. and Yun Chen Jia., **Applied Catalysis A: General.**, vol. 184, 1999. pp. 211-217.

[112] Rylander P.N., "Hydrogenation Methods", **Academic Press, London,** 1985.

[113] Shubhangi B., Umbarkarand T. and Kotbagi V. "Acetalization of glycerol using mesoporous MoO3/SiO2 solid acid catalyst", **Journal of Molecular Catalysis A: Chemical.**, vol. 310, 2009 pp. 150–158.

[114] Francesco A. and Nicola G. "Working Mechanism of Oxide Catalysts in the Partial Oxidation of Methane to Formaldehyde", **Journal of catalysis.**, vol. 67, 1997 pp. 66–76.

[115] Zhaoxia S. and Naoki M. "Gas-phase epoxidation of propylene through radicals generated by silica-supported molybdenum oxide", **Applied Catalysis A: General.**, vol. 316, 2007 pp. 142–151

This material is reserved for educational use only, not allowed for commercial use.
Forbidden to modify the content, and cite the document when use.

APPENDICES

This material is reserved for educational use only, not allowed for commercial use.
Forbidden to modify the content, and cite the document when use.

APPENDIX A

Reference X-ray Diffraction Pattern

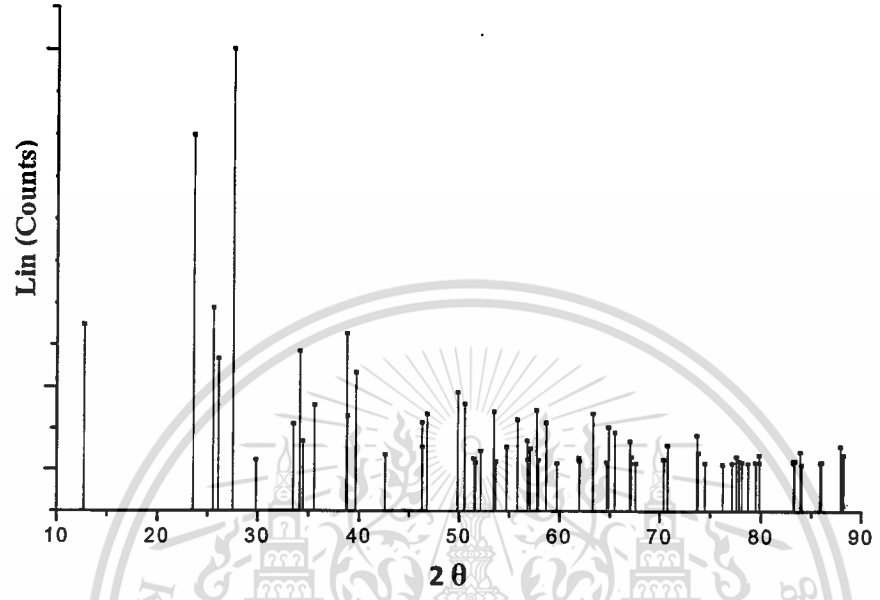

Figure A.1 Reference XRD pattern of α-MoO_3

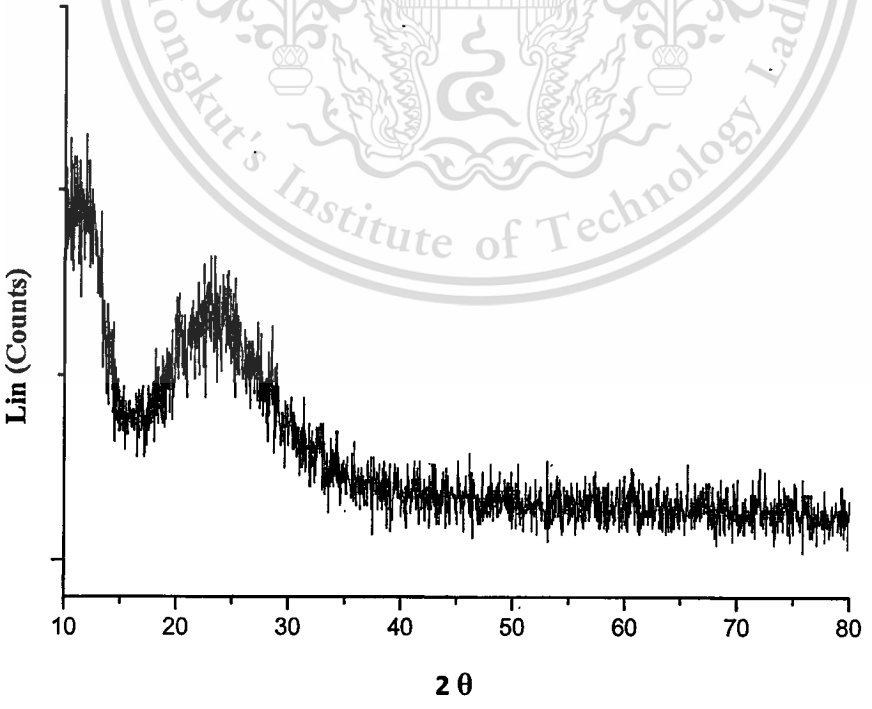

Figure A.2 Reference XRD pattern of amorphous silica

This material is reserved for educational use only, not allowed for commercial use.
Forbidden to modify the content, and cite the document when use.

APPENDIX B

Scanning Electron Micrograph

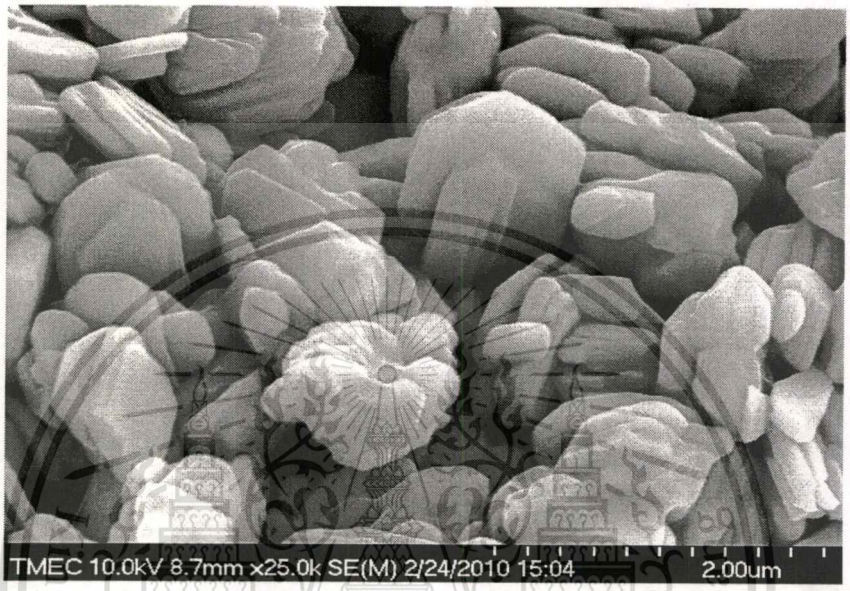

Figure B.1 SEM micrograph of α-MoO_3

Figure B.2 SEM micrograph of amorphous silica

This thesis is for study purpose only, not allowed for commercial use.
Forbidden to modify the content, and cite the document when use.

APPENDIX C

CALCULATION

C1. Calculation of catalytic parameters

Contact time (W/F)

$$W/F = \frac{\text{Weight of catalyst (g)}}{\text{Mole of gas reactant feed (mol/h)}}$$

In the reaction using 0.00536 mol/h (30 ml/min) of saturated vapour of butyraldehyde at -1.12 °C (0.06648 atm) and using 0.1608 grams of catalyst, the W/F is calculated as follow:

$$W/F = [0.1608 \text{ (g)} / 0.00536 \text{ (mol/h)}]$$

$$= 30 \text{ g.h.mol}^{-1}$$

In a similar manner; W/F of catalysts (10,20 and 60 $g.h.mol^{-1}$) with different catalyst weight and different feed rate were also calculated.

This material is reserved for educational use only, not allowed for commercial use.
Forbidden to modify the content, and cite the document when use.

Calculation of % weight of products from gas chromatography

The peak area of the components which were obtained from GC-chromatogram is shown in **Table C.1**

Table C.1 The peak area of components from butyraldehyde conversion over 3MoSi500(s) catalyst

Component	Peak area
C1-C2	16.8264
Propane	57.1704
Iso C4	83.2464
Butyraldehyde (feed)	271.9776
Butanol	115.62
2-ethyl-2-hexanal	251.5104
Butyl butyrate	6.396
4-octanone	5.2152
2-ethyl hexenal	2.3616
1-(1-ethyl-2,3-dimethyl-cyclopent-2-enyl)-ethanone	159.0144
2,4,6-triisopropyl-1,3,5-trioxane	7.9704
2,4-dimethyl-1-(1-methylethyl)-benzene	6.6912
Total	984

** Reaction conditions; Catalyst:3MoSi500(s), Carrier gas:H_2, Temperature:500 °C, Flow rate of saturated vapour of feed plus Carrier gas:30 ml.min^{-1}, Pressure:1 atm, The results collect from initial state.*

This material is reserved for educational use only, not allowed for commercial use.
Forbidden to modify the content, and cite the document when use.

In gas chromatography, area normalization is used for quantitative analysis. Area normalization, in its simple form, assumes that the sensitivity of the detector is the same for each component in the mixture. The composition of the mixture is then obtained by expressing the area of each individual peak as a percent of the total area of all the peaks in the chromatogram which is represented as a percent by weight of the component **(Table C.2)**.

Table C.2 The percentage of components from butyraldehyde conversion over 3MoSi500(s) catalyst

Component	Percent by weight (w %)
C1-C2	1.71
Propane	5.81
Iso C4	8.46
Butyraldehyde (feed)	27.64
Butanol	11.75
2-ethyl-2-hexanal	25.56
Butyl butyrate	0.65
4-octanone	0.53
2-ethyl hexenal	0.24
1-(1-ethyl-2,3-dimethyl-cyclopent-2-enyl)-ethanone	16.16
2,4,6-triisopropyl-1,3,5-trioxane	0.81
2,4-dimethyl-1-(1-methylethyl)-benzene	0.68
Total	100

This material is reserved for educational use only, not allowed for commercial use.
Forbidden to modify the content, and cite the document when use.

Conversion

The conversion of butyraldehyde at each time on stream was determined by subtracting the total mass of all fraction (w %) and the total mass of all unconverted feed (w %). Therefore, the conversion can be defined by the relation;

% Conversion = [Total mass of all fraction (100%)] - [Total mass of unconverted feed (w %)]

Selectivity

The selectivity of products at each time on stream is the ratio of mass of each product component (w %) to the total mass of all product (w %). It can be expressed as the following;

$$\text{\% Selectivity of product A} = \frac{\text{Mass of product A (w \%)}}{\text{Total mass of all product (w \%)}} \times 100$$

Yield

The yield of product is defined as the product obtained from the reactant. It can be expressed as the following;

$$\text{\% Yield of product A} = \frac{\text{Selectivity (\%) x Conversion (\%)}}{100}$$

This material is reserved for educational use only, not allowed for commercial use.
Forbidden to modify the content, and cite the document when use.

APPENDIX D

COLUMN PARAMETERS AND GAS CHROMATOGRAPH CONDITIONS

D1. Column parameter and gas chromatograph condition for oxygenated compounds

The GC operating condition is summarized in **Table D.1** and the chromatographic temperature program for gas phase product analysis is summarized in **Table D.2**

Table D.1 The GC operating condition for oxygenated compounds

Column	HP-5
Diameter (mm)	0.53
Length (m)	30
Column head pressure (psi)	2
Linear velocity (cm/s)	12.08
Carrier gas	He
Injection temperature (°C)	200
Detector	FID
Detector temperature (°C)	250
Sample loop (μl)	25

Table D.2 The chromatographic temperature program for oxygenated compounds analysis

Step	Temperature (°C)	Heating rate (°C/min)	Hold time (min)	Total time (min)
1	40	-	5	5
2	240	10	20	40

This material is reserved for educational use only, not allowed for commercial use.
Forbidden to modify the content, and cite the document when use.

D2. Column parameter and gas chromatograph condition for light hydrocarbon compounds

The GC operating condition is summarized in **Table D.3** and the chromatographic temperature program for gas phase product analysis is summarized in **Table D.4**

Table D.3 The GC operating condition for light hydrocarbon compounds

Column	HP-PLOT
Diameter (mm)	0.25
Length (m)	30
Column head pressure (psi)	5
Linear velocity (cm/s)	15
Carrier gas	He
Injection temperature (°C)	200
Detector	FID
Detector temperature (°C)	250
Sample loop (μl)	15

Table D.4 The chromatographic temperature program for light hydrocarbon compounds analysis

Step	Temperature (°C)	Heating rate (°C/min)	Hold time (min)	Total time (min)
1	40	-	20	20
2	200	10	14	30

This material is reserved for educational use only, not allowed for commercial use.
Forbidden to modify the content, and cite the document when use.

AUTHOR BIOGRAPHY

Name: Mr. Leenawat Kanda

Date of Birth: January 29, 1984

Nationality: Thai

University Education:

2003-2006 **Bachelor Degree :** Bachelor of Science, Industrial Chemistry
King Mongkut's Institute of Technology Ladkrabang

2006-2011 **Master Degree :** Master of Science, Chemistry (Inorganic chemistry)
King Mongkut's Institute of Technology Ladkrabang

Work experiences:

2007 –2009 Lecturer in Chemistry for Mattayom 4-6 levels, Long Life Learning CO., Ltd.

2007 –2010 Teacher Assistant, King Mongkut's Institute of Technology Ladkrabang

2010 - present Researcher Assistant, Project: Controlled deoxygenation of cellulose to low oxygen-leveled fuels, PTT public company limited.

2008- present R&D supervisor, Matt Chemie Co., Ltd.

Conferences

2009 Leenawat Kanda, and Tawan Sooknoi, Synthesis of high surface area molybdenum oxide supported silica catalyst by sol-gel method, Oral presentation, Pure and Applied Chemistry International Conference 2009 (PACCON 2009), January 14-16, 2009, Naresuan University, Phitsanulok, Thailand.

2011 Leenawat Kanda, and Tawan Sooknoi, Partially embedded molybdenum oxide in silica support for single site catalysis, Poster presentation, The 6th International Symposium on Advance Material in Asia-Pacific Rim (6th ISAMAP), November 21-23, 2009, Chulalongkorn University, Bangkok, Thailand.

This material is reserved for personal use only, not allowed for commercial use.
Forbidden to modify the content, and cite the document when use.